The American Mineralogist

Journal of the Mineralogical Society of America

Vol. 37 JANUARY-FEBRUARY, 1952 Nos. 1 and 2

Contents

Published bi-monthly by the Society

Mineralogical Society of America

ASSOCIATED WITH THE GEOLOGICAL SOCIETY OF AMERICA

President: **Michael Fleischer,** U. S. Geological Survey, Washington 25, D. C.

Vice President: **J. D. H. Donnay,** The Johns Hopkins University, Baltimore, Maryland.

Secretary: **C. S. Hurlbut, Jr.,** Harvard University, Cambridge, Massachusetts.

Treasurer: **Earl Ingerson,** U. S. Geological Survey, Washington 25, D. C.

Editor: **Walter F. Hunt,** University of Michigan, Ann Arbor, Michigan.

Councillors: **Lewis S. Ramsdell,** University of Michigan, Ann Arbor, Michigan.
E. F. Osborn, School of Mineral Industries, Pennsylvania State College, Pennsylvania.
George T. Faust, U. S. Geological Survey, Washington 25, D. C.
Victor T. Allen, Institute of Geophysical Technology, St. Louis, Missouri.
Adolf Pabst, University of California, Berkeley, California

The enlarged issues of this journal for 1952 are made possible by a grant from the Penrose Fund of the Geological Society of America.

The American Mineralogist—Journal of the Mineralogical Society of America

A journal containing articles on mineralogy, crystallography, petrography, and allied sciences, is issued every two months. Contributions are invited from everyone.

Office of Publication, Mineralogical Laboratory, Ann Arbor, Mich.

The general conduct of the journal is in the hands of the editor, **Walter F. Hunt,** Ann Arbor, Michigan, to whom all manuscripts should be submitted. To assist the editor the council of the Mineralogical Society has appointed **Lewis S. Ramsdell,** Ann Arbor, Michigan, assistant editor, and the following board of associate editors:

Michael Fleischer, U. S. Geological Survey, Washington, D. C.
Esper S. Larsen, Jr., U. S. Geological Survey, Washington, D. C.
Austin F. Rogers, 2412 Durant Ave., Berkeley, California.
M. N. Short, University of Arizona, Tucson, Arizona.
George Tunell, University of California at Los Angeles, California.

Contributors of leading articles are given without charge 100 reprints (without covers) of their article. If additional reprints are desired these can be purchased at the following rates:

Pages	*1–4*	*5–8*	*9–12*	*13–16*	*17–20*	*21–24*	*25–28*	*29–32*	*Covers*
Copies									
25	$3.50	$5.00	$ 8.00	$ 9.50	$11.00	$13.00	$15.00	$16.00	$4.90
50	3.80	5.55	8.80	10.40	12.10	14.20	16.40	17.50	5.50
75	4.10	6.10	9.60	11.30	13.20	15.40	17.80	19.00	6.10
100	4.00	6.65	10.40	12.20	14.30	16.60	19.20	20.50	6.70
Addl. C's	1.20	2.20	3.20	3.60	4.40	4.80	5.60	6.00	2.40

Cover Composition $1.55.

Sent to all members and fellows of the Mineralogical Society of America. Subscription price, $4.00 per year (single copies of normal issues, $1.00 plus postage).

Entered as second class matter at the post office at Menasha, Wis., under Act of March 3, 1879. Acceptance for mailing at the special rate of postage provided for in section 1103, Act of Oct. 3, 1917, paragraph 4 section 429 P. L. & R. authorized March 13, 1922.

Notice of change of address, orders, and remittances should be sent to Dr. Earl Ingerson, U. S. Geological Survey, Washington 25, D. C.

Printed by the George Banta Publishing Company, Menasha, Wisconsin
Printed in the United States of America

THE AMERICAN MINERALOGIST

JOURNAL OF THE MINERALOGICAL SOCIETY OF AMERICA

Vol. 37 JANUARY-FEBRUARY, 1952 Nos. 1 and 2

PRELIMINARY REPORT ON THE VARIATIONS IN DIFFERENTIAL THERMAL CURVES OF LOW-IRON DOLOMITES*

DONALD L. GRAF

TABLE OF CONTENTS

ABSTRACT

Soluble salts, present to the extent of as much as 0.3 weight per cent, principally potassium, sodium, calcium, and magnesium chlorides, are found to be a major cause of the variations in position and shape of the lower-temperature endothermic deflection in differential thermal analysis curves of a number of low-iron sedimentary dolomites. Finely ground dolomites from which soluble salts have been leached give DTA curves like those of salt-free specimens. Conversely, the curves of essentially salt-free specimens to which dilute salt solution has been added duplicate those of naturally occurring salt-rich dolomites.

The particle size to which specimens are ground before differential thermal analysis becomes increasingly important in more coarsely crystalline rocks and results in the shifting of deflection temperatures without marked change in the shape of the deflections. Dilution of samples with noncarbonate material lowers the deflection temperatures because of reduced CO_2 partial pressure in the furnace atmosphere.

The Na_2O and K_2O present in accessory-mineral illite and feldspar are not released from the lattices of these minerals at the temperatures of the lower dolomite endotherm.

Understanding of the significance of salt-dolomite interaction, and of area measurements under dolomite DTA curves, is believed to be contingent upon a more detailed knowledge of the mechanism of dolomite thermal decomposition.

The kind and amount of soluble salts in dolomites may be characteristic of different

* Published by permission of the Chief, Illinois State Geological Survey.

environments of deposition, but it does not appear to be possible to secure reliable salinity estimates from the extent of distortion of DTA curves of dolomite.

Introduction

Variations in differential thermal analysis curves of dolomite have been attributed by Faust (1949) largely to grain size and rate of heating. Sprague (1949) was unable to find evidence of cation disorder in a number of specimens, and suggested that a domain structure, destroyed by grinding during preparation of powder *x*-ray samples, might be responsible for the unusually large separation of the two endothermic deflections for "Ohio dolomite." According to this hypothesis, the grinding of DTA samples, to a coarser size than *x*-ray samples, would presumably not affect the domains. Murray (1950) noted that the curve for "Ohio dolomite" could be duplicated by soaking "non-Ohio dolomite" in a one-percent solution of sodium chloride overnight, but his DTA curves have not yet been published. A number of workers (Budnikov and Bobrovnik, 1938; Berg, 1943; Schwob, 1950) have described the effect of small amounts of alkali- and alkaline-earth salts upon thermal decomposition of dolomite. The principal findings of Berg's paper are substantiated by the present study.

The present investigation has centered around DTA curves, but the report includes some related stratigraphic and chemical information. Table 1 lists the specimens examined, all of which are low in ferrous iron, as may be seen from Table 2. It was felt that ferrodolomites and ankerites, whose high ferrous iron content is known to modify the curve strongly, would introduce an undesired additional variable into a preliminary study. The Fe^{++} values in Table 2 represent the maximum possible Fe^{++} in these dolomites, for some of the ferrous iron will be shown later in the paper to be present in illite, and furthermore the determination of Fe^{++} by permanganate reduction gives high values if $S^{=}$, organic material, or any other reducing substance is present. There is no evidence that significant amounts of Fe^{++} are oxidized to Fe^{+++} during the determination (McVicker, 1951).

The R-series of Illinois sedimentary dolomites are Chicago-area Silurian types from the suite assembled by Willman (1943) for his study of high-purity dolomites of Illinois. The K-series specimens are part of a group of dolomites having different colors, textures, and fossil types, collected from the reef-core and near-reef-flank beds exposed in a quarry north of Kankakee, Illinois.

The writer wishes to express his appreciation to his Illinois Geological Survey colleagues, J. E. Lamar, W. F. Bradley, J. S. Machin, H. B. Willman, W. A. White, and E. C. Jonas, for stimulating discussion and

TABLE 1. SPECIMEN LOCATIONS AND DESCRIPTION

Specimen	Series	Formation	Member	Relation to reefs	Lithology
R-1926	Niagaran	Joliet	Markgraf	Non-reef	Dense, fine-grained, slightly argillaceous, slightly silty, no visible porosity (common type)
R-1927	Niagaran	Joliet	Markgraf	Non-reef	Like R-1926 but more nearly pure, slightly coarser grained, more porous (common type)
R-1928	Niagaran	Joliet	Romeo	Non-reef	Very fine-grained, widespread unit
R-1929	Alexandrian	Kankakee	—	Non-reef	Well-bedded, some greenish shale partings (not in this sample)
R-1930	Niagaran	Brandon Bridge	—	Non-reef	Contains reddish shale partings, reddish crinoid stems
R-1931	Niagaran	Chicago	—	Reef flank beds	Highly porous unit, Thornton reef
R-1932	Niagaran	Chicago	—	Reef flank beds	Less porous than R-1931; Thornton reef
R-1933	Niagaran	Chicago	—	Non-reef (?) but (?) near reef	Rather pure, gray organic (?) banding
R-1934	Niagaran	Chicago	—	Flat non-reef beds just outside dipping reef flank beds	Rather pure, probably made up of reef detritus
R-1935	Niagaran	Elwood	—	Inter-reef	Intermixed silty dolomite and thin greenish clay laminae
K-1	Niagaran	Chicago	—	Fossil and texture varieties from loose blocks; reef core or reef flank near the core.	Very fine-grained, light yellow around vugs and darker elsewhere
K-2	Niagaran	Chicago	—		Fine-grained, porous, crumbling yellow rock
K-3	Niagaran	Chicago			Medium-grained porous red unit
K-5	Niagaran	Chicago			Mottled, dense medium gray and medium-grained light brown
K-6					Light yellow replacement and filling of Favosites
K-7	Niagaran	Chicago			Coarsely crystalline, non-porous, light brown
K-9	Niagaran	Chicago			Porous fine-grained gray rock, rock, light brown zones
Manteno, Illinois	Niagaran	Chicago		Near-reef-flank beds	Fine-grained non-porous brown rock
Carey, Ohio					Fine-grained vuggy cream-colored dolomite
Anna, Illinois					Light pink crystalline aggregates filling cavities in Ste. Genevieve limestone
Lee, Mass.					Fine-grained white dolomite marble (Wards)
Sierra das Eguas, Brazil					Large colorless, transparent cleavage fragment (Wards)
New York					Cavity lining of $\frac{1}{8}$″ white crystals in dense black limestone (Wards)

TABLE 2. CHEMICAL ANALYSES OF ILLINOIS DOLOMITES

1 Specimen	2 CaO	3 MgO	4 FeO	5 CO_2	6 SiO_2	7 TiO_2	8 Al_2O_3	9 Fe_2O_3	10 Na_2O	11 K_2O	12 H_2O	13 100 Total	14 Maximum possible weight % illite	15 Maximum possible K_2O in illite	16 Maximum possible Na_2O in illite
R-1926	27.72	18.76	0.36	42.45	8.54	0.16	1.50	0.16	0.12	0.73	0.10	100.60	5.85	.38	.02
R-1927	30.09	20.29	0.38	45.60	2.60	0.15	0.35	0.09	0.11	0.20	0.11	100.03	1.36	.09	—
R-1928	30.72	20.92	0.32	46.72	0.98	0.10	0.00	0.06	0.12	0.06	0.11	100.11	—	—	—
R-1929	29.57	20.16	0.29	44.89	3.71	0.11	0.69	0.17	0.10	0.34	0.09	100.12	2.69	.18	.01
R-1930	28.76	19.26	0.40	43.38	6.19	0.13	1.17	0.22	0.13	0.69	0.08	100.41	4.56	.30	.01
R-1931	30.57	21.54	0.07	47.12	0.06	0.00	0.25	0.02	0.11	0.01	0.19	99.94	0.98	.06	—
R-1932	30.91	21.60	0.08	47.38	0.12	0.03	0.19	0.01	0.20	0.03	0.23	100.78	0.74	.05	—
R-1933	30.80	21.56	0.13	46.96	0.36	0.03	0.26	0.12	0.09	0.05	0.08	100.44	1.02	.07	—
R-1934	30.76	21.32	0.18	47.03	0.68	0.02	0.25	0.09	0.15	0.07	0.10	100.65	0.98	.06	—
R-1935	25.86	17.89	0.25	39.16	13.58	0.13	1.85	0.17	0.10	0.95	0.08	100.02	7.21	.47	.02
K-1	30.53	21.60		46.81								(98.94)			
K-2	30.62	21.92		47.33								(99.87)			
K-3	30.63	21.60		47.11								(99.34)			
K-5	30.70	21.29		46.70								(98.69)			
K-6	30.60	21.50		46.82								(98.92)			
K-7	30.91	21.50		47.04								(99.45)			
K-9	30.65	21.26		46.50								(98.41)			
Pink	32.23	20.20		47.14								(99.57)			

Cupric nitrate staining tests (Rodgers, 1940; Hugi, 1945) reveal calcite intergrown with the Anna dolomite, as suggested by its MgO/CaO molar ratio of 0.870. Calcite was also found in small amount in several R- and K-series specimens examined, usually as a vug lining presumed to be secondary, but rarely intergrown with the dolomite as isolated grains that may be remnants of original $CaCO_3$ before dolomitization.

helpful criticism, and for reading part or all of the final manuscript. J. E. Melvin, State Geologist of Ohio, kindly furnished the specimen of Ohio glass-grade dolomite.

Differential Thermal Analyses Procedure

The equipment used for differential thermal analyses has been described (Grim and Rowland, 1942). The procedure for preparing samples used in the present study involves grinding the entire sample to minus 325-mesh in a mullite mortar, to minimize as much as possible the effect upon the curves of grain-size in coarsely crystalline rocks. In this way, too, the final portion of the sample used in the analysis is representative of the original rock, which might not be true of a specific size fraction. The dolomite powder is next mixed with an equal weight of α-Al_2O_3, prepared from $Al(OH)_3$ held at 1380° C. for 7 hours which dilutes the sample enough so that none of it is expelled from the sample block by rapid evolution of CO_2. Because of the dilution and the consequent lower partial pressure of CO_2 in the furnace atmosphere, temperatures at which the endothermic deflections occur are somewhat lower than those customarily reported for undiluted specimens. The details of the complex lower-temperature deflection are better resolved because of the dilution, and the higher-temperature deflection is unusually sharp because of the increased amplification used for diluted-sample curves.

The effect upon the DTA curves of particle-size obtained by grinding, and of dilution, is shown in Fig. 1 for a dolomite marble, a dense sedimentary dolomite (K-7), and a sedimentary dolomite (K-2) which readily breaks into a coarse sand. It is sufficient at this point to note from Fig. 1 that any dolomite DTA curve must be regarded as valid in detail only for a set of experimental conditions which have been arbitrarily selected; these curves are discussed at greater length below. The curves shown in figures 2, 3, 4, and 6 were run under conditions identical with those for curve 4 in Fig. 1.

Throughout the paper, DTA curves of salt-containing dolomites, diluted with α-Al_2O_3, are discussed, and the question of DTA deflection from reaction between the alkali- and alkaline-earth salts and the α-Al_2O_3 arises. DTA curves of mixtures of several of the pure salts and α-Al_2O_3 show no deflection below the melting points of the salts. Therefore there is apparently no solid-state reaction between salts and alumina which has a sufficiently rapid heat effect to be detected. The melting points of the chlorides and sulfates of K, Na, Mg, and Ca are at or above the temperature of maximum deviation from baseline of the sensitive lower-temperature dolomite deflection for diluted samples. Thus it

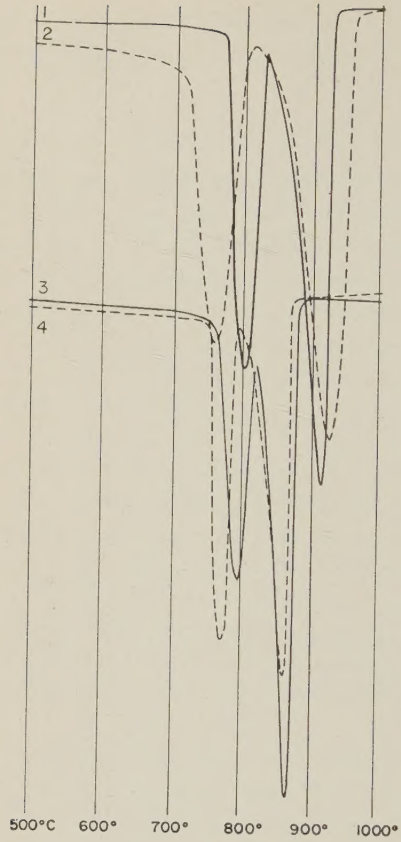

1A

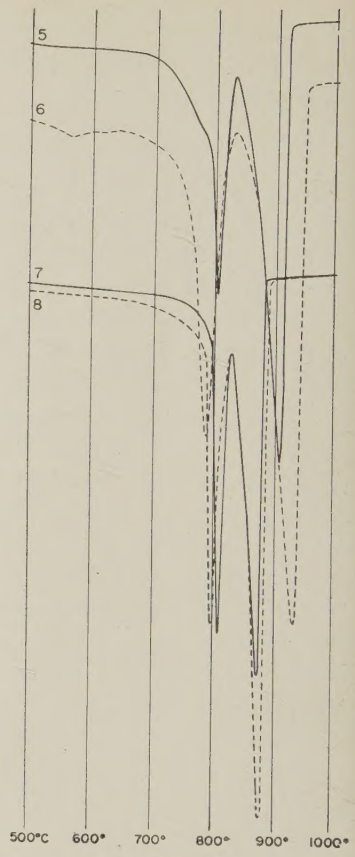

1B

FIGS. 1A, 1B, and 1C. DTA curves of dolomite samples of varying particle size and dilution. Curve 1 Brazilian dolomite—65 mesh, 0.345 gram, 300 ohms resistance in series. Curve 2. Brazilian dolomite—325 mesh, 0.345 gram, 300 ohms. . . . Curve 3. Brazilian dolomite—65 mesh, 0.14 gram+0.14 gram α-Al_2O_3, 200 ohms. . . . Curve 4. Brazilian dolomite—325 mesh, 0.14 gram+0.14 gram α-Al_2O_3, 200 ohms. . . . Curves 5–8. Specimen K-2. Curves 9–12. Specimen K-7.

seems unlikely that a chloride or sulfate melt has an opportunity to attack the α-Al_2O_3 before completion of the deflection, although the possibility of local melting of salt mixtures should be considered further. The validity of the diluted-sample curves is further indicated by the fact that the order of undiluted-sample curves arranged in a progression toward increasing "abnormality," a term that will be defined below, duplicates that of the diluted samples, even though the general shape of the lower-temperature endothermic deflection in the undiluted-sample curves is somewhat different.

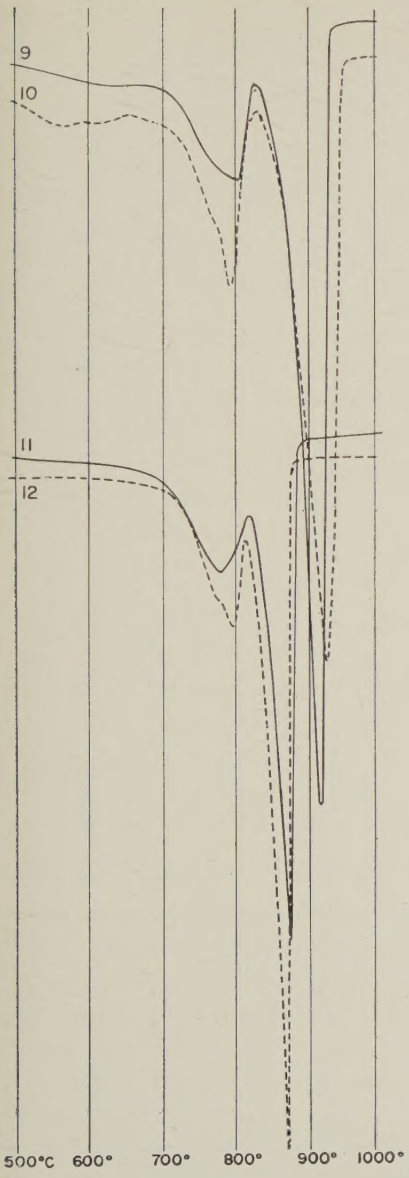

1C

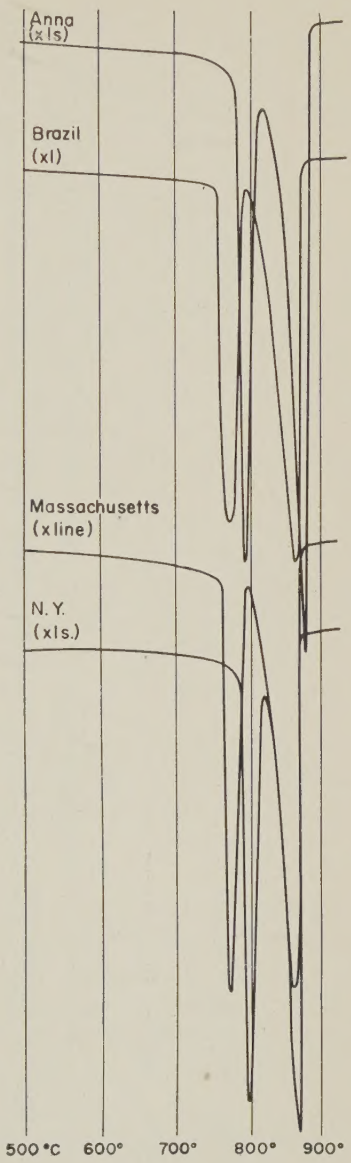

2A

Little importance has been attached to actual lengths of deflections, especially the sharp ones, because several different furnaces and thermocouple wire assemblies, yielding somewhat different sensitivities for the

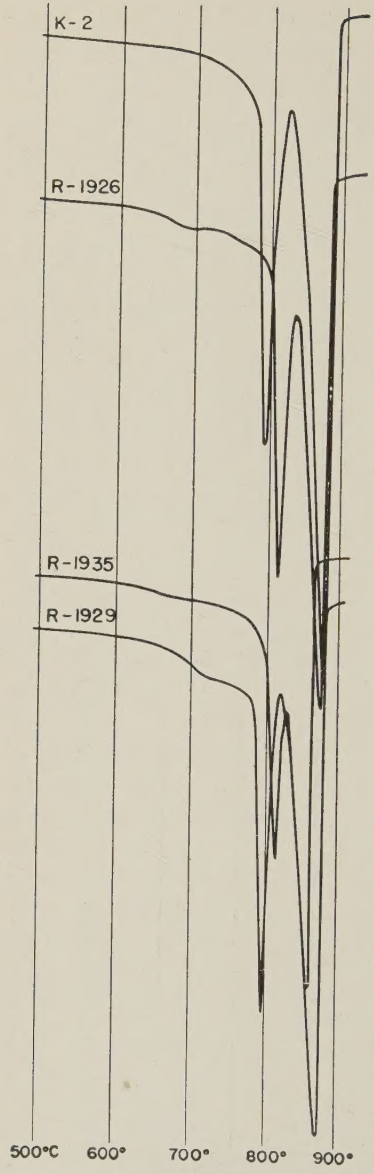

2B

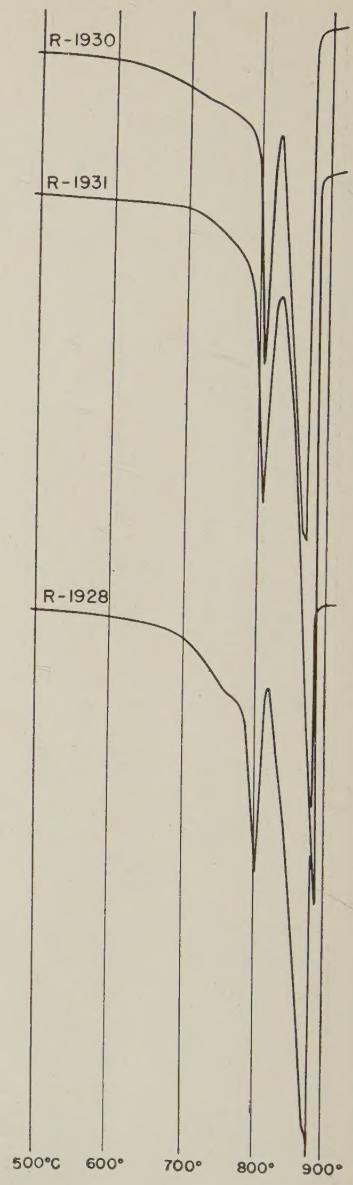

2C

FIGS. 2A, 2B, 2C, and 2D. DTA curves of dolomite samples, diluted with 50 wt. percent α-Al_2O_3.

same resistance in series, had to be used. The curves in Fig. 1, which should be directly comparable, are an exception. The shapes of deflections, ratios of deflection lengths within the same curve, and ratios of areas under the two deflections of a single curve are considered to be meaningful; limitations on their quantitative accuracy will be discussed.

Differential Thermal Analyses Curves

Typical curves for pure, low-iron dolomite are given by the specimens from Brazil, Massachusetts, New York, and Anna, Illinois, at the top of Fig. 2. The sharp break from the gently sloping low-temperature portion of the curve into the lower-temperature endothermic deflection is characteristic. Even among these specimens, however, there is a difference of 30° C. in the temperature of that deflection maximum, and some variation in the sharpness of both deflections.

The curves of a few sedimentary dolomites, such as K-2, are similar to those of the highly crystalline specimens, but for the most part the sedimentary dolomite curves have a smaller ratio of [lower-temperature deflection height]/[higher-temperature deflection height], a more gradual beginning of the lower-temperature deflection, and a lower-temperature deflection complicated by a shoulder (R-1928), a vague preliminary deflection (R-1929), or an actual separate deflection (R-1934). The curves are arranged approximately in order of increasing abnormality, using the criteria just enumerated.

All the curves from R-1927 to K-10 have higher-temperature endothermic deflections very similar in shape and length to that shown for R-1933, and the others have been omitted to save space.

The effect of soluble salts on DTA curves

In order to determine the composition and approximate amount of soluble salts in the specimens studied, two-hundred gram portions of Massachusetts dolomite, Ohio dolomite, a composite of the K-series Kankakee specimens, and Manteno dolomite were ground in a mullite mortar to a fine powder, placed in 400 ml. of distilled water, stirred intermittently for 8 hours, and filtered through Whatman #42 filter paper.

The leachate analyses are given in Table 3, both in weight per cent and in milliequivalents per 200 gram sample. The Massachusetts dolomite contains a much smaller amount of soluble salts than the sedimentary dolomites. The chloride content is from 6 to 30 times that of sulfate; inasmuch as DTA curves of dolomites artificially enriched with several per cent of various sulfates are not distorted, the sulfate content of the leachate analyses is not regarded as significant to the present discussion.

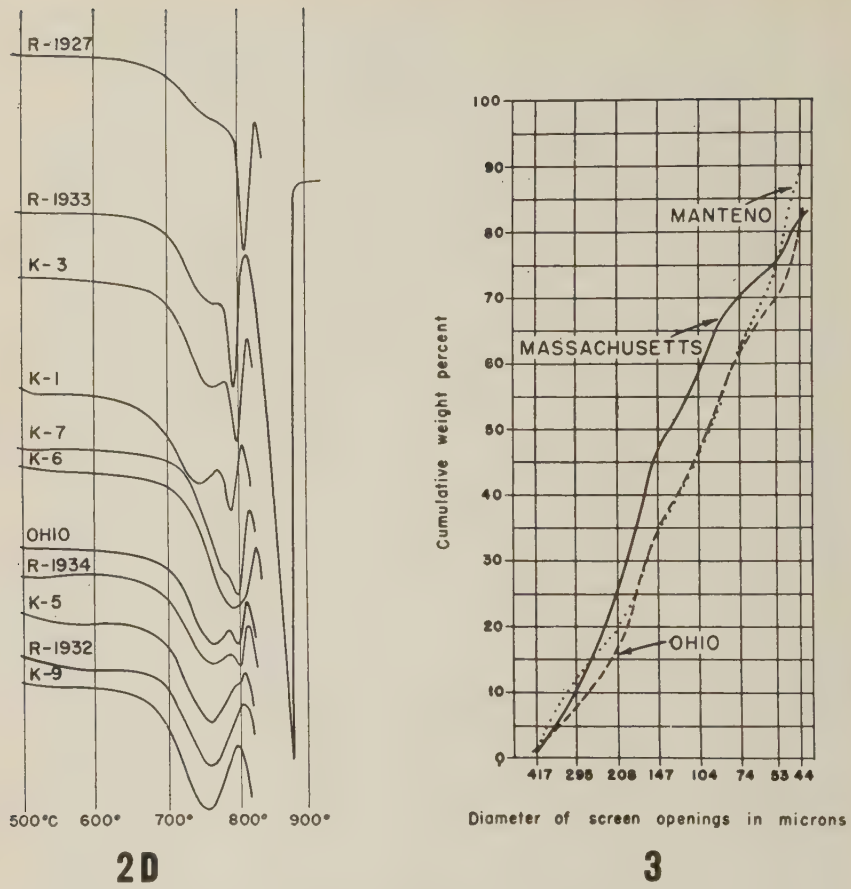

FIG. 3. The particle size distribution of several dolomite powders used in leachate experiments.

The amount of Na_2O is from 2 to 9 times that of K_2O, the reverse of the ratio in the total analyses given in Table 2.

As the soda and potash in the leachates satisfy a little less than one-third of the chloride and sulfate, alkaline-earth chlorides must be present in the specimens. At least part of the MgO and CaO left (column 5 of Table 3) after these calculations results from the solution of dolomite, but no attempt has been made to give the contribution from this source, both because of uncertainty in published values of dolomite solubility and because the dolomite in these experiments was almost certainly not in the water long enough to give an equilibrium solubility. Iron chloride, which might result from the oxidation of small amounts of pyrite, was

TABLE 3. LEACHATE ANALYSES

Specimen	Weight % of original rock							Milliequivalents/original 200 gm. sample							Meq. ($SO_4^=$ + Cl^-) unsatisfied by K_2O + Na_2O	Meq. (CaO + MgO) remaining after satisfying $SO_4^=$ and Cl^-
	CaO	MgO	K_2O	Na_2O	$SO_4^=$	Cl^-	Total	CaO	MgO	K_2O	Na_2O	$SO_4^=$	Cl^-	Total		
Massachusetts[1]	.003	.013	0.0005	.0007	.001	.000	0.0182	0.11	1.30	0.02	0.05	0.04	0.00	1.52	−0.03	1.41
Ohio[2]	.006	.010	.002	.011	.001	.030	0.060	0.43	1.00	0.08	0.71	0.04	1.67	3.93	0.92	0.20
Kankakee[3]	.011	.019	.004	.009	.0025	.055	0.1005	0.79	1.90	0.17	0.58	0.10	3.14	6.68	2.49	0.59
Manteno[4]	.007	.013	.002	.009	.0025	.031	0.0645	0.50	1.30	0.08	0.85	0.10	1.77	4.33	1.21	0.51

Analyst: L. D. McVicker.

[1] Crystalline dolomite, Lee, Massachusetts.

[2] High-purity dolomite, Carey, Ohio.

[3] Composite of Kankakee, Illinois, quarry specimens (K-series specimens in table 1).

[4] Niagaran dolomite, Manteno, Illinois.

not determined and could account for some of the variation in column 5 of Table 3. It is unlikely that any dolomite particles passed through the filter paper.

Not all the salts were leached from the dolomites, but a considerable fraction, believed to be representative, was recovered. The particle-size distribution of the fine powders used in the initial leachate experiments is given in Fig. 3. The differences among the three samples reflect variations in the ease with which the dolomites pulverized. The difference in particle-size distribution for the several powders presumably affected the quantity recovered.

The DTA curve of the unleached Ohio dolomite with the particle-size distribution of Fig. 3 is number 3 in Fig. 4. The next curve, which represents this material after it was leached, dried, and reground to pass 325 mesh (44 microns), is definitely more "normal" according to the criteria previously discussed. A 5-gram portion of the leached Ohio dolomite, reground to minus 325 mesh and then continuously agitated in 200 ml. of distilled water by means of a motor-driven stirrer for 8 hours, gave curve 5, which is typically "normal."

The Manteno dolomite, whose original DTA curve was very similar to that of the Ohio material, gave curve 6 after the two-stage washing described above. However, the Massachusetts dolomite, which as a "normal" curve, retained about the same ratio of deflection lengths after washing, although the deflections are somewhat less sharp.

The foregoing suggests that soluble salts are responsible for the DTA anomalies and that it should be possible to produce these anomalies in the curve of the Massachusetts dolomite by adding salts to it. Therefore a moderately concentrated distilled-water solution was prepared with HCl, H_2SO_4, MgO, CaO, KOH, and NaOH, in which the ratio $Cl^-:SO_4^=:Na^+:K^+:Mg^{++}:Ca^{++}$ in milliequivalents was 2.16:0.08:0.53:0.11:1.10:0.50, a close approximation to the average of the leachate analyses for the three sedimentary dolomites of Table 3. By diluting portions of this solution to different volumes, it was possible to add 0.3 ml. of solution to 0.14 gm. dolomite in each case and yet to use different salt concentrations. The ground dolomite samples were placed in the centers of watch glasses, and the solution added from a graduated pipette. After drying, the dolomite was briefly reground and the standard 0.14 gm. of α-Al_2O_3 diluent added.

DTA curves of the salt-treated samples, arranged according to the multiple of the original leachate concentration added, are given in Fig. 5, and closely duplicate the curves of the untreated dolomites. The temperature of the lower-temperature endothermic deflection in these artificial mixtures is somewhat higher than in most of the comparable natural curves for sedimentary dolomites, and the sharpness of that

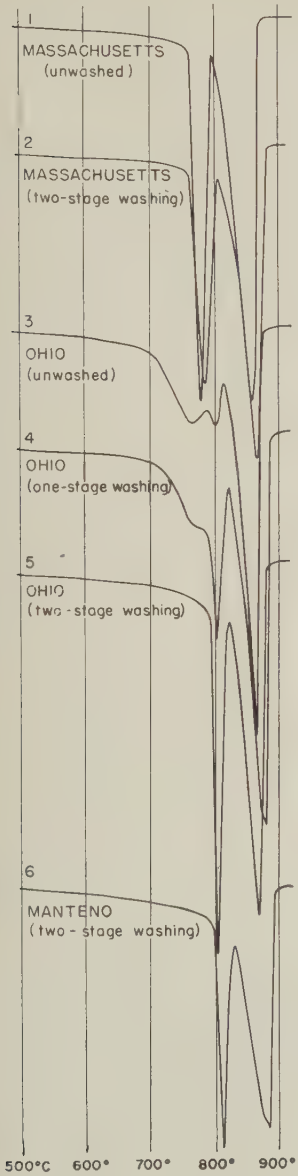

4

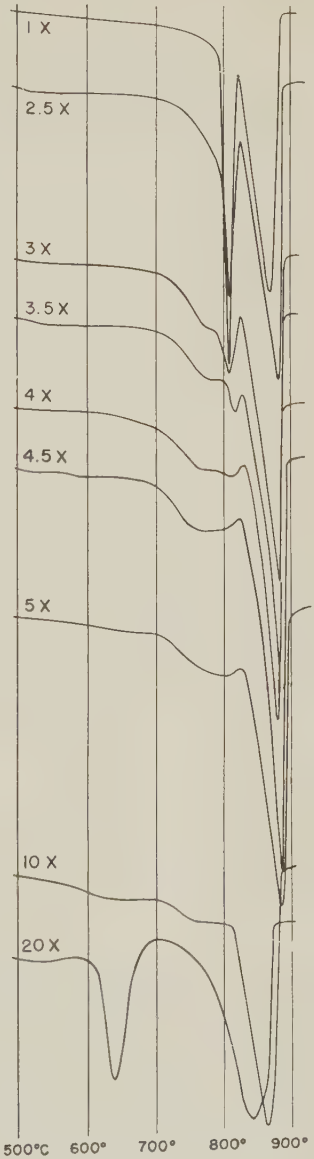

5

FIG. 4. The effect of distilled water leaching upon the DTA curves of dolomite.

FIG. 5. DTA curves of Massachusetts dolomite with added salts. The figures given are multiples of the average of salt content in leachates of three sedimentary dolomites (Table 3).

deflection in the "4.5X" and "5X" curves of Fig. 5 is not comparable, for example, with its equivalent in the K-9 and K-5 curves of Fig. 2. The curves of numerous other artificial mixtures investigated indicate clearly that small variations in the particle size of the added salts and in the ratios of the several ions of which they are composed would be enough to alter the shape of the lower-temperature deflection. The position of the deflection varies with particle size; thus the difference in position noted here may be due to the finer grain size of the sedimentary dolomites, compared to the Massachusetts dolomite marble.

It appears from a comparison of the "1X" curve of Fig. 5 with that of the original Massachusetts dolomite in Fig. 2 that the addition of a very small amount of the salts actually sharpens the lower-temperature deflection. Conversely, the Massachusetts dolomite curve in Fig. 4, after washing, has a more blunted lower-temperature deflection than before. It does not necessarily follow from the sharpness of the lower-temperature deflections in the curves of the Ohio and Manteno dolomites after two-stage washing (Fig. 4) that these specimens still contain a small amount of salts; although this is probably true. The difference in grain size between these specimens and the Massachusetts dolomite is an additional variable.

The leachate analysis figures, which are much too low, give 0.060, 0.101, and 0.064 wt. per cent total soluble salts for the three sedimentary dolomites. The curves of artificial salt-dolomite mixtures indicate that concentrations ranging from 2 to 5 times that of the average leachate duplicate the range of curves for the natural salt-containing dolomites. These figures are slightly high because of a small amount of salt film which clings to the watch glass after preparation of the salt-dolomite mixtures and cannot be removed. Accordingly, the maximum amount of soluble salts present in the specimens examined is estimated to be 0.3 wt. per cent.

Detailed discussion of possible mechanisms of salt-dolomite interaction is not included in this preliminary report. It seems desirable, however, to mention the necessity of giving serious consideration to solid-state reaction for which conditions are ideal because: (1) at the temperature of the lower-temperature decomposition, the alkali salts are beginning to show measurable vapor pressures, indicating strong thermal agitation of their component ions, and (2) the magnesium carbonate in dolomite is unstable above about 600°, if appropriate bonds in the dolomite lattice can be weakened enough to permit its segregation.

The effect of particle size

With information regarding the role of soluble salts in dolomite thermal decomposition in mind, the effect of the particle size of the samples

may be better understood. Its effect is to shift the position of the deflection with only a moderate change in deflection shape. This is shown by curves 1–4 of Fig. 1, for an essentially salt-free Brazilian dolomite which is a single crystal, at least in the macroscopic sense. In contrast, the effect of water-soluble salts in increasing amounts is to distort the lower-temperature deflection severely before there is any change in temperature. Curves 9–12, for a salt-rich Kankakee dolomite whose average grain size is only slightly greater than the minus 4-micron particle-size obtained by grinding, illustrate this phenomenon. The amount of salts needed to shift the temperature of the deflection noticeably, as determined from synthetic mixtures ("20X" curve, Fig. 5), has not been encountered in the natural specimens examined, but obviously exists in dolomites from evaporite sequences, for example.

The increase in separation of the two dolomite endothermic deflections when particle size is decreased (Curves 1 and 2, 3 and 4, of Fig. 1) is the result of a lowered temperature for the first deflection. The lowering is generally attributed to the fact that there is a smaller temperature differential between the surface and the center for smaller particles than for large ones, and consequently a lower furnace temperature is needed to raise the center of the particle to a temperature at which dissociation of the center area will take place. A contributing factor is the thickness of the layer of already dissociated material through which the CO_2 has to pass. Smyth and Adams (1923) noted an initial dissociation for calcite, followed by a decrease in heat absorption, after which dissociation increased rapidly. They believed that CO_2 pressure within the crystals had to build up sufficiently to break through the initially formed CaO coating before dissociation could continue. Zawadski and Bretsznajder (1938) note that in the thermal decomposition of coarsely powdered calcite the velocity of the reaction falls almost to zero "at a certain distance from equilibrium."

The sharpness of the lower-temperature deflection is affected by the rapidity with which CO_2 can escape from the sample well, and in turn from the furnace, as well as from within the particle. This is equivalent, of course, to saying that the partial pressure of CO_2 in the atmosphere between the particles is critical in determining how rapidly the dissociation will be completed. Thus, the 0.345 gram sample of minus-325 mesh material used for curve 2 of Fig. 1 had to be packed much more tightly to fit into the sample well than the same weight of minus-65 mesh material for curve 1, and the lower-temperature deflection is accordingly sharper in curve 1 than in curve 2. When the samples are diluted with α-Al_2O_3 (curves 3 and 4), the quantity of CO_2 which must escape from the sample well is decreased enough so that the partial pressure of CO_2 in the atmosphere around the sample does not approach the

magnitude of that within the particles. Consequently, particle size becomes the critical factor in determining deflection sharpness, and the minus-325 mesh material of curve 4 gives the sharper low-temperature deflection.

The next logical step in this line of investigation is experimentation with gas atmospheres directed through the sample, either to sweep CO_2 away as fast as it is formed, or to maintain the sample in an atmosphere of constant partial CO_2 pressure. Stone (1951) has carried out a similar series of experiments for kaolin, in which the partial pressure of water vapor was controlled.

Differences in the rate of particle-size growth of MgO undoubtedly have some effect upon the slope of the right side of the lower-temperature deflection, but this phenomenon can hardly be independent of the rate at which CO_2 escapes. No simple relation is evident in Fig. 1 between slope of the deflection and either particle size or the temperature of the deflection.

There is some variation in the closeness with which the curve approaches the baseline between the two deflections. The most striking difference can be seen by comparing curves 3 and 4 of Fig. 1. The coarse particle size of the curve 3 sample has brought the lower-temperature deflection to about the upper limit of the range in which it occurs in air at one atmosphere pressure. The higher-temperature deflection is at about the lower limit of the observed range for $CaCO_3$ decomposition because: (1) the $CaCO_3$ resulting from the dolomite lattice breakdown is extremely fine grained, and (2) dilution of the sample with Al_2O_3 makes it easy for CO_2 to escape from the sample well. Consequently the lower-temperature deflection partially overlaps the upper one in curve 3.

In this connection it is of interest to note that the doubling of the tip of the high-temperature deflection, as in the curve for specimen R-1929 (Fig. 1), and the shoulder at a similar position in the curve for R-1928 (Fig. 1), can very likely be attributed to a small amount of calcite which occurs in some of the dolomites (see Table 2). This calcite is more coarsely crystalline than that resulting from dolomite dissociation, and consequently should dissociate at a slightly higher temperature.

It is not clear from these curves to what extent finer grinding of the salt-containing dolomites alters the area in contact between salt and dolomite and thus affects the intensity of the salt-dolomite interaction. The gentle endothermic deflections at about 600° C. in curves 6 and 10, not present in curve 4, Fig. 1, may represent accelerated low-temperature decomposition at local points of high salt concentration, or decomposition of a fine fraction created by grinding.

The importance of lattice domains of the order of 0.1 to 0.01 micron diameter as the controlling factor in the rate of diffusion of CO_2 from

the lattice has been suggested for magnesite (Kahler, 1947; Cremer, 1949). Determination of the variation, from one dolomite sample to another, in the size and regularity of these units would be desirable, for these domains are not of constant size and disorientation for a given mineral species and are not necessarily related to the macroscopic particle size and orientation in the rock (see, for example, Ewald and Renninger, 1934). It is also known that grinding of ideal crystals or non-ideally imperfect crystals produces or increases domain structure in a surface layer so that the manner in which these dolomite samples have been prepared for thermal analysis may be important in determining the initial rates of nucleation of MgO and diffusion of CO_2.

Areas under curves

Berg (1943) states that the ratio of areas under the lower- and higher-temperature deflections changes from about 1.65 to about 1.25 if NaCl is added to depress the temperature of the lower-temperature deflection. It is not clear how much NaCl was added and how much the temperature was lowered. In accordance with his view that there is a preliminary dissociation of dolomite into $CaCO_3$ and $MgCO_3$, Berg cites the change of heat of dissociation of $MgCO_3$ with temperature to explain the differences in ratios.

The amount of soluble salts present in the Niagaran specimens is sufficient only to blunt the lower-temperature deflection, not to lower its temperature appreciably. The principal practical use of the area ratios—to determine the relative amounts of calcite and dolomite in dolomitic limestone—would thus not be affected by changes of carbonate heat of dissociation for specimens of this type. Likewise, the fact that soluble salts modify the shape of the lower-temperature deflection should not affect the heat of dissociation, for these salts are present in such small amounts that their action must be viewed as a catalytic or surface-active one rather than a true chemical reaction. To the extent that deflections become broader and shallower, errors in drawing the baseline have a greater percentage effect on the accuracy of area measurement. Beyond a certain point the sensitivity of the equipment to gentle prolonged heat drops off. There is probably some error because of differences in recrystallization. Experience thus far suggests that the combined effect of these errors is not great enough to mar the usefulness of area ratios as a routine semi-quantitative procedure. Berg (1945) obtained calcite and dolomite percentages from area measurements which agreed within two per cent with those from chemical analyses, even though the baseline for his area measurements is not completely defensible on theoretical grounds.

The accuracy of measurement and thoroughness of interpretation re-

quired for meaningful comparisons of area ratios for various pure dolomites and slightly salty dolomites is believed to be considerably greater than for estimating calcite/dolomite ratios. Measurement of areas for the curves in this paper has accordingly been deferred until a better understanding of certain fundamentals has been obtained:

(1) The precise mechanism of dolomite thermal decomposition has not been determined satisfactorily. Berg's concept of preliminary dissociation into $CaCO_3$ and $MgCO_3$ must compete with the idea of high-temperature carbonate solid solutions, and that of a preliminary dissociation into oxides followed by a recombination, $CaO+CO_2 \rightarrow CaCO_3$, as well as more specific hypotheses of ion migration and oxide nucleus formation within the disintegrating dolomite lattice (Hall, Stein, and Louw, 1951; Wilsdorf and Hall, 1951). Until this mechanism is understood in detail, the effect of specific cations and anions upon it, and perhaps indirectly upon the areas under curves, can hardly be appreciated.

(2) There seems at present to be no means of estimating from DTA curves the exothermic effect resulting from particle-size growth of newly formed MgO and CaO which is superimposed, respectively, upon the latter portions of the lower- and upper-temperature endothermic deflections. Bradley and Grim (1951) have recently discussed this problem of how energy changes resulting from the gradual formation of new phases are recorded in DTA curves. The recrystallization of CaO has been shown by Noda (1939, 1940) to be accelerated by the presence of salts like those found in sedimentary dolomites. The area ratio may thus be affected by the presence of these salts if MgO recrystallization is affected more than that of CaO, or vice versa, or if the supply of salts has been partly volatilized before the $CaCO_3$ dissociates.

(3) There is some uncertainty as to what areas under the curve should be measured, and what they mean. The curve for many specimens does not return to baseline between the two deflections, indicating that the two reactions overlap. The question may be raised whether a perpendicular from this point to the baseline, for example, gives two meaningful areas for measurement. A long sliver of area at lower temperatures results, at least in large part, from gradual CO_2 loss, because the partial pressure of CO_2 in the dolomite is greater than that in the atmosphere, at these temperatures. The sliver should, therefore, be measured, even though slight differences in the position of a baseline projected from below 400° C. unfortunately result in very considerable differences in the sliver area.

(4) There are questions of the behavior of equipment, and its effect upon some of the details of the DTA curves, which this paper does not

attempt to answer. The response of a moving-coil, ribbon-suspension type of galvanometer like that used in this study is not perfectly linear for the outer portions of the long endothermic dolomite deflections and in the setup used this instrument is not in a perfect critically damped condition when the various resistances are put in series with it, even though another resistance used in parallel minimizes deviation from critical damping. Likewise, the use of a nickel block of high heat capacity makes it necessary to be very careful in positioning all thermocouples exactly at the centers of the alumina-filled wells, if the baseline in the lower portion of the curves is to be straight enough for projection. It is generally believed that these instrumental errors can be avoided by experienced workers, but only detailed testing of individual setups will prove the point.

A further evaluation of instrumental performance is relevant to an explanation of the variation in baseline position of dolomitic DTA curves after complete dissociation (Fig. 6). Differences in heat of solution of MgO samples formed by calcining $MgCO_3$ were related to the particle size and lattice perfection of the oxide by Kahler (1947) and Treffner (1950). By analogy, it is possible that the variation in baseline position of the dolomite curves results from differences in heat diffusivity and specific heat related to the size and perfection of the CaO and MgO lattice blocks present.

Suggested Procedures for Dolomite

The specific procedure followed in making DTA curves of dolomite can be varied in accordance with the main objective of the study. As the design of the equipment currently in use in most laboratories is still being perfected, it is well to realize that the outlook presented here may soon require amplification and revision.

Measurement of areas under curves, in order to estimate calcite/dolomite ratios, requires a straight baseline and sharply-defined deflections as large in area as possible. The use of a rather large resistance in series to minimize baseline variation, plus undiluted samples to give larger areas under the curves, plus a CO_2 atmosphere (Rowland and Lewis, 1951) to sharpen the beginning of the lower-temperature deflection, plus a capping layer of α-Al_2O_3 to prevent ejection of part of the sample from the well by rapid CO_2 evolution, would seem to be called for.

On the other hand, it has been shown that dilution of the sample is useful in resolving details of the lower-temperature deflection in samples containing soluble salts, because of the decreased partial pressure of CO_2. Studies of the relation between deflection shapes, areas under deflections, temperature of CO_2 evolution, and amount of specific salts added

could probably be carried out best on curves of diluted samples.

Berg (1943) noted that there were still differences in dolomite DTA curves after soluble salts had been leached out, and tentatively attributed them to water-insoluble salts that affected the dolomite dissociation, or to "admixtures of calcite and magnesite in solid solution."

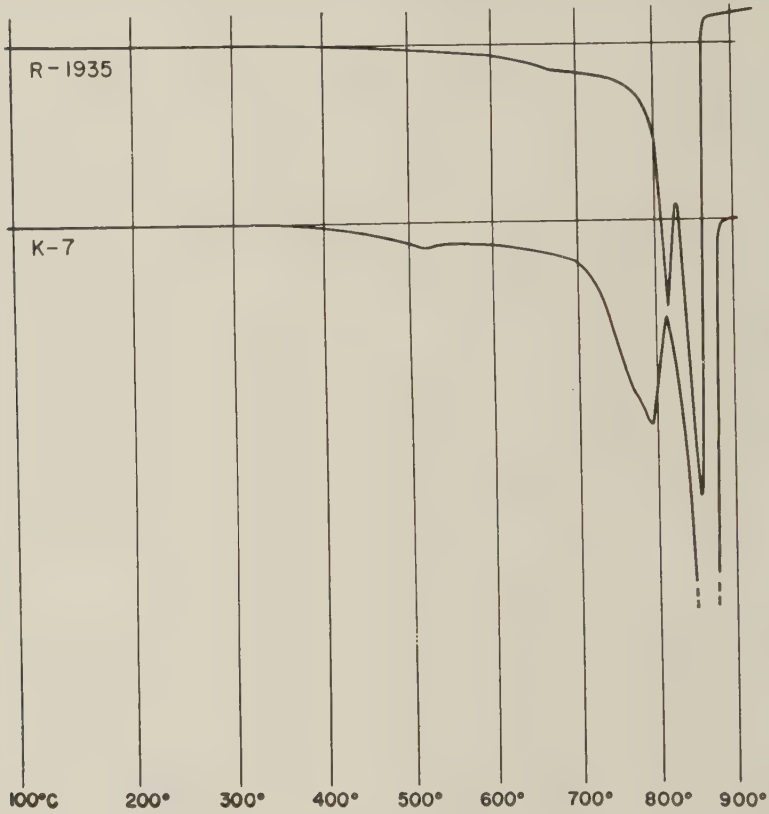

Fig. 6. Variation in baseline position after dolomite decomposition.

If further studies are to be undertaken of the effect of particle size, isomorphous substitution as in ferrodolomites and ankerites, and possible lattice disorder, the soluble salts present should first be removed as completely as possible, as Berg suggested, because their effect upon the curves is comparable to that of any of the other factors.

Mineralogical Distribution of Cations in the Sedimentary Dolomites

It is desirable to know accurately the mineralogical distribution in the sedimentary dolomites of K, Na, Mg, and Ca which are not present

as soluble salts, to be certain that there are no difficultly soluble accessory minerals which affect the dolomite deflections. The compilation of analyses of carbonates by Ford (1917), even though not accompanied by *x*-ray data, indicates that departures from a 1:1 molar Mg:Ca ratio occur in some iron-free single crystals of dolomite. It is impossible to determine the actual Mg/Ca ratio in the Illinois sedimentary dolomite minerals accurately enough to allot, for example, a small amount of excess Ca to clay minerals, feldspars, and anhydrite or gypsum. A number of comments can be made, however, about the distribution of K and Na.

A comparison of the R-series curves in Fig. 2 with the analyses of Table 2 shows that there is no correlation between increasing abnormality of the curves and total percentage of K_2O, Na_2O, or (K_2O+Na_2O). Much of the alkali may be presumed to be combined in insoluble accessory minerals, from which it is not released at temperatures up to that of the lower-temperature dolomite endotherm.

Muscovite, illite, and the feldspars are possible sources of alkalis. No muscovite could be found in an immersion study of the coarser fraction of the HCl-insoluble residue of a composite of the K-series specimens, but potash feldspar and Na-rich plagioclase together made up perhaps 15 or 20 per cent of the coarser residue. It was not possible to secure accurate determinations of the alkali content of these small amounts of feldspar, for the individual K-series specimens were too small to permit chemical analyses of the low percentages of insoluble residue in each of them.

The less-than-1 micron fraction of the insoluble material from a 200-gram composite of the K-series specimens was obtained, using 1 N acetic acid, and Na polyphosphate as a deflocculating agent. The *x*-ray powder diffraction pattern of this material gives a basal spacing of 10.0 Å, which does not expand on treatment with glycol. The presence of an illite-group clay mineral is thus confirmed, according to the agreement reached at the International Soils Science Congress, Amsterdam, 1950, that illite should be used as a general, nonspecific term for both heptaphyllite and octaphyllite mica-clay minerals which show no significant swelling characteristics and which give a first order basal reflection of about 10 Å which is unaffected by mild chemical or thermal treatments. This determination is in agreement with the finding of Grim, Lamar, and Bradley (1937) that illite is abundant in Niagaran limestones from Illinois, some of which contain considerable kaolinite as well.

It is possible to estimate the maximum amount of alkalis which could be contained in the accessory mineral illite of these dolomites. The average of a number of illite analyses assembled by Grim and Bradley (1949) gives 6.5 wt. per cent K_2O, 0.3 Na_2O, and 25.6 Al_2O_3 for a "typical" illite from well-indurated sedimentary beds. These figures are not fun-

damentally different from the average of the percentages given for illite with associated chlorite, or for illite with some mixed layers of montmorillonite. This average illite composition, obtained chiefly from analyses of illites from shales, probably applies as well to illites from dolomites, for laboratory experiments indicate (White, 1951) that K is able to remain in only 3 to 5 per cent of the exchange positions in the presence of a considerable excess of Ca, a situation which obtains in most natural environments. In an extreme situation such as a bed containing alkali halide brine, of course, the amount of alkali ions in base-exchange position could increase sharply and the average figures cited would not be valid. Degraded illites (Grim, Dietz, and Bradley, 1949) low in alkali are formed during weathering, but regain most or all of the alkali loss when carried into a marine environment; therefore the illites in the Niagaran samples should not be degraded.

Column 15 of Table 2 indicates the amount of illite, expressed as weight per cent of the dolomite rock, that would exist if all the alumina in the analysis were converted to a "typical" illite containing 25.6 weight per cent alumina. Column 16 gives the maximum amount of K_2O, expressed as weight per cent of the dolomite rock, which could be tied up in the illite. For specimens high in K_2O, only about half can be accounted for in this manner. Figs. 7 and 8, based upon the chemical analyses of Table 2, indicate that the alkali/alumina ratios for the dolomite specimens lie between that for illite and that for orthoclase.

The predominance of Na over K in the soluble salts is suggested by comparison of Fig. 8, in which the band of $(Na_2O+K_2O)/Al_2O_3$ plots intersects the positive side of the horizontal axis, indicating that some alkali oxide is not combined with Al_2O_3, with Fig. 7, in which the band of K_2O/Al_2O_3 plots goes through the origin.

Dolomite-illite interaction

In order to determine whether any of the alkalis in base exchange position in illite are released to affect the lower-temperature dolomite deflection, a mixture of 85 wt. per cent Massachusetts dolomite marble and 15 wt. per cent $<2\mu$ Fithian illite was thoroughly ground together in a mullite mortar and mixed with an equal weight of α-Al_2O_3 diluent in accordance with the usual procedure. The Massachusetts rock is very low in alkalis (Table 2) and has a sharp lower-temperature deflection. The quantity of illite added is greater than that which could possibly be present in any of the dolomites examined. In the DTA curves of this mixture, the lower-temperature deflection is completely undistorted, and characteristic illite deflections are not developed at the instrumental sensitivity and dilution used. Nor did any recognizable illite deflections occur in the DTA curves of the natural specimens.

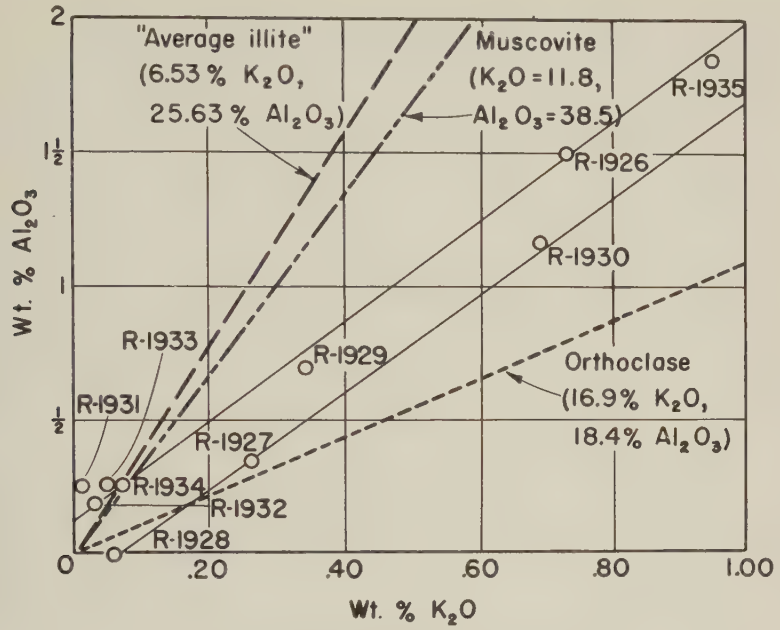

FIG. 7. K_2O-Al_2O_3 relations for R-series specimens

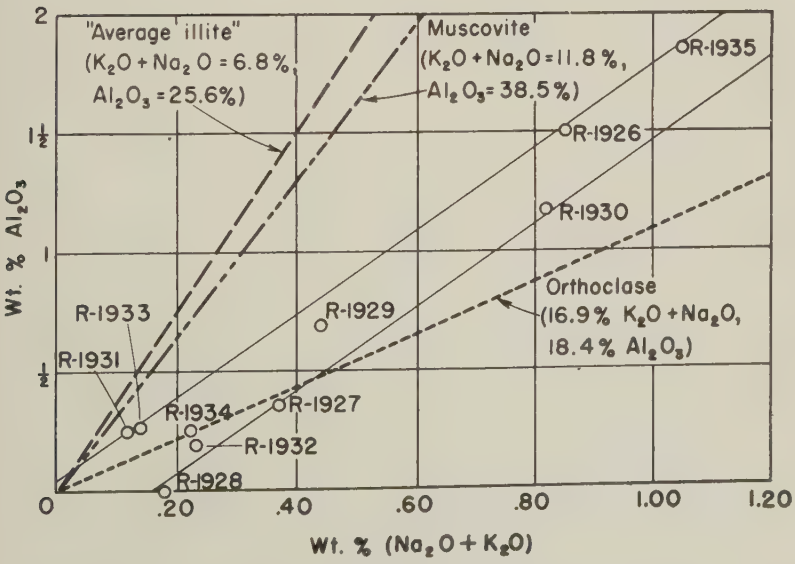

FIG. 8. (K_2O+Na_2O)-Al_2O_3 relations for R-series specimens.

Grim (1942) found that the degree of intimacy of mixing of layer lattice minerals, particularly certain poorly crystallized varieties, had a significant effect upon the DTA curves, and accordingly allowed mixtures to settle from a water suspension. Interaction between alkalis in illite, and in dolomite, whether expressed in terms of mobilities of ions at elevated temperatures or very low vapor pressures, should be related to the area in contact between the two compounds per unit weight. Although no structural relationship comparable to the interlayered clay minerals has ever been suggested for illite and dolomite, a certain doubt as to the validity of artificial dolomite-illite mixtures should remain until more is known of the physical relationship of these two minerals in natural dolomites. In the present case, this doubt is largely dispelled by the fact that illite-containing dolomites give undistorted curves after washing (Fig. 4), a procedure which is quite inadequate for the removal of base-exchange cations from the illite.

Another method of evaluating possible dolomite-illite interaction involves consideration of the detailed thermal behavior of illite. Grim and Bradley (1940) state that destruction of the "anhydrous modification" of illite is completed around 800 or 850° C., at which temperature spinel begins to form from the middle sheet of the illite lattice, while the alkalis and the silica from the outer sheets go to amorphous glass. An indication of the effect of temperature on the equilibrium existing between cations in base-exchange positions and those in fixed positions, below 850° C., is given by Hofmann's studies (Hofmann and Endell, 1939; Hofmann and Klemen, 1950) of the decrease in base-exchange capacity of montmorillonite on heating. The loss of 80 per cent of exchange capacity by Li-saturated montmorillonite after heating to 200° C. over a protracted period is attributed to the migration of Li ions from the surfaces to the interiors of the silicate sheets. Higher temperatures are required, in the order $Li,^{+}$ $H,^{+}$ $Ca,^{++}$ $Na,^{+}$ to achieve comparable effects for these larger ions, whose movement into the lattice is believed to be more difficult. K^{+}, of course, is even larger, but is not discussed by Hofmann. Wear and White (1951) found that illite, heated to 105° C. for 12 hours after its base-exchange positions had been saturated with K^{+}, fixed the least K^{+}, 2.4 milliequivalents, of the several clay minerals so treated. They attribute this to the fact that the large amount of K^{+} already present in the lattice almost balances the negative charge existing in the tetrahedral layers.

The differential thermal analysis of dolomite-illite mixtures in the present study does not correspond precisely to any of the experimental situations described in the preceding paragraph, for the base-exchange positions of the illite are assumed to be largely filled by Ca^{++} and Mg^{++}, and the times used are less and the temperatures greater than in the

other experiments. Nevertheless, the evidence seems to indicate that the base-exchange cations are held more and more tightly, whatever their final position in the lattice, with rising temperature and progressive dehydration, and that by the time the illite lattice breaks down to release these cations into a liquid alkali silicate phase, the sensitive lower-temperature dolomite reaction has already occurred.

Soluble-Salt Content as an Environmental Indicator

The sensitivity of the lower-temperature deflection to tiny amounts of salts suggests, on first thought, that examination of routine DTA analyses might furnish information about the salinity of the environments of deposition of carbonate rocks. Thus, the variability of DTA curves for the Niagaran specimens contrasts with the virtual identity of a series of slightly abnormal curves for specimens from a section through the Prosser member of the Ordovician Galena formation near Galena Junction, Ill. More of the Niagaran specimens from reef-core and near-reef-flank beds have highly abnormal curves than those from inter-reef and non-reef areas.

On further consideration, however, it becomes clear that there are several inherent limitations in the use of DTA analyses of dolomite in estimating salinity of depositional environments. These limitations, which are in addition to the usual difficulty involved in selecting a sampling method that integrates local variation, are: (1) Alkali- and alkaline-earth chlorides and alkali carbonates distort the curves, but sulfates do not, so that specimens having a high sulfate content will give misleading curves. Likewise, it is unlikely that the cations in a salt mixture will have a simple additive effect upon decomposition, regardless of whether they act as a melt or by solid-state reaction. (2) It seems likely that in many cases a portion of the soluble salt cations in the sea water trapped in carbonate sediment would be used in forming authigenic feldspar and illite, changing the relative proportions of the cations remaining in solution. (3) Because groundwater movement after lithification may redistribute soluble salts present as intergranular films, determinations of salt content of liquid inclusions within grains, where they exist, would be highly desirable. A crushing and leaching procedure which will preferentially remove intergranular salt films, so that only the liquid inclusion material remains to affect the DTA curves, is not apparent from this study, for it cannot be assumed that compact dolomites will break apart into their component grains before breaking across these grains.

References

Berg, L. G. (1943), Influence of salt admixtures upon dissociation of dolomite: *Comptes Rendus (Doklady) de l' Academie des Sciences de l' URSS*, **38**, no. 1, 24–27 (in English).

——— (1945), Area measurements in thermograms for quantitative estimations and the determination of heats of reaction: *Comptes Rendus (Doklady) de l' Academie des Sciences de l' URSS*, **49,** no. 9, 648–651, (in English).

Bradley, W. F., and Grim, R. E. (1951), High temperature thermal effects of clay and related minerals: *Am. Mineral.*, **36,** 182–201.

Budnikov, P. P., and Bobrovnik, D. P. (1938), The influence of admixtures on the decarbonation of dolomite: *J. Appl. Chem. (USSR)*, **11,** 1151–1154.

Ewald, P. P., and Renninger, M. (1934), The mosaic texture of rock salt: *Int. Conf. on Physics*, **2,** 57–61.

Faust, G. T. (1949), Dedolomitization, and its relation to a possible derivation of a magnesium-rich hydrothermal solution: *Am. Mineral.*, **34,** 789–823.

Ford, W. E. (1917), Studies in the calcite group: *Trans. Conn. Acad. Arts and Sciences*, **22,** 211–248.

Grim, R. E. (1947), Differential thermal curves of prepared mixtures of clay minerals: *Am. Mineral.*, **32,** nos. 9–10, 493–501.

Grim, R. E., and Bradley, W. F. (1940), Investigation of the effect of heat on the clay minerals illite and montmorillonite: *Jour. Am. Ceram. Soc.*, **23,** no. 8, 242–248.

——— (1949), The illite clay minerals, Manuscript on file at the Illinois Geological Survey.

Grim, R. E., Dietz, R. S., and Bradley, W. F. (1949), Clay mineral composition of some sediments from the Pacific Ocean off the California coast and the Gulf of California: *Geol. Soc. Am. Bull.*, **60,** 1785–1808.

Grim, R. E., Lamar, J. E., and Bradley, W. F. (1937), The clay minerals in Illinois limestones and dolomite: *Jour. Geol.*, **45,** no. 8, 829–843.

Grim, R. E., and Rowland, R. A. (1942), Differential thermal analysis of clay minerals and other hydrous materials: *Am. Mineral.*, **27,** no. 11, 746–761.

Haul, R. A. W., Stein, L. H., and Louw, J. D. (1951), $C^{13}O_2$ exchange between solid carbonates and gaseous carbon dioxide: *Nature*, **167,** no. 4241, 242.

Hofmann, U., and Endell, J. (1939), Die Abhängigkeit des Kationenaustausches und der Quellung bei Montmorillonit von der Vorerhitzung: *Zs. angew. Ch.*, **52,** 708.

Hofmann, U., and Klemen, R. (1950), Verlust der Austauschfähigkeit von Lithiumionen an Bentonit durch Erhitzung: *Zs. anorg. Ch.*, **262,** 95–99.

Hugi, Th. (1945), Gesteinsbildend wichtige Karbonate und deren Nachweis mittels Farbmethoden: *Schw. min. petr. Mitt.*, **25,** 114–140.

Kahler, F. (1947), Elektronenmikroscopische Untersuchung des Sintervorganges von Magnesiumoxyd: *Radex Rundschau*, no. 3, 50–55.

McVicker, L. D. (1951), Personal communication.

Murray, J. A. (1950)—See Avery, W. M., *Pit and Quarry*, November, **1950,** 91; *Rock Products*, November, **1950,** 76–81.

Noda, Tokiti (1939), Calcination of lime, XII. Effect of the addition of alkali chlorides, alkali fluorides, alkaline earth chlorides, and alkaline earth fluorides on the crystal growth of calcium oxide: *J. Soc. Chem. Ind. Japan*, **42,** Suppl. binding 265.

——— (1940), Calcination of lime, XV. The effect of addition of salts on the crystal growth of CaO: *J. Chem. Ind. Japan*, **43,** Suppl. binding 40.

Rodgers, J. (1940), Distinction between calcite and dolomite on polished surfaces: *Am. Jour. Sci.*, **238,** 788–798.

Rowland, R. A., and Lewis, D. R. (1951), Furnace atmosphere control in differential thermal analysis: *Am. Mineral.*, **36,** nos. 1–2, 80–91.

Schwob, Yvan (1950), Les carbonates rhomboedriques simples et complexes de calcium, magnesium, et fer, Publication Technique No. 22, *Centre d' Etudes et de Recherches de L' Industrie des Liants Hydrauliques*, Paris, 105 pp.

SMYTH, F. H., AND ADAMS, L. H. (1923), The system calcium oxide-carbon dioxide: *Jour. Am. Chem. Soc.*, **45,** 1167–1184.

SPRAGUE, R. S. (1949), A critical experimental study of the hydration and reactivity of oxides, Dissertation, University of Illinois.

STONE, R. L. (1951), Thermodynamics applied to differential thermal analysis: Presented at the American Ceramic Society meeting, Chicago, Illinois, April 24.

TREFFNER, W. (1950), Kalorimetrische Studien an aktiven Magnesiumoxyd aud naturlichem Magnesit: *Radex Rundschau*, No. 2, 125–131.

WEAR, J. I., AND WHITE, J. L. (1951), Potassium fixation in clay minerals as related to crystal structure: *Soil Science*, **71,** No. 1, 1–15.

WHITE, W. A. (1951), Personal communication.

WILLMAN, H. B. (1943), High-purity dolomite in Illinois: *Rept. of Investigations*, **90,** *Illinois Geological Survey*, 87 pp.

WILSDORF, H. G. F., AND HAUL, R. A. W. (1951), *X*-ray study of the thermal decomposition of dolomite: *Nature*, **167,** no. 4258, 946–947.

ZAWADSKI, J., AND BRETSNAJDER, S. (1938), Some remarks on the mechanism of reactions of the type: Solid=Solid+Gas: *Trans. Faraday Soc.*, **34,** pt. 2, 951–959.

Manuscript received July 13, 1951.

THE STRUCTURAL DISINTEGRATION OF SOME AMPHIBOLES*

MARK WITTELS,** *Massachusetts Institute of Technology, Cambridge, Mass.*

ABSTRACT

The structural disintegration characteristics of some selected species of amphiboles were investigated by thermal, *x*-ray, optical, and chemical methods. Except for some limited cases of fusion all of the reactions involving structural collapse occur in the solid state and are heat absorbing (endothermic). In the temperature range 900°–1125° C most species have heats of reaction of the order of 5 calories per gram.

Monoclinic amphiboles yield the following substances among the products of structural disintegration: monoclinic pyroxenes, cristobalite, hematite, magnetite, olivine, plagioclase feldspar, water, and glass. The magnetite and olivine minerals occur as disintegration products of hastingsite at 1145° C. Orthorhombic amphiboles collapse above 900° C. to form orthopyroxenes, cristobalite, water, and glass.

The amphiboles containing Al that proxies for Si in the double-chains have higher disintegration temperatures than the non-aluminous types. The heats of reaction at these higher temperatures are lower, however, than those for the pure silicon types.

The amphiboles that contain large amounts of Na and F undergo extensive fusion near the breakdown temperatures. Fluorine remains in the glass product of disintegration and is not driven off at temperatures up to 1125° C. due to its high electronegativity.

The oxidation of ferrous iron at temperatures bordering near structural collapse make calorimetric measurements of the disintegration process less accurate in those specimens bearing ferrous iron.

INTRODUCTION

Thermal studies of the amphiboles were initiated more than fifty years ago by Doelter and Hussak[1] when they determined that green hornblende broke down into magnetite plus augite, or olivine, at a high temperature. These observations were made without the benefit of a precise knowledge of the structure and composition[2,3] of the amphiboles which remained undetermined for many years. The dehydration experiments with tremolite[4] and magnesian anthophyllite[5] confirmed the previously established presence of 2 (OH,F) ions per mole formula. In these same experiments it was shown that the removal of hydroxyl groups

* An investigation as part of a Ph.D. thesis by the author.

** Now at the Oak Ridge National Laboratory, Oak Ridge, Tenn.

[1] Doelter, C., and Hussak, E., Ueber die Einwirkung geschmolzener Magmen auf verschiedene Mineralien: *Neues Jahr. für Min., Geol.*, und *Pal.*, Band **1**, 18–44 (1884).

[2] Warren, B. E., The crystal structure and chemical composition of the monoclinic amphiboles: *Zeit. für Krist.*, **72**, 493–517 (1930).

[3] Warren, B. E., and Modell, D. I., The structure of anthophyllite, $H_2Mg_7(SiO_3)_8$: *Zeit. für. Krist.*, **75**, 161–178 (1930).

[4] Posnjak, E., and Bowen, N. L., The role of water in tremolite: *Am. Jour. Sci.*, **22**, 203–214 (1931).

[5] Thilo, E., and Rogge, G., Chemische Untersuchungen von Silikaten, mitteil VIII: *Ber. der Deut. Chem. Gesell.*, **72**, 341 (1939).

in the form of water was closely associated with the disintegration of the crystal structure.

The investigation described here is a re-examination of some of the previous experiments by a quantitative method[6] of differential thermal analysis that permitted the heats of reaction for the structural disintegrations to be measured. In addition, *x*-ray, optical, and spectrochemical methods of analysis were employed as supplementary tools in the investigation.

The chemical analyses for the eight specimens tested are shown below.

Several differential thermal analyses of diverse members of the amphibole group indicated that the range of stability of these minerals lies between 600° and 1125° C., a region of high efficiency for the thermal equipment used in this investigation. No changes were observed below 600° C. and so only the thermographic records above that temperature are exhibited. A heating rate of 30° C. per minute with a furnace evacuated to a pressure of 1 mm. Hg was used to obtain the thermographic curves.

The structural disintegration of all the specimens analyzed occurred in the temperature range 925°–1125° C., and this reaction is designated by the peaks (y) in Figs. 1 and 2. Only the thermographic peaks so designated are concerned in this investigation. In all cases the transformation is a solid state reaction requiring heat absorption (endothermic). Other reactions, such as inversions[7] in the magnesian varieties, and oxidation of Fe^{++} in the ferrous varieties, are thermographically recorded at temperatures below the disintegration level.

Tremolite

Posnjak and Bowen[8] demonstrated the role of water in tremolite by static weight-loss experiments. At 900° C. the theoretical water content (2.22%) is driven off, and the following reaction takes place in the solid state:

$$\underset{\text{tremolite}}{Ca_2Mg_5Si_8O_{22}(OH)_2} + \Delta H = \underset{\text{diops.-clinoenst.}}{2CaSiO_3 \cdot 5MgSiO_3} + \underset{\text{cristobalite}}{SiO_2} + H_2O$$

A thermographic record of the removal of hydroxyl groups from tremolite (Fig. 1) gives a graphical representation of this dissociation reaction. The specimen from which the analysis was obtained was a portion of the

[6] Wittels, M., Some aspects of mineral calorimetry: *Am. Mineral.*, **36**, 760–767 (1951).

[7] Wittels, M., Structural transformations in amphiboles at elevated temperatures: *Am. Mineral.*, **36**, 851–858 (1951).

[8] Posnjak, E., and Bowen, N. L., *op. cit.*

Specimen	SiO_2	Al_2O_3	TiO_2	Fe_2O_3	MgO	FeO	MnO	Na_2O	CaO	K_2O	H_2O	F	Total
Tremolite[1]	58.59	0.10			24.78			0.12	13.95	0.10	2.31	—	99.75
Richterite[2]	57.74	0.37	tr	0.29	23.67	tr	2.40	3.14	9.01	0.64	2.39	0.37	99.86
Soda-Trem.[3] Glaucophane (A)	54.30	2.02	0.04	7.37	17.71	2.96	0.52	7.80	3.30	2.10	0.61	2.14	100.87
Soda-Trem.[3] Glaucophane (B)	52.28	4.34	0.57	4.32	18.14	5.30	0.26	5.56	6.74	2.18	0.15	n.d.	99.86
Anthophyllite[4] (A)	57.02	1.40	—	—	28.81	8.71	0.09	0.66	1.48	—	1.59	—	99.76
Anthophyllite[4] (B)	48.49	13.26	0.41	1.28	20.56	14.60	—	0.11	0.04	—	1.48	—	100.23
Hastingsite	43.60	11.33	2.09	4.02	12.41	9.88	0.19	1.38	12.03	1.34	1.63	—	99.95
Pargasite[3]	40.18	14.26	1.79	4.73	14.87	5.76	0.22	2.22	12.88	1.86	0.60	0.79	100.19

Note: Glaucophane (A), glaucophane (B), and pargasite are designated IH39, U-184e, and U-1993, respectively, in the paper by Larsen. Anthophyllite (A) and anthophyllite (B) are designated CC 200A and CC 121, respectively, in the paper by Rabbitt.

[1] Posnjak, E., and Bowen, N. L., *op. cit.*

[2] Sundius, N., The position of richterite in the amphibole group: *Geol. Förh.*, Band **67,** 266–270 (1945).

[3] Larsen, E. S., Alkalic rocks of Iron Hill, Gunnison County, Colorado: *U.S.G.S.P.P.* **197A** (1942).

[4] Rabbitt, J. C., A new study of the anthophyllite series: *Am. Mineral.*, **33,** 263–298 (1948).

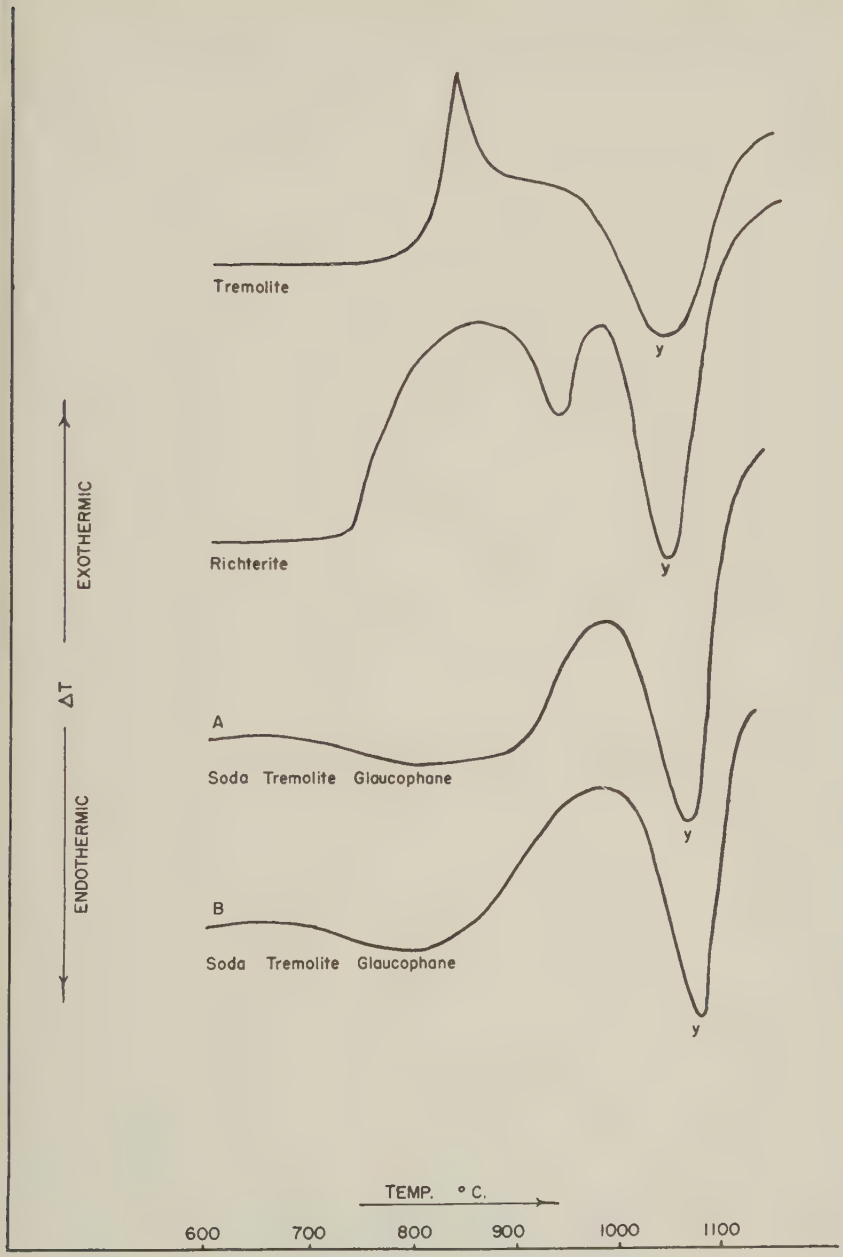

FIG. 1. Thermographic curves of amphiboles.

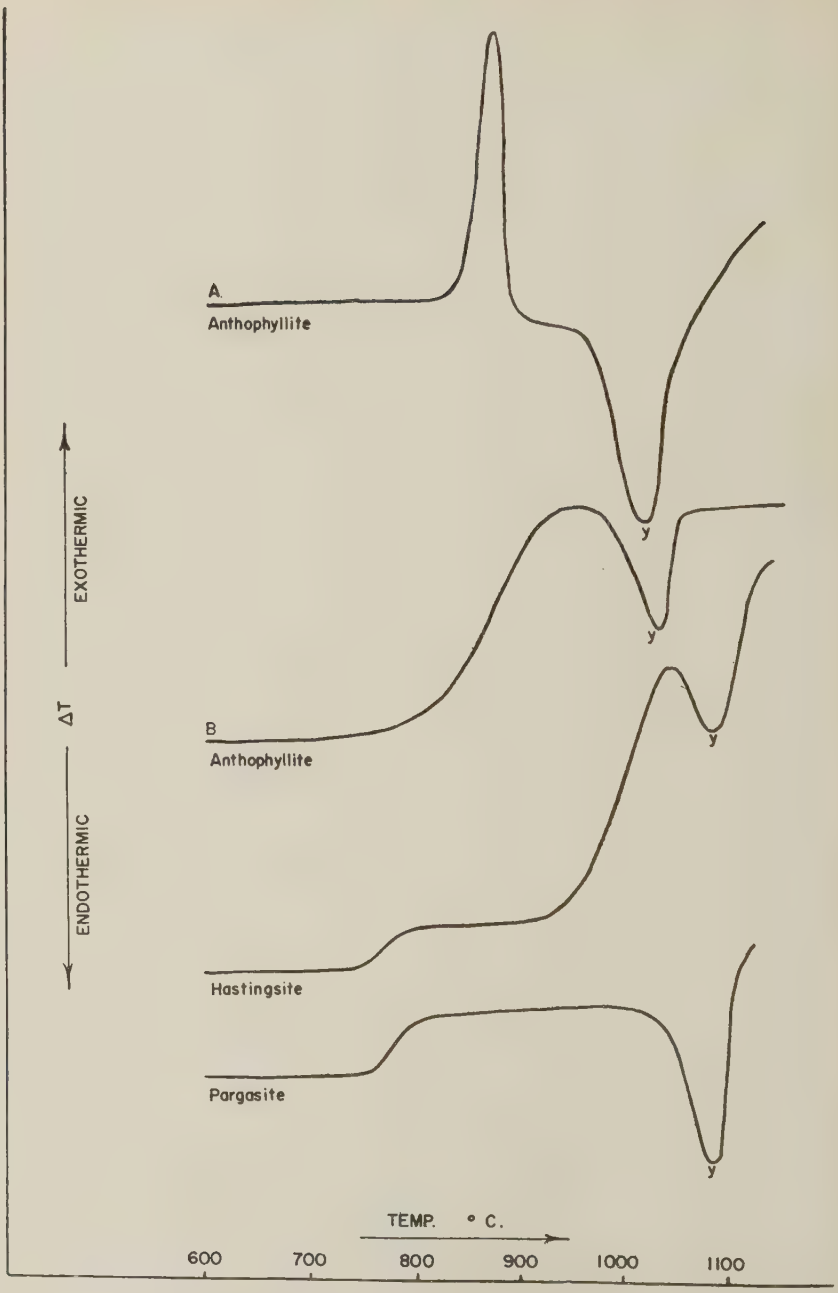

FIG. 2. Thermographic curves of amphiboles.

very pure material investigated by Posnjak and Bowen. The results are in complete accord with those described in the earlier investigation, where the reaction went only to partial completion after 24 hours at 900° C.

Specimens heated to 960° C. and immediately cooled showed no structural changes upon x-ray examination. This observation was a reflection of the dynamic nature of differential thermal analysis in that there is a noticeable reaction-temperature lag which static tests do not give. Where the reaction is not instantaneous and when high heating rates (30° C. per minute) are employed, this relation is all the more evident.

At 1125° C. the disintegration reaction is completed. It was noted that an original 200 mesh amphibole powder transformed into reaction products which were still part of the original powder. This material did not melt, fuse, or cohere. Each grain became a pseudomorph of pyroxene plus cristobalite after amphibole in a simple reaction of solid state disintegration. The close relation of the amphibole and pyroxene structures reveals a mechanism of structural collapse whereby the double-chain units split into single-chain units plus a residue which are stable at these elevated temperatures. The heat absorbed (ΔH) in the reaction was 6.40 calories per gram, and the accuracy of the determination is estimated at $\pm 15\%$.

Richterite

The disintegration reaction for this specimen was similar to that for tremolite, except that a more complex pyroxene formed due to the presence of Mn, plus a glassy residue from the Na and F constituents. A hypothetical reaction for the thermal collapse of the mineral is

$$\underset{\text{richterite}}{2NaCa_{1.5}Mg_{4.5}Mn_{0.5}Si_8O_{22}(F)(OH)} + \Delta H = \underset{\text{pyroxene}}{\left|\begin{matrix}3CaSiO_3\\9MgSiO_3\\1MnSiO_3\end{matrix}\right|} + \underset{\text{glass}}{2NaF\cdot 3SiO_2} + H_2O$$

The reaction products included a complex pyroxene with a composition in the diopside-clinoenstatite-johannsenite series, water, and an alkali fluor-silicate glass. A heat of reaction of 6.85 calories per gram was determined and the accuracy of the measurement was somewhat lower (approximately $\pm 20\%$) as a result of the errors imposed by the slight sintering action.

Soda-Tremolite-Glaucophane

The structural disintegration of amphiboles whose composition includes portions of tremolite and glaucophane end-members was parallel to the rupture of tremolite and richterite samples. The breakdown prod-

ucts included a pyroxene of the acmite-augite series, hematite, cristobalite, and water. A hypothetical reaction for this process is

$$\underset{\text{soda-trem.-glaucophane}}{Na_2Mg_2Fe^{2+}Fe_2^{3+}Si_8O_{22}(OH)_2} + \tfrac{1}{4}O_2 + \Delta H = \left|\begin{array}{l} 2NaFe^{3+}Si_2O_6 \\ 2MgSiO_3 \\ \tfrac{1}{6}Fe_2O_3 \\ \text{polyaugite} \end{array}\right| + \underset{\text{hema-tite}}{\tfrac{1}{3}Fe_2O_3} + \underset{\text{cristo-balite}}{2SiO_2} + H_2O$$

This reaction will vary in amphiboles of this variety depending upon the chemical composition of each specimen. Small amounts of Ca and Al alter the reaction only slightly since both are acceptable constituents of the augite reaction product. Indeed, the ability of the augite structure to accept small amounts of Al^{+++}, Fe^{+++}, and Ti^{++++}, in addition to regular amounts of Ca^{++}, Mg^{++}, Fe^{++}, and Mn^{++}, makes it almost impossible for any precise reaction to be written. Slight differences in the amounts of the isomorphous constituents of the amphibole minerals definitely alter the proportional amounts of the reaction products. The presence of fluorine causes, at the distintegration temperature, the formation of a glass, and may eliminate the cristobalite component. In a limiting case hematite may not form if the iron content of the amphibole is so low that all of the iron goes into the formation of pyroxene. In any case, the bulk of the disintegration products always consists of a complex pyroxene of the acmite-augite-clinoenstatite series while the remaining substances described above form in minor amounts or are absent.

Both specimens fused into glassy masses at 1100° C., and as a result, the accuracy of the calorimetric measurement was reduced to about $\pm 25\%$. The peculiar heat effects accompanying glass formation is detrimental to the type of heat analysis employed in this investigation where the test specimen must maintain its physical characteristics if accurate measurements are to be made. The high alkali and fluorine contents of both samples was largely responsible for this glass formation. Spectrochemical analyses of the disintegration products revealed no loss of fluorine in samples heated to 1125° C. This might be expected in view of the very high electronegativity of fluorine. The heat absorbed by specimens A and B in the disintegration reaction was 4.68 and 5.24 calories per gram, values of the same order as those determined for tremolite and richterite.

Pargasite-Hastingsite

These amphiboles are members of the lime-alkali varieties of hornblendes that are high in calcium as well as aluminum. At 1100° C. the disintegration products included some plagioclase feldspar flakes in addition to polyaugite, hematite, and water. The complex composition of both the amphibole and its reaction products prohibits the writing of an

exact expression for the reaction but a possible reaction may be expressed as follows:

$$2NaCa_2MgFe_3^{2+}Fe_{1.5}^{3+}Al_{1.5}Si_6O_{22}(OH)_2 + \tfrac{3}{2}O_2 + \Delta H$$

hornblende

$$= \left|\begin{matrix} NaFeSi_2O_6 \\ 2MgSiO_3 \\ 3CaSiO_3 \end{matrix}\right| + \left|\begin{matrix} CaAl_2Si_2O_8 \\ NaAlSi_3O_8 \end{matrix}\right| \quad \left|\begin{matrix} Fe_2O_3 + 2H_2O. \\ \text{hema-} \\ \text{tite} \end{matrix}\right.$$

polyaugite plagioclase

The hastingsite specimen heated to 1145° C. reacted to form all the products above plus some olivine and magnetite. Evidently temperatures greater than 1100° C. are necessary for the formation of these reaction products.

The differential thermal curve for hastingsite (Fig. 2) reveals a disintegration peak temperature of about 1090° C., approximately 40° C. higher than the peak temperature for tremolite. Buerger[9] stated that the presence of aluminim proxying for silicon in a silicate increases the disintegration temperature for that silicate. Comparing the disintegration temperatures of tremolite and the aluminous hastingsite we see that this relation holds true in this instance.

The heats of reaction for the pargasite and hastingsite specimens are 2.83 and 0.83 calories per gram, respectively. These heats are noticeably lower than those determined for the other monoclinic amphiboles and should be interpreted with care. Since the disintegration temperatures for aluminous species are considerably higher than for non-aluminous types direct comparison of the reaction heats at different temperatures are not justifiable. In addition, the oxidation of ferrous iron at temperatures closely bordering on the disintegration temperatures is an exothermic reaction that interferes with the heat determination of disintegration. The accuracy of these determinations is probably no better than $\pm 50\%$.

The thermographic curves of pargasite and hastingsite show that some transformation is occurring in the 750°–800° C. range. It is possible that this is supporting evidence for the inversion reported by Kozu, *et al.*[10]

Magnesian Anthophyllite

The disintegration of magnesian anthophyllite closely parallels the collapse of tremolite, its monoclinic counterpart. The products of structural disintegration are orthopyroxene, cristobalite, and water.

[9] Buerger, M. J., The role of temperature in mineralogy: *Am. Mineral.*, **33**, 101–121 (1948).

[10] Kozu, S., Yoshiki, B., and Kani, K., Note on the transformation of common hornblende into basaltic hornblende at 750° C.; *Sci. Rept. Tohoku Imp. Univ.*, Ser. 3, No. **2**, 143 (1927).

The reaction[11]

$$\underset{\text{anthophyllite}}{Mg_7Si_8O_{22}(OH)_2} + \Delta H = \underset{\text{enstatite}}{7MgSiO_3} + \underset{\text{cristobalite}}{SiO_2} + H_2O$$

has a peak temperature of about 1020° C., and absorbs 4.50 calories per gram. The estimated accuracy of the heat measurement is the same as that for tremolite ($\pm 15\%$). Rabbitt's[12] thermographic curve for anthophyllite (A) was described as "a vague continuing loss . . . of H_2O at 1050° C." From the present investigation it is seen that his interpretation overlooked the fact that the more extensive reaction, shown above, was taking place.

Ferrous Anthophylite

Specimen (B), Fig. 2, gave orthopyroxene, cristobalite, and water as disintegration products according to the reaction

$$\underset{\text{anthophyllite}}{\left|\begin{matrix}Mg\\Fe^{++}\\Al^{+++}\end{matrix}\right|_7 \left|\begin{matrix}Si\\Al\end{matrix}\right|_8 O_{22}(OH)_2} + \Delta H = 7 \underset{\text{hypersthene}}{\left|\begin{matrix}Mg\\Fe^{+++}\\Al^{+++}\end{matrix}\right| \left|\begin{matrix}Si\\Al\end{matrix}\right| O_3} + \underset{\text{cristobalite}}{SiO_2} + H_2O$$

where the pyroxene is hypersthene, the variety that accommodates Fe and Al in its structure. Once again ferrous iron oxidation interferes with the calorimetric measurement of the disintegration reaction, and makes the heat determination of 2.00 calories per gram accurate to about $\pm 30\%$. It may be expected that alkali fluoriferous specimens would yield a glass among the disintegration products.

[11] Thilo, E., and Rogge, G., *op. cit.*

[12] Rabbitt, J. C., *op. cit.*

Manuscript received April 25, 1951.

NOTES ON MINIMUM-DEVIATION REFRACTOMETRY

H. W. Fairbairn, *Massachusetts Institute of Technology, Cambridge, Massachusetts*

Abstract

Minimum-deviation refractometry problems are presented at the maximum precision level likely to be required by mineralogists. Using a medium-precision spectrometer equipped with a Gauss ocular for auto-collimation, it is concluded that for solids the probable error of a single determination should not exceed ± 2 or 3×10^{-5}. For liquids, where temperature coefficients are relatively high, probable errors between $\pm 1\times10^{-4}$ (for methylene iodide) and $\pm 4\times10^{-5}$ (for water) need not be exceeded. Tests of the accuracy of this spectrometer, using a Bureau of Standards calibrated glass prism, check within $\pm 2\times10^{-5}$. It is emphasized that the level of precision of index determination of a liquid used in the immersion procedure should ideally be much higher than the precision of index determination aimed at for the solid. Under any circumstances, however, an estimate of the error in index of the liquid should accompany the statement of index error assumed for solids determined by the immersion method.

Introduction

It is generally agreed by competent authorities (Tilton, 1929) that the minimum-deviation method of refractive index determination is inherently superior to any other. For solids, single determinations with a probable error of ± 2 or 3×10^{-6} are routine and precision can be improved if replicate measurements are made. For liquids, on the other hand, which have relatively high refractive index variation with temperature, a precision of $\pm 1\times10^{-5}$ is about the limit obtainable, and for ordinary work with open, hollow cells a considerably lower goal of precision must be faced. As a major use of the minimum-deviation method in mineralogical work is in calibrating liquids for the immersion method of refractive index determination, it is important to know what precision is obtained under given conditions. The immersion method assumes particular importance in investigations of rock-forming minerals because of the impossibility of obtaining fragments large enough for preparation of oriented prisms to be used on a spectrometer. Since there is always an unavoidable random error in matching a grain with its embedding liquid, it is only common sense to devote considerable care to the calibration of the liquid being used as the standard. Depending on the nature of the problem, a degree of precision may be required which makes advisable calibration of a liquid beyond the precision limit ($\pm .0002$) of the ordinary Abbe refractometer. This can not be done, as is usually attempted in mineralogical laboratories, by pressing into service a one-circle crystal goniometer, since auto-collimation is not provided on these instruments

and sufficiently precise prism angle determinations can not be carried out. A spectrometer designed for the purpose must therefore be used. The author uses a medium-precision Gaertner instrument (Type LIII) which reads directly to 20 seconds and by interpolation to 10 seconds. It is provided with a Gauss ocular (for auto-collimation) which can be illuminated by any small concentrated light source such as a Penlite battery lamp. A sodium-vapor lamp supplies monochromatic radiation[1] for the minimum-deviation measurements.

Temperature control is provided by a constant-temperature assembly supplied by American Instrument Co. Temperature in the supply tank is controlled to .05° C., but is probably not better than .1° C. elsewhere in the circulating system. Air temperature is checked by a thermometer suspended directly above the prism table.

Tolerances in Measurement

Tilton (1929, 1931, 1933, 1935) has thoroughly investigated the sources of error in minimum-deviation refractometry and has established tolerances based on a probable error of $\pm 1 \times 10^{-6}$ in refractive index. Table 1 lists most of the errors discussed in his papers and gives, for selected refractive index values, the larger tolerances based on a probable error of $\pm 1 \times 10^{-5}$, which is the goal under consideration here.

All the sources of error may be either positive or negative except errors in prism orientation, which, from the mechanics of the method, can be positive only. As noted in the table, most of the tolerances are large enough in terms of measurement and control that the desired error of $\pm 1 \times 10^{-5}$ need not be exceeded. Exceptions are (1) the prism angle determination, where the observed tolerance (see Table 2) is commensurate with a refractive index error of $\pm 2 \times 10^{-5}$ rather than $\pm 1 \times 10^{-5}$, and (2) the control of temperature for organic liquids, where the tolerances are too small for ordinary control equipment. This matter will be discussed on a later page.

If it is desired to find tolerances for other values of refractive index error, the relations are linear throughout except for prism orientation error, where a second power relation obtains (see Table 1).

The flatness of the prism faces is critical because of its influence on the tolerances in prism translation, eccentricity of prism-table axis, and collimator focusing. However, it is routine procedure to obtain surfaces deviating from true flatness by less than .25 λ per 1 cm. area. Where this holds, these three dependent sources of error acquire large tolerances and may be neglected for work at $\pm 1 \times 10^{-5}$.

[1] In addition to the strong doublet (5890 and 5896), lines 6563, 4861, and 4340 may also be used with this lamp.

TABLE 1. TOLERANCES FOR A PROBABLE ERROR IN REFRACTIVE INDEX OF $\pm 1\times10^{-5}$
PRISM ANGLE ASSUMED TO BE 60°

Source of Error	Refractive Index				Notes	Reference
	1.3	1.5	1.7	1.9		
Prism Angle (A)	5.7 sec.	3.3 sec.	2.2 sec.	1.6 sec.	Tolerances are in general too small for a refractive index error of only $\pm 1\times10^{-5}$	Tilton 1929
Double Deviation (2D)	5.6 sec.	6.2 sec.	8.0 sec.	15.0 sec.	Tolerances large, varying directly with index.	Tilton 1929
Prism Orientation Azimuth at the Minimum Deviation Setting	~6°	~5°	~4.5°	~4°	Error is always positive. $\Delta n \propto$ (P.E. azimuth).[2] Tolerances large.	Tilton 1931
Prism Flatness	2.7λ	1.4λ	.8λ	.4λ	Referred to an area 1 cm. diameter. Tolerances large, varying inversely with index.	Tilton 1933
Prism Translation Eccentricity of Prism-Table Axis Collimator Focussing					Tolerances dependent on flatness of prism, and are large enough to be ignored if prism flatness <.5λ	Tilton 1933
Air Temperature	8° C	7° C	6° C+	6° C−	For λ=5893 and room temperature. Tolerances cannot be ignored.	Tilton 1935
Air Pressure	22 mm. Hg.	19 mm. Hg.	16 mm. Hg.	15 mm. Hg.	Tolerances are fairly critical.	Tilton 1935
Temperature of Solids	Sylvite ~.3° C(−) n_ϵ Calcite ~.1° C(+) Fused quartz ~1° C(+) Light Flint Glass ~2° C(+)				For λ=5893. Coefficients positive or negative. Tolerances ample.	Tilton 1935
Temperature of Liquids	Water 0.1° C(−) Most organic liquids about .025° C(−) Methylene iodide .015° C(−)				For λ=5893. Tolerances too small (water excepted) for $\pm 1\times10^{-5}$ probable error. Coefficient always negative.	Tilton 1935
Wavelength of Light Source	Water 1.0 Å Fluorite 1.3 Å				For λ=4000. Tolerances ample when using sodium, mercury, etc., vapor lamps	Tilton 1935

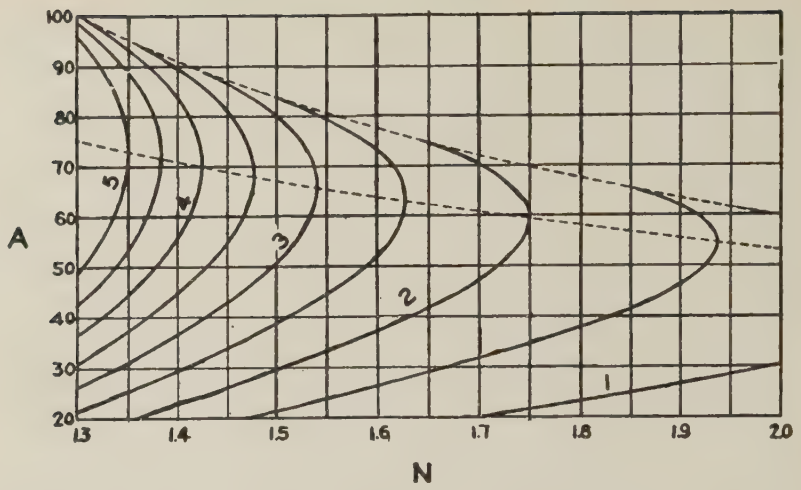

FIG. 1. Iso-tolerance curves (in seconds) for various combinations of prism angles A and refractive indices N, based on an arbitrary error of $\pm 1 \times 10^{-5}$. The merit of using prism angles close to 60° (for this range of indices) is indicated by the broken line connecting the crests of the curves. The upper broken line shows the largest prism angle which could possibly be used for various refractive indices. Modified from Tilton (1929).

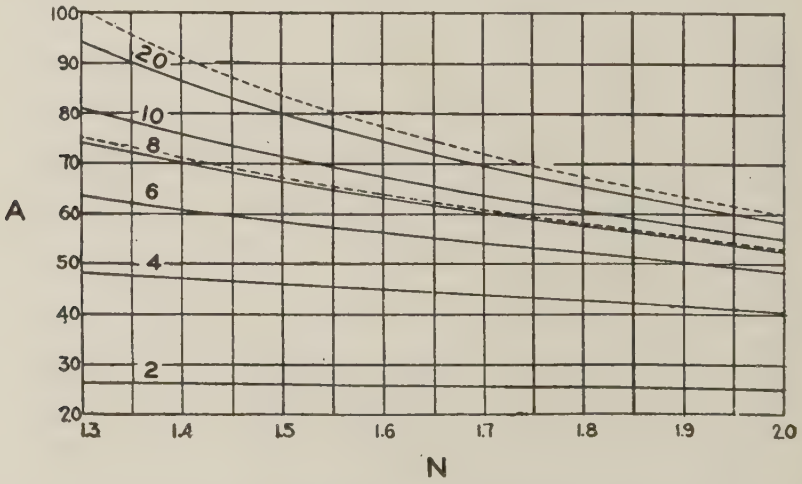

FIG. 2. Similar to Fig. 1, but drawn to show tolerances (in seconds) in the double-deviation angle $2D$. The broken lines are identical with those in Fig. 1. Note the larger tolerances compared with prism angle tolerances. Modified from Tilton (1929).

The tolerances for prism angle determinations are shown in Fig. 1. The general merit of using 55–75° prisms is evident from the broken line connecting the peaks for each curve. The tolerance varies inversely with index.

Figure 2 applies to errors in double-deviation. The tolerances vary directly with prism angle and refractive index. The broken lines have the same positions as in Fig. 1.

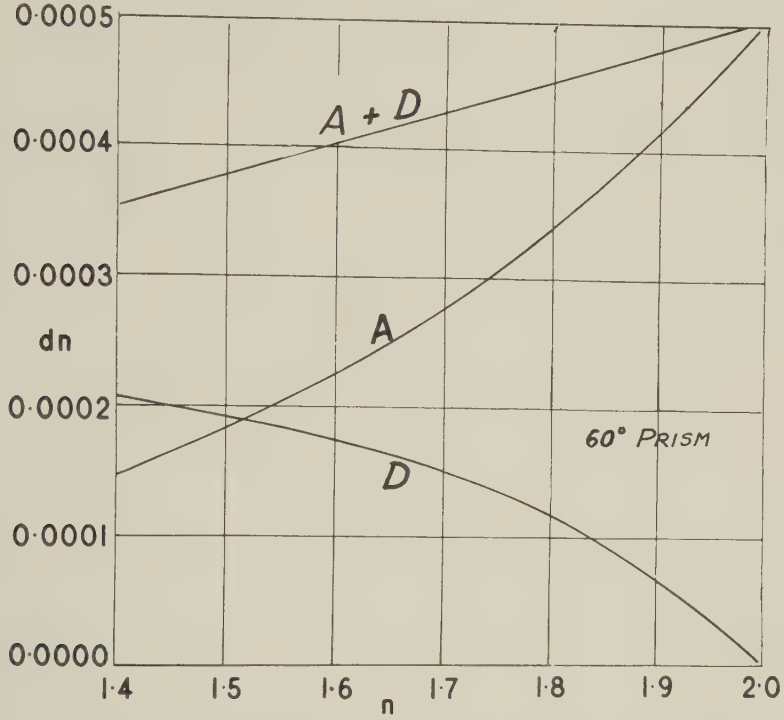

FIG. 3. Diagram showing relative trends of error in prism angle A and deviation angle D for a *fixed* prism angle. The opposing trends in the A and D curves show the need for particular care in determining A. From Fairbairn and Sheppard (1945), based on a maximum error of 1 minute in measuring A and D.

Figure 3 shows, for a 60° prism, the opposing trend of errors in prism angle and double deviation. Except for low-index materials, tolerances are less liberal for prism angles than for double deviation angles, thus emphasizing the requirement of auto-collimation in prism angle determination.

TESTS WITH A STANDARD GLASS PRISM

In order to test the precision and accuracy of the present spectrometer, measurements were made with a glass prism furnished by the Optics Section, National Bureau of Standards. Two determinations of its prism angle are stated to differ by less than one second and the refractive index varies less than 3 units in the sixth decimal place. Table 2 gives a sum-

mary of measurements made for comparison with the Bureau of Standards data. The probable error of 5 seconds in the prism angle computed for one set of measurements is about twice the tolerance given in Fig. 1 for an index error of $\pm 1 \times 10^{-5}$ and is therefore commensurate with an error of $\pm 2 \times 10^{-5}$. The double-deviation error on the other hand is well within the limits set by Fig. 2. This contrast in the two errors is striking, but nevertheless normal, and points up the fact that even with the autocollimation method, prism angle determination is a much greater source of error than the double-deviation determination.

Table 2. Summary of Tests with Standard Prism

Prism Angle Data (A)			Double Deviation Angle Data (2D)				Refractive Index
Angle	Probable Error	No. of Trials	Angle	Probable Error 2D	Probable Error D	No. of Trials	
60°14′55″	5 sec.	5	87°51′48″	2 sec.	1 sec.	4	1.57205
60°14′50″	n d	3	87°51′56″	n d		2	1.57211
60°14′50″	n d	2	87°51′50″	n d		2	1.57209
60°14′50″*			87°51′53″*				1.57210*

* Data supplied by Optics section, Bureau of Standards, Washington, D. C. Two determinations of prism angle varied <1 second. Refractive index varied about 3 units in the sixth decimal place and is here rounded off to five places. Compare with corresponding data immediately above.

The flatness of the glass prism is about .25 λ, well within the tolerance range given in Table 1, and also below the threshold value of .5 λ where dependent errors due to prism translation, eccentricity of the prism table axis, and collimator focussing would be significant.

Data on relative values of air temperature and pressure at the Bureau of Standards and in our laboratory are not available. However, in view of ordinary room temperature ranges, it is unlikely that the corresponding tolerances given in Table 1 have been exceeded. The tolerances for air pressure are slightly more critical and the present measurements may be affected beyond $\pm 1 \times 10^{-5}$, but not above $\pm 2 \times 10^{-5}$.

The prism is a light flint glass having a tolerance of about 2° C. for our arbitrary index error of $\pm 1 \times 10^{-5}$. As the writer's measurements were made at somewhat higher room temperature (2–4° C.) than the standard 20° C. used at the Bureau of Standards, the index error limit may need to be raised to $\pm 2 \times 10^{-5}$. Any correction applied would be negative (see Table 1 for details for various solids).

The average refractive index of the three trials reported in Table 2 (1.57208) agrees very closely with the standard value of 1.57210. A probable error based on so few determinations would not give a very significant statistic and no computation has been made. However, in assessing the magnitude of such errors it must be kept in mind that practically all the component sources of error may be either positive or negative. This compensating factor tends to reduce the magnitude of the combined probable error in refractive index. Tilton (1935) states that high precision determinations in the Bureau of Standards laboratory have a probable error of about ± 2 or 3×10^{-6}. In view of the evaluation of errors of measurements made in the writer's laboratory, a probable error not greater than ± 2 or 3×10^{-5} may be assumed. The Gaertner instrument may therefore be considered adequate, both from the standpoint of precision and accuracy, for refractive index determinations correct to at least four decimal places and approximate in the fifth.

Tests with a Hollow Prism

Calibration of the spectrometer with solid prisms gives a sound basis for tests with hollow prisms.[2] As is well known, hollow prisms are subject to two inherent defects (1) non-parallelism of the inner and outer surfaces, and (2) curvature of the prism faces. For satisfactory work, therefore, a good grade of optical glass should be obtained. Glass recently used by the writer deviates from true parallelism by 6 seconds and from true flatness by 2 rings ($= 1 \lambda$) per 1 cm. diameter. It would be possible for given orientations of the symmetry planes related to the wedging and curvature of the glass to work out an assembly for the hollow prism in which these defects are minimized. It is simpler, however, to proceed empirically and to calculate a cell "constant" for the particular prism used. For example, from trials with distilled water as a reference liquid, the writer determined a systematic excess in its refractive index, at the temperature used, amounting to .00005. For unknown liquids this value is therefore subtracted from the calculated refractive index. If a new cell is assembled its "constant" must be independently determined.

If the cell is built as in Fig. 4, it may turn out that no "constant" need be used. This would be the case if error from the flatness of the surfaces was negligible and if the "wedging" of the glass was so small that the tolerance for prism translation (Table 1) was not exceeded.

As already stated on a previous page (see also Table 1) the temperature of liquids is a critical parameter and the limits of control must be known. In the writer's laboratory thermometers are installed in the

[2] Same design as illustrated by Butler (1937).

pump-driven bath circuit at equal distances on each side of the hollow cell. These read to 0.1° and had previously been checked against each other. Since temperature control in the bath is rated at ±.05°C., it is probable that the fluid flowing through the cell does not vary more than ±.1° C.

For purposes of calibration it is a fortunate circumstance that the temperature tolerance of distilled water is about five times larger than that of the organic liquids used for immersion refractometry of minerals. Its tolerance of .1° C. is of the same order of magnitude as the probable temperature variation of the circulating fluid and makes possible determination of a cell "constant" as already outlined. It also permits investi-

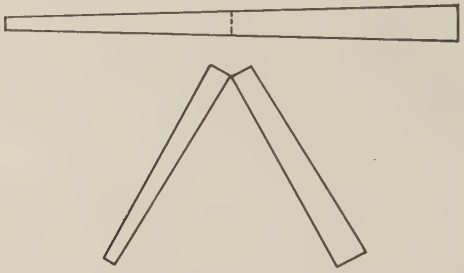

FIG. 4. Sketch showing preferred method of reducing error due to non-parallelism of glass plates in construction of a hollow cell.

gation of the problem of temperature differential between the circulating fluid and the refracting liquid. As the hollow cell is not insulated in any way, the refracting liquid will usually be at a different temperature than that of the circulating fluid unless steps are taken to have the room and bath temperatures the same. As this is rarely possible without a thermally-controlled laboratory, an estimate must be made of the actual temperature of the refracting liquid for known values of room temperature and bath temperature. The thermal coefficient of water, in addition to being relatively low, is also known with greater precision than for other liquids important in immersion work and can, therefore, be used as a standard. A constant volume of distilled water (0.1 ml) was used for the test and refractive indices were determined at bath temperatures varying between 28° C. and 51° C. The room temperature varied between 24° C. and 28° C. The table in *Handbook of Physics and Chemistry*[3] gives the temperature corresponding to the measured refractive index. These data, plotted as differences, are shown in Fig. 5, with the bath-air differential plotted against the bath-cell differential. Up to 10° bath-air

[3] Chemical Rubber Publishing Co., Cleveland, Ohio.

differential, the relation is unequivocal and reasonably linear; above this range the data are difficult to interpret. This may be due to convection currents in the cell; minimum-deviation angles for example are notoriously less precise for liquids considerably above room temperature.

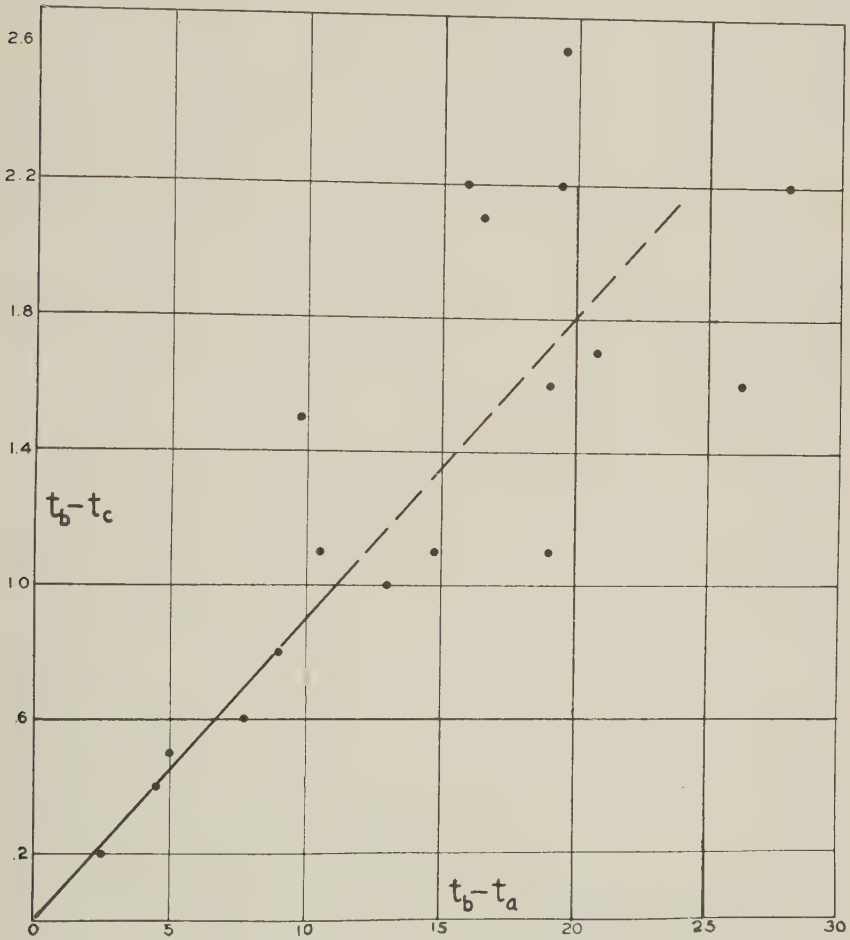

FIG. 5. Diagram showing hollow cell temperature corrections ($t_b - t_c$) required for various room temperatures (shown as a differential $t_b - t_a$ above temperature of circulating water bath).

However, since air temperature will not normally vary as much as 10° C. from the desired cell temperature, corrections may be read from the graph as needed. If the error in the bath-air differential be taken as .2°, the corresponding error of the correction (bath-cell differential) would not exceed about .02° C. and may be neglected.

An alternative technique was also carried out, based on direct determination of the temperature of the refracting liquid with a thermocouple and precision potentiometer.[4] A larger volume of liquid (cell filled) was used in these experiments. As would be expected with this larger volume, the bath-cell differential temperature is greater than shown in Fig. 5. Measurements on distilled water, methylene iodide, carbitol, and α-chloronaphthalene are, however, inconsistent, ranging from 2° to 4° ($t_b - t_c$) for a $t_b - t_a$ of 10° C. A variety of reasons could be adduced for this discrepancy, but until further refinements in the technique are made, the indirect approach by calculation of the refractive index (Fig. 5) is preferable. This correction should be determined with distilled water for each cell for a fixed volume of liquid. The temperature of an equal volume of an unknown liquid in the same cell can then be read from the graph.

As Table 1 indicates, a precision level of $\pm 1 \times 10^{-5}$ cannot be maintained for minimum-deviation work with organic liquids if the temperature of such liquids can be controlled only to .1° C. The index errors corresponding to $\pm .1$° C. are $\pm 7 \times 10^{-5}$ for methylene iodide and $\pm 4 \times 10^{-5}$ for most other organic liquids. Since the probable error of a single index determination of a solid prism has been set at ± 2 or 3×10^{-5}, the total error for index determination of an organic liquid would in the worst case be $\pm 1 \times 10^{-4}$ (methylene iodide) and for other liquids somewhat less. Both of these values are appreciably smaller than can safely be assumed for Abbe refractometer determinations, where error in the setting alone will never be less than about $\pm 2 \times 10^{-4}$. Addition of the temperature error increases this to almost $\pm 3 \times 10^{-4}$.

From the above analysis of error it would therefore seem eminently worth while to take considerable pains to calibrate adequately any liquid intended for precise refractive index work by the immersion method. Where a pure liquid is used, this need only be done once for any particular lot; for mixtures, frequent checks will be necessary, particularly if methylene iodide is one of the ingredients. In all cases, in reporting a refractive index obtained by the immersion method, the level of precision in the index of the embedding medium is a factor which must be considered in assessing the total error of index determination.

Appendix

A detailed statement of minimum-deviation procedure scarcely needs to be included here, but the writer will be glad to supply instructions to any reader in need of them. There are a number of special points, how-

[4] The writer is indebted to H. S. Yoder for generous assistance with this phase of the investigation.

ever, not covered in the instructions issued by the manufacturer, which are worth enumerating.

1. Since hollow prisms and most prisms of mineral crystals are smaller than the telescope objective aperature, they may be centered on the prism table fairly accurately by observation through the telescope with ocular removed.

2. The prism should be so centered that no re-focusing of the telescope is needed during measurement of the prism angle.

3. The position of the lamp used for illumination of the cross-hairs should not be altered during measurement of the prism angle.

4. If hollow prisms are filled with mercury during measurement of the prism angle the confusing double set of reflected cross-hairs (due to non-parallelism of the walls of the prism) will be resolved into a very strong and a very faint reflection. Use of the former for measurement gives the true internal angle of the hollow prism.

5. In order to utilize the central light rays in the telescope, the prism, after measurement of the prism angle, should be re-centered for minimum-deviation measurement. Possible error through neglect of this re-centering will be greater for high than for low refractive index liquids.

6. When the prism table clamp is loosened preparatory to making the minimum-deviation measurement, observe whether there is any disorientation of the reflected cross-hairs. Re-set the prism (by the autocollimation procedure) in the unclamped position if the original orientation is not maintained.

7. Maintain a fixed slit width in measuring any given double deviation.

8. In making the minimum deviation measurement set the vernier table approximately at zero as a convenience in finding the minimum-deviation angles on either side. If an approximate refractive index is already known a nomogram such as that prepared by Winchell (1951) may be used to find the approximate minimum deviation position.

9. Interpolate vernier readings to the nearest 10 seconds and use six-place tables in calculating the refractive index.

References

Butler R. D., (1937), Imersion liquids of intermediate refraction: *Am. Mineral.*, **18,** 386.

Fairbairn H. W., and Sheppard C. W. (1945), Maximum error in some mineralogic computations: *Am. Mineral.*, **30,** 673.

Tilton L. W. (1929, 1931, 1933, 1935) Standard conditions for precise prism refractometry: *Nat. Bur. Standards Jour. Res.*, **2,** RP64; **6,** RP262; **11,** RP575; **14,** RP776.

Winchell, Horace (1951), Alignment chart for calculation of refractive index etc.: *Am. Mineral.*, **36,** 287.

Manuscript received May 10, 1951

GRAPHICAL INDEXING OF POWDER PATTERNS OF CUBIC SUBSTANCES AND THE CHOICE OF RADIATION FOR PRECISION MEASUREMENTS OF LATTICE PARAMETERS

M. E. Straumanis, *University of Missouri, School of Mines and Metallurgy, Department of Metallurgy, Rolla, Missouri*

Abstract

A convenient graphical method is described showing how to find the most suitable x-radiation for precision determination of lattice parameters. At the same time, the method allows one to index the powder patterns. The method is based on the application of three dimensional reciprocal lattice and becomes very simple if used in the case of cubic crystals.

Introduction

For the precision determination of lattice parameters sharp powder lines (or spots of a single crystal) are necessary in the very back reflection region of the patterns.[1,1a]

It is nearly always possible to find the proper radiation producing lines with a glancing angle ϑ greater than 78°, even in the case of small lattice constants. However, the choice of the wave length[2] takes considerable time and, as far as know by the author, no convenient methods have been described in order to find the best possible radiation.

A simple graphical method, which is easy to apply especially in the case of the cubic powders, is described below. It can be used at the same time for the indexing of powder patterns and is based on the application of the reciprocal lattice constants.

The Theory

The section normal to the cylindrical axis of a Debye-Scherrer camera is drawn in Fig. 1 showing the path of the direct and reflected x-ray beams.

It follows directly from the figure that

$$\frac{x}{2r} = \operatorname{Sin}\vartheta \qquad \text{and} \qquad \frac{p}{x} = \operatorname{Sin}\vartheta \qquad \text{(1 and 2)}$$

[1] Straumanis, M. E., *J. Appl. Phys.*, **20**, 726 (1949).

[1a] Straumanis, M., and Ievins, A., Die Präzisionsbestimmung von Gitterkonstanten nach der asymmetrischen Methode: (Verlag J. Springer, Berlin, Germany, 1940), reprinted by Edwards Brothers, Inc., Ann Arbor, Michigan (1948).

[2] Buerger, M. J., *X*-ray Crystallography: John Wiley and Sons, Inc., New York (1942), pp. 171, 393 and 459.

If now the inside wall of the camera, as shown in Fig. 1, is regarded as the sphere of reflection,[3,4] then the chord x represents the reciprocal lattice vector (Fahrstrahl)[5] of the three dimensional reciprocal lattice. This chord connects the origin O of the reciprocal lattice with the reflection (powder line) on the circle of reflection (wall of the camera). Thus,

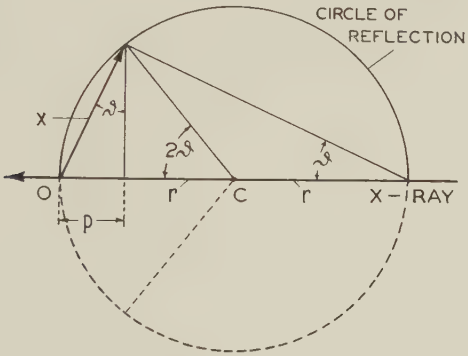

FIG. 1. Path of the x-ray beam in a Debye-Scherrer Camera.
c = the powder sample
x = vector of the reciprocal lattice

p is the projection of the reciprocal lattice vector x on the diameter (marked by the x-ray) of the camera. This p has very interesting properties.

It follows from the combination of Bragg's equation

$$\text{Sin } \vartheta = \frac{n\lambda}{2d} \qquad n = 1$$

with (1 and 2):

$$p = \frac{r\lambda^2}{2d^2}. \tag{3}$$

For the cubic substances d^2 can be replaced by $a^2/\Sigma h^2$, the sum of the squares of the indices h, k, l of the reflecting plane, a, being the lattice parameter of the substance under investigation:

$$p = \frac{r\lambda^2}{2a^2}\,\Sigma h^2. \tag{4}$$

Working with the same radiation and substance, the part $r\lambda^2/2a^2$ of

[3] Bernal, J. D., *Proc. Roy, Soc. London*, A, **113,** 117 (1926).
[4] Buerger, M. J., *X*-ray Crystallography, J. Wiley and Sons, Inc., New York (1942) pp. 128.
[5] Ewald, P. P., *Z. Krist.*, **56,** 129 (1921); **93,** 396 (1936).

(4) becomes constant and the length of p, resulting from the other lines on the reflection circle, is simply proportional to Σh^2, which represents the integers 1, 2, 3. . . . :

$$p = k\Sigma h^2. \tag{5}$$

This means that all differences of the projections p of two subsequent reciprocal lattice vectors of a cubic substance are equal, including extinct lines and those the Σh^2 of which cannot be split into 3 integers that are squares.

This difference is equal to the smallest p_{min}, resulting if $\Sigma h^2 = 1$; it can also be calculated from (4) if the lattice parameter a is known. Likewise, the lattice parameter a can be calculated if p_{min} is known:[6]

$$a = \lambda\sqrt{\frac{r}{2p_{min}}}. \tag{6}$$

Now, if p is kept constant, the change in radiation from λ_1 to λ_2 will result in a changed radius (r_2) of the reflecting circle. Applying eq. (6) r_2 can be computed using the r_1 adopted previously: .

$$r_2 = r_1\left(\frac{\lambda_1}{\lambda_2}\right)^2. \tag{7}$$

Thus, by means of equation (5) a cubic film can easily be indexed and by means of equation (7) the best radiation for precision determination of lattice parameters can be found. How to apply these two formulas is shown in the next section.

Indexing Procedure and Choice of Radiation

The best radiation for the precision determination of the lattice constant of germanium had to be found. The first trial photograph was made with Co-radiation. A very thin germanium powder mount was prepared[1,1a] and the photographs were made in a 64-mm precision camera, using the asymmetric film arrangement.[1] Working with this method standard substances are unnecessary, as well as the knowledge of the camera diameter. Film shrinkage is eliminated and the absorption corrections can be neglected. The exact values of the glancing angles and the lattice constants can be calculated directly from the film, provided the construction of the camera is correct. An example of calculation of the mentioned quantities from an asymmetric film has been given previously.[1]

The measurement of the asymmetric germanium powder film obtained led to the following 2ϑ angles in degrees (only the α or α_1 lines were measured):

[6] Straumanis, M., *Z. Krist.*, **104**, 167 (1942).

31.81; 53.28; 63.42; 87.29; 101.72; 110.65; 126.87; and 138.58°.

Now a reflection circle, corresponding to the inside wall of the camera must be drawn. It is convenient to take the radius of the reflecting circle for copper radiation as being equal to 100 mm. The radii for other radiations, assuming that the projection p_{min} does not change, are calculated by equation (7) and listed in Table 1.

Table 1. Radii of the Reflection Circles in mm for Different Radiations, Assuming that p_{min} Is Constant and the Radius for Cu Radiation Is Equal to 100 mm

Cu α_1	100 mm	Fe α_1	63.4 mm
Cu β	121.3 mm	Fe β	76.9 mm
Co α_1	74.1 mm	Cr α_1	45.3 mm
Co β	90.4 mm	Cr β	54.6 mm

Further, the following operations must be performed:

(1) The already mentioned 2 ϑ angles of germanium are carried on the reflection circle for Coα_1 radiation as shown in Fig. 2, starting from the origin O on the left side. The figure shows simply the positions of the peaks of the powder lines in a camera with a radius of 74.1 mm. (Table 1).

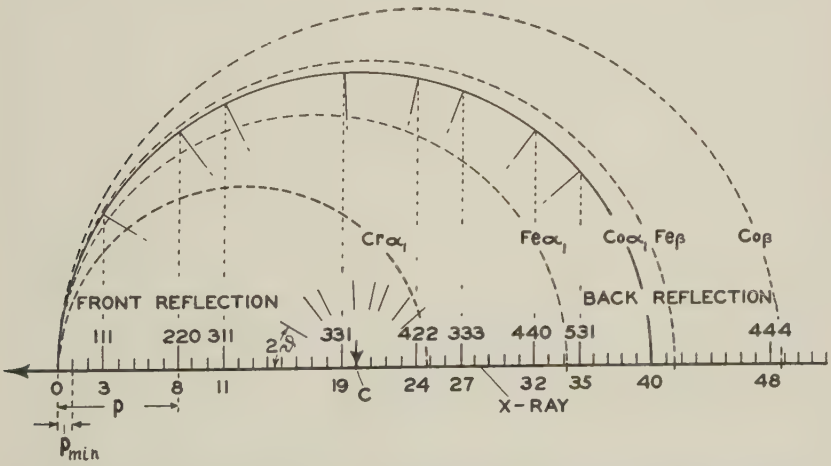

Fig. 2. Graphical indexing of the lines of a germanium film. Choice of best radiation for precision determination of the lattice constant. Crα_1 (and Crα_2) radiation is the best. C = center of the reflecting circle for Coα_1 radiation (place of the powder mount).

(2) The 2 ϑ angles (or more correctly the reciprocal lattice vectors) are projected onto the diameter of the circle as represented by the x-ray beam and the end points are marked as shown on Fig. 1.

(3) Starting from the origin O, the distances between the projection points are divided into the largest possible divisions (equal p_{min}), so that the end point of any one projection from the origin O is an integral multiple of p_{min}. This can be found by trial. Or, since it is known that the first interference of a germanium powder pattern is 111 ($\Sigma h^2 = 3$), the distance between O and 3 should be divided into 3 parts, each part representing p_{min}. Or, if the lattice constant is known p_{min} can be calculated from equation (4), assuming that $\Sigma h^2 = 1$.

(4) The p divisions on the diameter of the circle are numbered successively, starting from the origin as shown in Fig. 2. Each number represents the Σh^2 of the corresponding line and the indices can be easily found.

If all the projections of the points on the reflecting circle coincide with the integers of p_{min} on the diameter (x-axis), the indexing of the cubic crystal is right and there is no other possibility. These are difficulties if the lattice constants are larger; in such cases one must start with a larger radius of the reflecting circle.

The best radiation for the precision measurement of lattice constants is that one which produces lines in the very back reflection region ($\vartheta > 78°$). To find the best radiation, the x-axis with its p-scale is extended if necessary, and reflection circles for the various other radiations (Table 1) are drawn so that the origin O on the x-axis is common to all reflection circles (the centers of the reflection circles are on the x-axis). These reflection circles (broken curves on Fig. 2) intersect the x-axis at different points. Since these intersections correspond to $2\vartheta = 180°$ (back reflection region), that radiation the reflection circle of which intersects closest to a p division is the best one. Of course, the line to which the p belongs must be intense enough. For instance, Fig. 2 shows that Crα_1 and α_2 radiation is the best one in the case of germanium. Coβ radiation would be good also, but the photograph showed that 444β is too weak. In the other cases the very back reflection lines are extinct and the corresponding radiations are unsuitable for precision measurements.

Of course, the whole procedure can also be carried out by calculation using the formulas as given above.

A similar graphical method for the choice of radiation and for indexing of rotation crystal photographs based on the two dimensional reciprocal lattice was described previously.[1a]

Manuscript received July 20, 1951.

BYSTROMITE, MAGNESIUM ANTIMONATE, A NEW MINERAL

Brian Mason and Charles J. Vitaliano, *Indiana University, Bloomington, Indiana.*

Abstract

Antimony ores from El Antimonio, Sonora, Mexico, contain a new mineral corresponding in chemical composition and structure with magnesium antimonate, $MgSb_2O_6$, although in the mineral the lattice is deficient in magnesium and some of the oxygen is replaced by hydroxyl groups. The mineral is massive, color blue-gray, streak light gray, hardness about 7, density 5.7. The mean index of refraction varies from 1.86 to 1.91, the birefringence is approximately 0.01. The mineral occurs in quartz veins associated with stibiconite. *X*-ray investigation shows that it is tetragonal (ditetragonal dipyramidal), $a=4.68$ Å, $c=9.21$ Å, $c/a=1.968$, space group $P4/mnm$; the structure is of the trirutile type, and the mineral is isomorphous with tapiolite and with many artificial antimonates and tantalates. The name bystromite is proposed after Anders Byström, Swedish crystal chemist, who worked out the structure of synthetic magnesium antimonate in 1941.

During an investigation of antimony ochers we received a number of specimens from Dr. D. E. White, of the U. S. Geological Survey, who had collected them from various deposits in Mexico. *X*-ray powder photographs showed that the common mineral was stibiconite. One specimen, however, gave a different powder photograph, the strong lines of which practically coincided with those recorded for cassiterite. Spectrographic analysis showed magnesium and antimony, with only traces of other elements. A synthetic magnesium antimonate with formula $MgSb_2O_6$ and structure and lattice dimensions similar to those of cassiterite was described in 1941 (1). The synthesis of magnesium antimonate was repeated and its identity with the new mineral confirmed. This is the first magnesium antimonate recorded as a mineral, and we propose for it the name bystromite,* after Dr. Anders Byström, the senior author of the paper describing the structure of synthetic $MgSb_2O_6$.

Bystromite occurs in the antimony deposits of El Antimonio district in the province of Sonora in Mexico. The geology and mines of this district have recently been described by White and Guiza (2). The specimens provided by Dr. White came from La Fortuna and San Jose mines, the type material being that from La Fortuna. In August 1950 one of us visited El Antimonio, without however finding any more of this new mineral, perhaps because at that time little mining was in progress and many of the claims were not being worked.

* The spelling bystromite without the dieresis follows the convention established in the Seventh Edition of Dana's System of Mineralogy. See, for example, lindstromite (Vol. 1).

The ore of antimony in El Antimonio district is stibiconite, and the bystromite is always associated with it. The two minerals are so intimately admixed that the purest specimens of bystromite always contain some stibiconite. This is borne out by the powder photographs, which always show some stibiconite lines, even though this mineral can seldom be detected optically. All the bystromite we have seen has a blue-gray color in hand specimen, and it was thought for a while that this might be characteristic, until similar material proved to be pure or practically pure stibiconite. We have concluded that the only certain identification of bystromite is by means of powder photographs, combined with positive tests for magnesium and antimony.

As mentioned above, the color is blue-gray. The streak is pale gray. The hardness is about 7, but often appears to be much less, due to the porous nature of the specimens. The density measured with the Berman balance on selected grains from the analyzed material was found to be 5.5 ± 0.1. The chemical analysis indicates admixture of about 8% stibiconite, and when allowance is made for this (assuming a density of 3.9, found for pure stibiconite from El Antimonio) the density of the pure bystromite becomes 5.7. The density calculated from the analysis and the dimensions of the unit cell is 5.80. The agreement is reasonable in view of the assumptions behind the calculations and of the porous and impure nature of the material.

The mineral is massive and non-crystalline and optical examination shows that even the smallest grains consist of aggregates of submicroscopic particles. Mr. T. B. Rhinehammer of the Department of Chemistry of this university kindly examined samples in the electron microscope and reports that even at the highest magnification most of the material appeared as structureless aggregates; a few grains with roughly square or rectangular cross-sections were occasionally seen. The powder photographs confirm its fine-grained nature; the lines on the photographs of the mineral are not as sharp as those on photographs of synthetic $MgSb_2O_6$, and the back reflections are not clearly separated into α_1 and α_2 lines.

The measurements of x-ray powder photographs of bystromite, taken with Cu-K_α radiation in a camera of 114.6 mm. diameter, are reproduced in Table 1. Apart from the weak lines of admixed stibiconite, it can be completely indexed in terms of a tetragonal unit cell, with $a = 4.68$ Å, $c = 9.21$ Å., $c/a = 1.968$. A powder photograph of synthetic $MgSb_2O_6$, made by heating a mixture of MgO and Sb_2O_3 in the correct proportions in air at 1000° C. for 18 hours, showed complete agreement with that of bystromite. Byström, Hök and Mason (1) showed that for synthetic $MgSb_2O_6$ $a = 4.63$kX, $c = 9.21$kX, space group $P4/mnm$, with two formula groups in the unit cell.

TABLE 1. X-RAY POWDER DIFFRACTION DATA FOR BYSTROMITE (ANALYZED SPECIMEN), Cu-K_α RADIATION

Intensities estimated by visual inspection: 100=strongest line; 90=very strong; 80=strong; 50–70=medium; 30–40=weak; 20=faint; 10=very faint; *=stibiconite line.

I	*d*	*hkl*	*I*	*d*	*hkl*
30	5.93	*	40	1.39	116
40	4.63	100			303
70	4.19	101	10	1.28	206
100	3.32	110	30	1.19	323
30	3.09	*	20	1.13	226
40	2.96	*	10	1.10	330
30	2.69	112	30	1.06	316
90	2.57	103			413
50	2.34	200	10	1.04	420
20	2.25	113	10	1.00	109
30	2.08	210	20	.919	219
		202			510
30	2.04	211	30	.894	336
20	1.81	*			503
90	1.73	213	10	.864	426
40	1.65	220	10	.856	309
10	1.55	*	20	.832	523
20	1.54	006	10	.804	329
40	1.48	310	20	.786	516

Five specimens of bystromite from El Antimonio were selected for the determination of optical properties, thus permitting a measure of the variability. In general, all material examined was divisible into two types; a clear colorless material appearing as an aggregate of tiny crystals under crossed nicols, and turbid grains, also possessing aggregate structure.

In view of the fine-grained structure, the determination of optical characters was limited to birefringence and indices of refraction. The indices of refraction were determined by the immersion method, using a set of newly prepared high-index liquids, whose values were determined by the method of minimum deviation.

The birefringence of the clear material varied from 0.005 to 0.009. The higher value was determined in sample Z61, the analyzed specimen, in which both fractions were found. In this specimen the indices of refraction had a somewhat wider range in the clear fraction than the turbid material. Two specimens (Z90 and Z91) consisted entirely of clear colorless material and had identical indices of refraction—1.855 for the low value and 1.860 for the high value. The colorless fraction of Z61 had a slightly higher index range: 1.862 and 1.871.

The birefringence and indices of refraction are shown in Table 2. In the turbid fraction, the minimum and maximum indices of refraction

Table 2. Indices of Refraction and Birefringence of Different Specimens of Bystromite

	Turbid Fraction		Biref.	Clear Fraction		
Z61	1.908	1.915	0.007	1.862	1.871	0.009
Z87	1.904	1.908	0.004			
Z89	1.908	1.915	0.007			
Z90				1.855	1.860	0.005
Z91				1.855	1.860	0.005

are 1.904 and 1.915. For two of the specimens, Z61 and Z89, the indices were almost identical, while for a third, Z87, the lower index was 1.904 and the higher one 1.908. In specimens Z87 and Z89 turbid material made up the entire specimen. The only impurity observed in these specimens, which were carefully selected, was an occasional grain of quartz.

The variation in refractive indices from one specimen to another and within the same specimen may be due to variation in composition or to the disturbing effect of intimately admixed stibiconite.

A specimen from La Fortuna mine, only slightly contaminated with stibiconite, was selected for analysis. The admixed stibiconite could not be removed in any way. The only other contaminant was quartz, which was largely eliminated by careful picking. The chemical analysis (Table 3) was made by Mr. M. E. Coller, to whom we express our thanks. The material was found to dissolve completely (with the exception of the quartz) in concentrated HCl containing KI as a reducing agent. Antimony was precipitated with H_2S, the precipitate dissolved by digestion with H_2SO_4 and Na_2SO_4, the resulting solution reduced with Na_2SO_3, and the antimony determined by titration with standard $KMnO_4$ solution at 5° C. A separate sample was used for the determination of SiO_2, Al_2O_3, Fe_2O_3, CaO, and MgO. It was dissolved in the same way, and the insoluble quartz filtered off and weighed after ignition. The antimony was removed from the filtrate by precipitation with H_2S. Iron and alumina were precipitated with NH_4OH, calcium determined as oxalate, and magnesium as the phosphate. The $H_2O(+)$ was determined by the Penfield method. Oxygen was found by ignition of a weighed sample in a stream of purified hydrogen at 850° C. and weighing of the water thereby produced; this weight was corrected for the water in the mineral, and the remainder reported as reducible oxygen. The result obtained (21.9%) agrees, within the limits of accuracy of the method, with the theoretical value if all antimony is in the quinquivalent state (22.05%).

The analysis must first be corrected for the presence of admixed stibiconite. Using the figures for an analyzed stibiconite from El Antimonio and assuming that all the calcium is present in that mineral, the corrected analysis is obtained (Table 3, col. 3). The correction corresponds to 8.3%

TABLE 3. THE CHEMICAL COMPOSITION OF BYSTROMITE

	1	2	3	Molecular Proportions		
Insol.[a]	0.25					
Al_2O_3	0.08					
Fe_2O_3	0.03					
CaO	1.44	1.44				
MgO	6.65		6.65	Mg	165	0.65
Sb	67.15	6.25	60.90	Sb	500	1.97
O[b]	21.9	1.9	20.0	O	1306	5.14 } 6.00
H_2O-	0.17					
H_2O+	2.60	0.63	1.97	OH	218	0.86
	100.27					

1. Bystromite, La Fortuna Mine, El Antimonio, Sonora, Mexico, M. E. Coller, analyst.

2. Correction for admixed stibiconite.

3. Bystromite, corrected composition.

[a] Quartz.

[b] Theoretical for Sb_2O_5=22.05.

stibiconite, which agrees with the amount suggested by the powder photographs. The corrected analysis shows that magnesium is considerably deficient for the composition corresponding to the formula $MgSb_2O_6$. This deficiency is evidently balanced by a replacement of part of the oxygen by hydroxyl groups. The correctness of this supposition is indicated by the low density of bystromite compared to the calculated value for $MgSb_2O_6$, which is 6.08.

Little can be said regarding the mode of origin of bystromite. The deposits in which it is found consist of quartz veins containing irregular masses of stibiconite. White and Guiza believe that the stibiconite is secondary after stibnite, as is usual in most deposits of this kind. In the specimens which we have examined bystromite is intimately intermingled with stibiconite. It may have formed contemporaneously with the stibiconite or alternatively it can have been produced from stibiconite by metasomatic action of magnesium-bearing solutions. The latter theory is perhaps supported by the comparatively local distribution of bystromite at El Antimonio, where it apparently occurs in a few of the veins only. Further research in the field is however necessary to provide the evidence required for solving this question.

REFERENCES

1. BYSTRÖM, A., HÖK, B., AND MASON, B., The crystal structure of zinc metantimonate and similar compounds: *Arkiv. Kemi, Mineral., Geol.*, **15B,** no. 4 (1941).

2. WHITE, D., AND GUIZA, R., Antimony deposits of El Antimonio district, Sonora, Mexico: *U. S. Geol. Survey, Bull.* **962-B** (1949).

Manuscript received June 9, 1951.

TRANSPARENT, PLASTIC–BALL, CRYSTAL STRUCTURE MODELS*

R. A. Hatch, J. E. Comeforo, and N. A. Pace, *Electrotechnical Laboratory, U. S. Bureau of Mines, Norris, Tenn.*

Abstract

A method is described for making crystal structure packing models from transparent, hollow, plastic balls. The special advantage of such models is their high degree of transparency which permits easy identification of the different constituent atoms on the basis of their color and size, and which facilitates the study of atomic arrangement in the interior of the model. The plastic model is easier to assemble than most types; it is light-weight, and it can be handled without undue fear of breakage. The principal structural features of the phlogopite mica model are illustrated in color plates.

Introduction

The development of the science of crystal structure analysis, based on x-ray diffraction measurements, has created a need for three-dimensional models to represent the geometric and bond relationships between the various atoms or ions constituting crystal structures. Experience has shown that these relationships cannot be represented adequately in all aspects by two-dimensional drawings. Indeed, models become increasingly valuable as the complexity of the structure increases, because the mind experiences great difficulty in visualizing the many-sided aspects of intricate geometric structures. The primary use for such models is for teaching the fundamentals of x-ray crystallography and crystal chemistry to students. However, their usefulness by no means ends here, for they are used to good advantage by crystallographers to solve structure problems that involve multiple choices. Additionally, scientists have found them indispensable for understanding the dependence of crystal chemistry and crystal physics on structure such as, for example, the extensive investigations on the nature of gliding mechanisms in crystals by Seifert (12).

Types of Models

As might be expected, the need for crystal structure models has been met in a variety of ways, as attested by the many articles on the subject that have been published during the last 25 years. In most cases the sphere has been chosen to represent the atomic or ionic units comprising the structure because, to a reasonably good first approximation, atoms behave as if they were more or less rigid spheres in contact. The great

* Illustrated by phlogopite mica.

majority of the ball-unit models that have been described can be classified (6, 8) as ball-and-stick models (2, 3, 8, 9, 18, 19) or as geometric-packing models (4, 7, 10, 15, 16), although a third type, consisting of flattened spheres in contact, are preferred for models representing many types of organic compounds (6, 13, 14, 17).

Ball-and-stick models

Ball-and-stick models are constructed with small, widely-spaced balls which may represent the centers or nuclei of the atoms. The balls are usually held together by rods or wires representing the valence bonds, but sometimes they are strung on vertical wires stuck in a baseboard. Although models of this type are useful for showing atomic positions and elements of symmetry, they do not convey much of an idea of how the packing of the atoms controls the structure and many of the properties of the crystal. Nevertheless, ball-and-stick models are still popular, partly because they are relatively inexpensive and, in the case of a recently developed type (2), because they can very readily be constructed and taken apart. This agreeable state of affairs has been achieved by the use of rubber balls with molded holes in them, the balls being connected with plastic rods. An important feature of this type of model is its flexibility, making it especially useful for demonstrating distortion and strain effects.

Geometric-packing models

Geometric-packing models are constructed with spheres that are approximately proportional in size to the constituent atoms of the structures one wishes to represent. A second essential feature is that the spheres are packed together in contact with or in close proximity to each other, thus forming models that are similar in structure and proportional in size to the corresponding unit cells as determined from x-ray diffraction measurements. Consequently, such models, when carefully made, are very useful for semiquantitative measurements of dimensions, interplanar spacings, and angular relations of the structure as related to crystal form, growth peculiarities, cleavage, slip planes, twinning, polymorphism, and isomorphism. In addition, packing models are helpful in understanding the dependence of many physical properties on the structure such as density, hardness, refractive index, and thermal expansion, to mention a few of the more commonly measured ones.

A wide variety of materials are available for the construction of packing models, including metals, wood, cork, rubber, glass, celluloid "Ping-pong" balls, and various other kinds of plastics. Well-known models of this type have been made from wooden balls by Buerger (4) and his

students (7), the balls being joined together by metal pins. These models are very neat and strong, but they are time-consuming and expensive to build, especially those having complex structures. Although relatively inexpensive wooden balls suitable for the purpose may be purchased, their use involves considerable calculation and preparation, as indicated by the following steps in the procedure for constructing this type of model (4).

1. Calculation of the atomic environments in the actual crystals.
2. Adjustment of atomic environments to available material.
3. Calculation of drilling coordinates.
4. Painting the balls.
5. Drilling the balls.
6. Assembling the model.

It is evident that steps 1, 2 and 6 are involved in the construction of packing models from any type of material but that steps 3, 4, and 5 are primarily characteristic of wooden-ball models. In any case, it is the latter set of operations that contribute substantially to the time and expense of building wooden-ball models, although step 5 is facilitated by the use of a special ball-orienting device (5) attached to the drill press.

Possibly the major disadvantage in using opaque balls in a packing model is that the arrangement of the atoms usually is not clearly visible. For simple structures this obstruction of view may not be particularly important, but for complex structures involving many different kinds of atoms, several of which may occupy equivalent positions, it can be a serious disadvantage. In other words, the ability to see the arrangement of the atoms and to trace rows and planes of atoms through the structure in all possible directions are deemed to be highly desirable features of a packing model.

It was such considerations as these that led to the idea of a transparent, plastic-ball, packing model. However, the authors make no claim for the originality of this idea. Undoubtedly it had occurred to many scientists, as for example, Badgeley (1) who illustrated and described the use of several types of three-dimensional plastic models.

Transparent Plastic-Ball Packing Models

Development of the idea

The need for an improved type of crystal structure model became apparent during the early stages of the research on the synthetic analogues of mica, amphibole asbestos, and other complex silicate minerals currently being conducted at the Electrotechnical Laboratory. As a consequence, a method for making transparent plastic balls was developed at this laboratory during the early part of 1950, and models of phlogopite

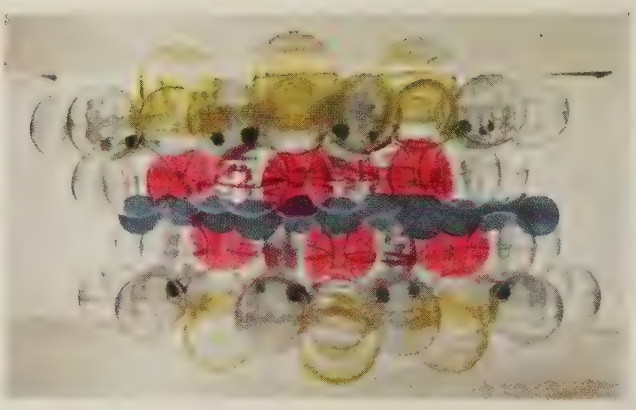

FIG. 1-*A*. A single layer of the phlogopite crystal structure viewed along the (130) direction, showing the layer structure and the "monoclinic shift" of $AlSi_3O_{10}F$ sheets. Yellow balls on top and bottom represent potassium in plane of cleavage; oxygen—colorless; fluorine or hydroxyl—pink; magnesium—blue; and silicon and aluminum—black.

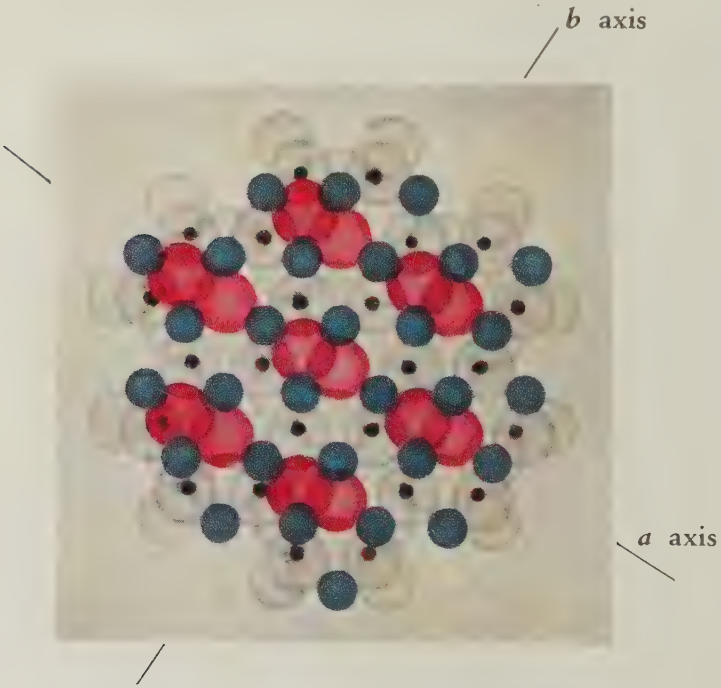

FIG. 1-*B*. A single sheet of the phlogopite structure viewed along the direction perpendicular to the layer structure, showing the hexagonal symmetry of the silicon-oxygen network, the trigonal symmetry resulting from the placement of magnesium between the sheets, and the monoclinic symmetry resulting from the shift of the fluorine (hydroxyl) ions.

mica and tremolite amphibole were assembled. Subsequently, the mica model was exhibited at the April 1950 meeting of the American Crystallographic Association at Pennsylvania State College, and the tremolite model was exhibited at the November 1950 meeting of the Mineralogical Society of America in Washington, D. C. The many expressions of interest in these models and requests for information on their construction, together with the fact that a review of the literature did not reveal any published description of models of this type, led to the preparation of this article.

General description

The most important features of the plastic crystal structure model can be illustrated to best advantage by natural color photographs such as those of the phlogopite mica structure reproduced in Fig. 1, *A* and *B*. It can be seen readily that the one feature that is new and unique to this type of model is its high degree of transparency. In this case, transparency was achieved by using colorless, transparent, plastic balls to represent the oxygen atoms that constitute about 72 per cent of the total volume occupied by the atoms in the mica structure. The other cations and anions represented in the model are distinguishable from the oxygen balls on the basis of color and usually by size. Thus, the fluorine or hydroxyl anions, whose ionic radii are nearly identical to that of oxygen, are represented by the pink balls; the potassium ions in (K-O_{12}) coordination are represented by the large yellow balls at the top and bottom of the model as viewed in Fig. 1-*A;* the magnesium ions in (Mg-O_4F_2) coordination are represented by the medium-sized blue balls; and the silicon plus aluminum ions in (Si, Al-O_4) coordination are represented by the small black balls. The sizes of the various balls are approximately proportional to the ionic radii of the atoms they represent. However, it should be noted that the mica model is not scaled to unit cell dimensions; several unit cells of the single-layer structure are represented.

The plastic model possesses other features and advantages that are not so readily evident from an inspection of the color reproduction. For example, the model is light in weight in spite of its relatively large size because the balls used in its construction are hollow and thin-walled. The mica model is 16″ in diameter by $9\frac{3}{4}$″ high, and it weighs 4 pounds. Because it is light in weight and relatively strong, the plastic model is readily transportable if normal precautions are practiced.

Considered as a structural problem, the strength of a packing model depends chiefly on the bonds or fastenings that hold the balls together. The plastic model differs from most types in that the balls are cemented together at their points of contact instead of threaded with wire or fast-

ened with pegs. Although a single, cemented bond is relatively weak, the model is sufficiently strong and rigid for practical purposes owing to the fact that each ball usually is bonded to six to eight neighbors. Those occupying corner or edge positions have fewer bonds, therefore, they are more likely to break loose. However, ordinary care in handling the model virtually eliminates this source of trouble. And even though breaks may occur occasionally, it is one of the advantages of the cemented bond that repairs are quickly and easily made.

Assembling the model

It has been indicated that the use of colored plastic balls and the cemented bond between balls eliminates steps 3, 4, and 5 followed by Buerger and Butler (4) in the construction of their wooden-ball models. As the other steps involved in the construction of packing models are adequately described in their paper, to which the reader is referred, present remarks are confined to those aspects of assembling the model that are peculiar to the plastic-ball type.

Assuming that the atomic environments in the actual crystal already have been calculated, and that a sufficient number of plastic balls of the proper sizes are available, the next step is that of assemblage. On the basis of the authors' limited experience, there appear to be two general approaches to the problem. Models of layered structures usually are prepared most easily by assembling layer by layer. With other structural types, it is usually convenient to first assemble small units, such as clusters, rows, or chains of atoms, and then to attach these together, thereby completing the model. Regardless of the procedure followed, it should be noted that serious distortion of the model can result from the use of imperfectly shaped balls unless proper compensation is made. In any case, minor imperfections in a model are difficult to avoid, but in general they do not detract significantly from its value. For example, small deviations from perfect alignment of the blue "magnesium" balls may be seen in Fig. 1-*B* of the mica model.

The cemented bonds are made by applying one or two drops of a suitable solvent to each of the points of contact between the plastic balls. Within a few seconds the solvent softens the plastic, and a circular area of contact $\frac{1}{8}$ to $\frac{1}{4}$ inch in diameter is formed. Within a minute or two the bond is strong enough to support the weight of several balls. However, several hours are required for the complete evaporation of the solvent and attainment of full bond strength. A suitable solvent for the acrylic resin type of plastic used in these models (Lucite or Plexiglas) is ethylene dichloride.

More specific directions for assembling plastic ball models, which

would be applicable to all types, cannot be formulated. Each structural type presents its own peculiar problems which are best mastered by the experience gained during the actual construction of a model.

The Manufacture of Plastic Balls

Before undertaking the development of plastic crystal structure models, an attempt was made to obtain suitable plastic balls from a dozen or more companies that manufacture or fabricate plastics. Failing to locate a source of supply of plastic balls of the desired sizes and colors, there seemed to be no alternative but to make them ourselves. As other investigators who wish to construct this type of model may encounter the same difficulty, a brief description of the method used at this laboratory may prove useful.

The essential steps in the process were as follows: The plastic material (Lucite or Plexiglas) was obtained in the form of transparent and translucent sheets of various colors. The colors were selected on the following basis: A colorless, transparent plastic was used for the principal anion, for example, oxygen in oxides and silicates; light-colored, transparent plastics were used for large cations, such as potassium; darker-colored, transparent plastics for the cations of intermediate size, such as magnesium; and dark- or light-colored, translucent plastics for the small cations, such as silicon and aluminum. After choosing an appropriate set of colors for the particular model to be built, circles for forming hemispheres were cut from the plastic sheets (Fig. 2-*A*), each circle having a diameter $\frac{1}{4}$ inch larger than the intended sphere diameter. Balls that were larger than 1 inch in diameter were made from $\frac{1}{8}$ inch sheet, whereas smaller balls were made from 1/16 inch sheet.

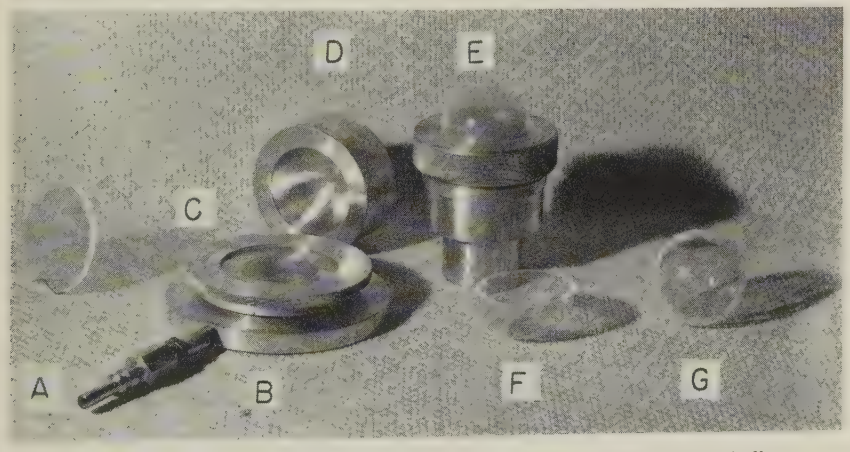

Fig. 2. Apparatus for the manufacture of transparent, hollow, plastic balls.

A plastic disk was clamped tightly in an assembly machined from aluminum, consisting of a base plate (Fig. 2-*B*) threaded to receive a clamping ring (Fig. 2-*C*). Each size ball required a different clamping ring bored to the correct diameter (2 inches for the oxygen ball illustrated in Fig. 2). The base plate contained an air inlet to a pressure chamber which was sealed on one side by the plastic disk. This entire assembly was placed in an oven and heated at about 300° F. for 5 to 6 minutes to soften the plastic. Then (1) the assembly was removed quickly from the oven (wearing asbestos gloves), (2) a cold, hemispherical, aluminum mold (Fig. 2-*D*) whose diameter was the same as that of the hole in the ring plate was fitted into a recess machined in the ring plate, (3) an air line was attached to the inlet by means of a quick-acting air coupler, and (4) a plastic hemisphere was blown into the cold mold, which was manually held in place. The mold contained several very small holes to prevent the trapping of air between the plastic and the mold. After several seconds, the air pressure was reduced and the entire assembly was quenched in water to cool and harden the plastic. The resulting dome of plastic material had a rim, similar to that on a derby hat, which had to be cut off to form a true hemisphere. This operation was done on a lathe using the usual cut-off tool and a special holder (Fig. 2-*E*), which was chucked in the lathe. The plastic dome was clamped around its rim to the end of the holder by means of a threaded ring, which was bored to the correct diameter.

After cutting off the rim on the plastic dome, the trimmed edge of each hemisphere (Fig. 2-*F*) was ground flat by rubbing it on a sheet of fine emery paper. Before cementing pairs of hemispheres together, each one was cleaned with a rag to remove dust and grease. The final step in making a ball was to press together two hemispheres and apply several drops of ethylene dichloride along the edge of the crack. The solvent was drawn rapidly around the crack by capillary attraction, welding the halves within a few seconds. The finished ball (Fig. 2-*G*) should not deviate significantly from a true sphere, otherwise it will introduce distortions in the model.

Although it appeared that the above-described method of making plastic balls was one of the simplest that could be devised, the number of balls made per man-hour was quite limited, averaging about ten. As a result, the cost of manufacturing them was undesirably high. This serious disadvantage can be overcome only by the adoption of a mass-production method. A step in this direction would be the use of gang molds, in which several hemispheres were blown at one time. Even more desirable would be the development of a technique whereby a complete ball could be formed in one operation. As such techniques as these

require more elaborate and costly equipment, especially molds of different sizes, they would be practical only if one desires to manufacture a large number of balls at an efficient rate. It is to be hoped that some company will undertake this development to supply scientists with transparent plastic balls in sizes and colors suitable for use in crystal structure models.

Utility of the Model

As stated earlier, the ability to see the arrangement of the atoms and to trace rows and planes of atoms through the structure in all possible directions is deemed to be a highly desirable feature of a packing model. To illustrate the utility of transparent models, several structural relationships that can be observed on a packing model of phlogopite, such as the one shown in Fig. 1, are described briefly.

One sees that a single layer of the phlogopite structure is composed of two $(AlSi_3O_{10})_n$ sheets which, together with hydroxyl or fluorine anions, are bound together by magnesium cations. Especially worth noting is the virtual hexagonal arrangement of the oxygen anions in the individual sheets, yet the single-layered mica structure as a whole is monoclinic. The lower symmetry is the result of a displacement of one sheet over the other by an amount approximately equal to one-sixth of the *a* unit cell dimension (indicated by the displacement of the pink fluorine anions in Fig. 1). The model shows that such a displacement is necessary to stabilize the structure. The shift minimizes the repulsion between the apex oxygen anions in opposing sheets and makes it possible for each magnesium to be octahedrally coordinated as $Mg\text{-}O_4F_2$.

Hendricks (11) has shown that polymorphism occurs rather commonly among micas of the phlogopite-biotite subfamily. He described hexagonal, monoclinic, and triclinic multi-layer forms and showed how they might be derived from the single-layer form by the application of various combinations of symmetry operations. Not only is the transparent model useful for illustrating these symmetry operations, but also it shows clearly the structural basis for the origin of multi-layer mica polymorphs. During the growth of aphlogopite crystal, the magnesium ions continually have a choice of occupying one or the other of two sets of positions between the sheets, each position being related to the other by a rotation of 180° about an axis perpendicular to the sheet. For each set of positions, the displacement of one sheet over the other may take place in any one of three equivalent directions 120° apart, or a total of six equivalent directions 60° apart. Thus, a large number of multi-layered mica polymorphs are possible owing to the simple fact that certain ions in the mica structure have a choice of several equivalent posi-

tions in that structure during crystal growth. It is to be expected, however, that the frequency of occurrence of phlogopite polymorphs composed of many layers should be small compared with the frequency of single-, double-, and three-layer forms.

The geologist long has made use of percussion and pressure figures (glide planes or secondary cleavages) to determine the crystallographic directions of sheet mica and for the purpose of relating common structural imperfections to these directions. Due to the ease with which one can visually trace rows and planes of atoms through the transparent model, it is readily apparent that the orientation of percussion figures parallel to (010), (110), and ($1\bar{1}0$) is controlled by the rows of densely packed oxygen atoms in the basal hexagonal network. On the other hand, the orientation of pressure figures parallel to ($13l$) and ($10l$) (planes that are inclined about 67° to the prominent basal cleavage of mica) is controlled by the densely packed planes of inner or "apex" oxygen and magnesium atoms.

Although many other geometric and structural realationships can be observed on the mica model, those described above will serve to illustrate the special advantages inherent in the use of transparent, packing models for the study of crystal structures. A detailed description of the structural features and the defects found in mica will be given in a later paper. In the meantime, it is hoped that this description will serve to stimulate the interest of teachers, students, and scientists in the construction and use of transparent, plastic models. If a demand for such models can be created, the problem of finding a manufacturer for plastic balls in the necessary sizes and colors will be greatly simplified.

Acknowledgments

The authors are greatly indebted to Messrs. I. N. Dockery, E. E. Dwyer, M. L. Kinamon, L. L. Hall, P. J. Jones, and W. A. Hassett for making the plastic balls; to Mr. E. F. Nichols for suggestions on molds; and to Drs. Alton Gabriel, Wilhelm Eitel, and J. A. Kohn for reviewing the manuscript.

This work was financed in part by the Office of Naval Research, the Bureau of Ships, and the Army Signal Corps on the synthetic mica contract.

References

1. Badgeley, C. D., Three-dimensional models: *Plastics*, **3**, 56, 90, (Oct. 1945).
2. Brenner, F. C., New crystal model sets aid education and research: *Laboratory*, **18**, No. 1.
3. Brode, W. R., and Board, C. E., Molecular models in the elementary organic laboratory; I: *Jour. Chem. Educ.*, **9**, 1774 (1932).

4. Buerger, M. J., and Butler, R. D., A technique for the construction of models illustrating the arrangement and packing of atoms in crystals: *Am. Mineral.*, **21,** 150–172 (1936).
5. Buerger, M. J., A device for drilling oriented holes in spheres required in the construction of crystal structure models: *Rev. Sci. Instruments*, **6,** 412–416 (1935).
6. Campbell, J. A., Structural molecular models: *Journ. Chem. Educ.*, **25,** 200–203 (1948).
7. Dorris, J. E., Frondel, C., Gussow, W. C., Lopez, V. M., Lord, C. S., Parrish, Wm., and Shimer, J. A.: Atomic packing models of some common silicate structures: *Am. Mineral.*, **23,** 65–84 (1938).
8. Fisher, D. J., and Stevens, E. H., Building nuclear crystal structure models: *Am. Mineral.*, **22,** 268–278 (1937).
9. Grunér, J. W., A new method of building crystal structure models: *Am. Mineral.*, **17,** 35–37 (1932).
10. Hauser, J. E., A simple method of building close-packed molecular and crystal models: *Journ. Chem. Educ.*, **18,** 164–166 (1941).
11. Hendricks, S. B., Polymorphism of the micas: *Am. Mineral.*, **24,** 729–771 (1939).
12. Seifert, Hans, Einseitiges Gleitvermögen und seine kristallstrukturelle Deutung: *Zeit. f. Phys.*, **124,** 144–153 (1944). *Ibid.*, Verformung von Salzkristallen: *Zeit. f. Elektrochem.*, **50,** 78–91 (1944). *Ibid.*, Über das Gleitvermögen der Glimmer: *Heidelberger Beitrage zur Kristallographie*, **1,** 486–504 (1948).
13. Stuart, H. A., New molecular models: *Zeit. physik. Chem.*, **27,** 350–358 (1934).
14. Taylor, H. S., Construction of molecular models: *U. S. Patent No. 2,308,402, Jan. 12, 1943.*
15. Terpstra, P., Wooden balls for structure models: *Naturrw. Tijdschr.*, **21,** 284–290 (1940).
16. Wear, J. I., Steckel, J. E., Fried, M., and White, J. L., Clay mineral models: Construction and implications: *Soil Science*, **66,** 111–117 (1948)
17. Wepster, B. M., Stuart's Atomkalotten: *Rec. trav. chim.*, **65,** 318 (1946).
18. Wooster, W. A., The construction of molecular models: *Jour. Sci. Instruments*, **21,** 125 (1944).
19. Wyckoff, R. W. G., and Ksanda, C. J., A simple model for illustrating the atomic arrangements in crystals: *Am. Jour. Sci.*, **11,** 377–380 (1926).

Manuscript received June 14, 1951.

ANTIGORITE FROM THE VICINITY OF CARACAS, VENEZUELA*

H. H. Hess, R. J. Smith, *Princeton University, Princeton, N. J.*,

AND

G. Dengo, *Direccíon de Minería y Geología, Caracas, Venezuela.*

Abstract

A chemical analysis of antigorite from Venezuela indicates the formula $Mg_7Si_5O_{13}(OH)_8 \cdot n\ H_2O$, rather than the formula for serpentine commonly given. *X*-ray diffraction data, thermal analysis data, optical and physical properties of the antigorite are given.

Field evidence indicates that the chrysotile type of serpentine goes to antigorite under dynamothermal conditions slightly higher than the chlorite-biotite subfacies of the greenschist facies. In the process chromite and magnetite are gradually resorbed and disappear leaving a rock composed entirely of antigorite.

Introduction

A monomineralic antigorite rock was found by Dengo in the course of making a geological map of the Federal District of Venezuela (Dengo, 1949). Inasmuch as antigorite has been the subject of considerable debate in petrological and mineralogical literature it was thought worth while to describe this specimen in some detail.

Chemical Composition

Though much has been written on antigorite there are no superior chemical analyses of the mineral available in the literature so far as the writers are aware. An analysis by Peck is given in Table 1. The material analyzed is a rock consisting almost entirely of antigorite, the only impurity noted being a fraction of a per cent of unidentified dusty inclusions of fibrous character and having much lower indices of refraction than antigorite.

An attempt to recalculate the analysis into the usual serpentine formula, $Mg_6Si_4O_{10}(OH)_8$ shows a poor fit (columns 7 and 8, Table 1). It is evident that the Mg:Si ratio is close to 7:5. A number of trial calculations to determine the probable relationship of (OH) and H_2O in the mineral assuming Mg:Si = 7:5 resulted in arriving at columns 5 and 6 of Table 1 as the most likely solution. The formula deduced indicates 21 O(OH) of which 8 are (OH) and leaves a remainder of H_2O. What information is available in the literature indicates a rather wide range of variation in H_2O content—from slightly less than 12 weight per cent to somewhat over 14 per cent. This suggests that the number of molecules

* Princeton Investigations of Rock Forming Minerals, number 6.

TABLE 1. CHEMICAL COMPOSITION

	1	2	3	4	5	6	7	8
			Ion Ratios		Cations to 21 O(OH)	Theoretical	Cations to 18 O(OH)	Theoretical
SiO_2	43.60	Si^{+4}	726	$741\frac{1}{2}$	4.97	5	4.16	4
			$15\frac{1}{2}$					
Al_2O_3	1.03	Al^{+3}	20					
			$4\frac{1}{2}$					
Cr_2O_3	.02	Cr^{+3}	—					
Fe_2O_3	.90	Fe^{+3}	11					
FeO	.81	Fe^{+2}	11	1048	7.03	7	5.88	6
MnO	.04	Mn^{+2}	$\frac{1}{2}$					
MgO	41.00	Mg^{+2}	1017					
NiO	.16	Ni^{+2}	2					
CaO	.05	Ca^{+2}	1					
Na_2O	.01	Na^{+1}	—					
K_2O	.03	K^{+1}	1					
H_2O+	12.18	Ti^{+4}	—					
H_2O-	.08	H	1201	1201	8.05	8	7.57	8
TiO_2	.01	O	3131					
	99.92	H_2O	78	78	1.40	1 to 3		

Analyst Lee C. Peck, Rock Analysis Laboratory, University of Minnesota.

Density 24° C/4° C = 2.607.

Approximate general formula: $Mg_7Si_8O_{13}(OH)_8 \cdot nH_2O$, Ni^{+2}, Fe^{+2}, Mn^{+2}, etc., may substitute for Mg^{+2} in part.

$Al^{+3}Al^{+3}$, $Fe^{+3}Al^{+3}$, $Cr^{+3}Al^{+3}$, etc., may substitute for $Mg^{+2}Si^{+4}$ to a limited extent.

of H_2O in the formula (represented by "n" in Table 1) might vary from $n=1$ to $n=3$. In the present analysis n is near the lower value, $n=1.4$.

X-RAY DIFFRACTION DATA

The powdered antigorite was examined with a low powered Philips *x*-ray spectrometer. Three records were made using an iron target with a manganese filter and three with a copper target and nickel filter. The averaged values for three runs on each sample are given in Table 2, columns 2 and 3. In the conversion of 2θ to d spacings the tables made by Switzer, Axelrod, Lindberg and Larsen (1948) were used. In these K_α Cu is 1.5418 Å. and K_α Fe is 1.9373 Å. The estimated relative intensities are given in columns adjacent to the d spacings of columns 2 and 3 but are not directly comparable to the intensities of column 1.

Dr. H. S. Yoder of the Carnegie Geophysical Laboratory very kindly offered to run the same powder on a Philips *x*-ray spectrometer having greater accuracy with respect to 2θ and higher resolving power. His results are given in Table 2 column 1. The following pertinent data with

TABLE 2. *X*-RAY DIFFRACTION PATTERN

1		2		3	
Copper Target (Yoder)		Iron Target (aver. 3)		Copper Target (aver. 3)	
d_{hkl} Å	I	d_{hkl} Å	I	d_{hkl} Å	I
8.05	10	7.97	½	—	
7.30	<400	7.23	8	7.34*	8
6.95	24	—	—	—	—
6.51	16	—	—	—	—
6.10	6	—	—	—	—
5.78	8	—	—	—	—
4.67	6	—	—	—	—
4.62	7	4.62	1	4.64	1
4.27	4	4.27	1	—	—
4.01	6	3.99	2	—	—
3.63	<300	3.612	10	3.625	10
3.51	24	—	—	—	—
2.88	2	—	—	—	—
—	—	2.777?	½	—	—
—	—	2.686?	¼	2.685	¼
2.59	4	—	—	—	—
2.57	8	2.554	½	—	—
2.52	70	2.522	5	2.531	6
2.46	9	2.443	½	2.462	¼
2.42	38	2.419	6	2.429	1
2.39	9	2.392	½	2.399	2
2.35	5	2.286	½	—	—
2.237	6	2.239	½	2.243	¼
2.208	7	2.199	¼	2.209	1
2.167	22	2.163	6	2.167	3
2.150	20	—	—	—	—
2.126	4	2.119	½	—	—
2.035	4	2.032	½	—	—
1.886	3	1.884	½	—	—
1.830	12	1.833	½	1.833	½
1.815	23	1.813	4	1.820	2
1.781	14	1.779	2	1.784	1
1.755	4	—	—	—	—
1.736	10	1.733	2	1.738	¼
1.688	2	—	—	—	—
1.640	2	—	—	—	—
1.584	3	—	—	—	—
1.560	12	1.559	½	1.559	1
1.540	9	—	—	—	—

*=7.28 compared to Muscovite standard.

TABLE 2—(*continued*)

1		2		3	
Copper Target (Yoder)		Iron Target (aver. 3)		Copper Target (aver. 3)	
d_{hkl} Å	I	d_{hkl} Å	I	d_{hkl} Å	I
1.535	9	1.532	½	1.537	¼
1.524	13	1.520	½	1.523	2
1.509	8	—	—	—	—
1.497	10	1.497	½	1.496	1
1.479	7	1.477	½	1.480	½
1.466	6	—	—	—	—
1.462	6	—	—	1.460	½
1.451	10	1.451	2	1.452	½
1.448	9	—	—	—	—
1.443	5	—	—	—	—
1.438	3	1.440	½	—	—
—	—	—	—	1.339	½
1.328	3	—	—	—	—
—	—	—	—	1.314	1
—	—	—	—	1.279	2
—	—	—	—	1.261	1
—	—	—	—	1.209	1

regard to the measurements were supplied by Yoder:

Dry powder, −150 +250 mesh x-rayed in shallow cell mount using Philips Geiger counter spectrometer. Copper radiation, nickel filter 25 Kv, 20 Ma, scan speed ½° per minute, time constant 4 seconds, angular aperture 1°, receiving slit 0.006 inch, goniometer radius 170 mm. Calibrated with silicon using:

Plane	°2θ (Cu K)
111β	=25.654
220α_1	=47.302
311α_1	=56.122
400α_1	=69.130
331α_1	=76.376
422α_1	=88.030

Error is approximately 0.01° 2θ over region investigated, intensities subject to error as probable result of preferred orientations in sample. Scale intensity arbitrary. Spacings based on Cu K_α=1.5418 Å in range 10°–40° 2θ and on Cu K_{α_1}=1.54050 for 40°–70° 2θ.

THERMAL ANALYSIS DATA

Thermal curves of the antigorite from room temperature to 1000° C. are given in Fig. 1. They show a strong endothermal peak at 782°±5° C.

and a broad shallow endothermal peak starting a little above 100° C. The exothermal peak at 810° to 830° C. commonly reported for antigorite is absent. The broad shallow low temperature endothermal effect probably represents the loss of H_2O while the larger peak at 782° C. represents dissociation of the antigorite structure probably with loss of its (OH).

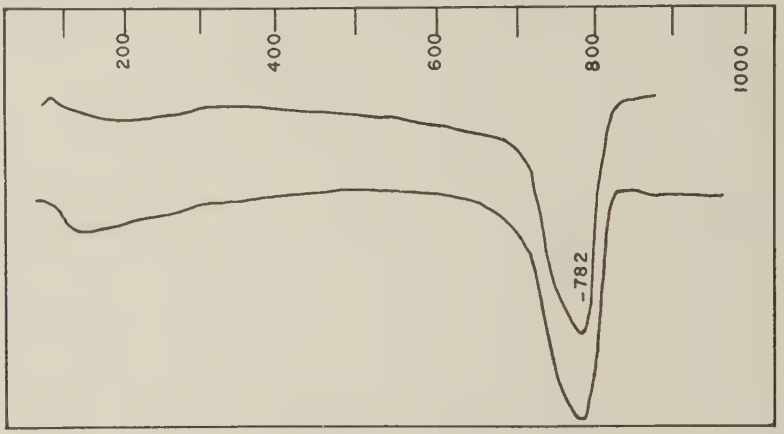

FIG. 1. Thermal curves for antigorite DF180. Scale along top of diagram is in degrees C.

PHYSICAL PROPERTIES

The antigorite rock is pale green in color, massive rather than foliated and has a dull luster rather than the resinous or the waxy luster common for serpentines. It is comparatively hard, approximately $3\frac{1}{2}$ on Mohs scale.

The density determined on seven 20 milligram fragments with a Berman balance using toluene averaged 2.603, 23° C/4° C. A seven gram cube weighed in air and toluene gave a density of 2.609, 24° C/4° C.

Examination in thin section and in powders shows a well developed {001} cleavage. The presence of a {100} parting is indicated in the powders but is rarely seen in the thin sections.

The antigorite occurs in bladed aggregates. The crystals reach as much as a millimeter in length and are generally elongated parallel to *a*. There is considerable variation in grain size, some portions of the rock being exceedingly fine-grained aggregates.

OPTICAL PROPERTIES

The indices of refraction were determined by immersion methods using a temperature control cell on the microscope stage and sodium light. Taking advantage of the {100} parting and {001} cleavage the three principal indices of refraction were determined as follows with an accuracy of ± 0.0005:

$$N_z = 1.5670$$
$$N_y = 1.5660$$
$$N_x = 1.5615$$
$$N_z - N_x = 0.0055$$

The optic angle was measured on the universal stage and found to be $47\frac{1}{2} \pm 1/2°$ with dispersion $r > v$ moderate and sign negative.

Z is in the plane of the {001} cleavage and X is perpendicular to this cleavage so far as it was possible to determine. A very slight departure from parallel or perpendicular might be overlooked inasmuch as the cleavage traces are not quite straight as a rule and many of the antigorite blades have been slightly bent. The same difficulty arises in trying to measure the crystallographic angle β which is close to 90°. Y is parallel to the b crystallographic axis, assuming the cleavage represents {001} and the parting {100}.

Under crossed nicols the antigorite shows anomalous interference colors. This is one of the most distinctive features of most antigorite as compared to chrysotile. Grains oriented so that they show moderate to low path difference—in the grays—have a distinctly bluish tint.

Petrological Data and Conclusions

Antigorite has not been found in laboratory investigations of the MgO-SiO_2-H_2O system, hence its field of stability is not known (Bowen and Tuttle, 1949). Two natural modes of occurrence have often been described: (1) in dynamothermally metamorphosed ultramafic igneous rocks; and (2) as bastite, a replacement of magnesian orthopyroxene in serpentinized periodotites. In the latter the bulk of the rock has been serpentinized to form chrysotile serpentine or serpophite, probably a variety of the same mineral.

Thus far the grade of metamorphism at which chrysotile serpentine goes to antigorite has not been determined. Smith, however, has found chrysotile serpentinites intruded into a sedimentary sequence in the Los Teques area, south of Caracas, Venezuela, which have suffered low grade metamorphism without alteration to antigorite. The sediments were originally tuffs, silicified tuffs, cherts, shales and a minor amount of limestone. Metamorphism altered them to phyllites with the following minerals characteristic: fine flakes of sericite and chlorite, recrystallized chert now fine-grained quartz aggregates, chloritoid, minor amounts of fine biotite locally and epidote. This assemblage represents the chlorite-biotite subfacies of the greenschist facies. Inasmuch as the serpentinite has been subjected to this metamorphism and has not developed antigorite, a higher degree of metamorphism must be required to produce the

change. In the northern portion of the area mapped by Smith metamorphic rocks belonging to the albite-epidote amphibolite facies are found. In these the serpentinites have been antigoritized. The rocks containing these serpentinites have probably suffered two episodes of metamorphism, one preceding and the other subsequent to the intrusion of the ultramafics. Whether the second stage of metamorphism was equivalent to the albite-epidote amphibolite facies, or slightly lower in grade, cannot be exactly determined. This places the grade at which antigoritization takes place as above the chlorite-biotite subfacies of the greenschist facies, but equal to or slightly less than the albite-epidote amphibole facies.

Antigorite develops generally in rocks which have been subjected to strong shearing stress, so far as the writers are aware. Pure thermal metamorphism such as where basaltic magmas intrude serpentinites does not generally result in the development of antigorite, even up to temperatures where regenerated olivine is being developed in the ultramafic (Leech 1949). This suggests that the reaction chrysotile→antigorite occurs at rather low temperature but is so sluggish that ordinarily it does not occur unless assisted by the catalytic action of shearing. Shearing alone, however, is evidently not enough to produce antigoritization or it would be found in the greenschists mentioned above. Both shearing and a temperature higher than that at which the greenschist facies develops must generally be necessary to promote this reaction even though antigorite may well be the stable phase at the temperature of formation of the greenschist facies. A favorable chemical environment may result in crystallization of antigorite without shearing as indicated below in the discussion of bastite.

The Formation of Bastite

Bates and Mink (1950) postulate that chrysotile and antigorite are morphologically analogous to endellite and kaolinite crystallizing as tubes and plates, respectively. All of these are layered structures. In the case of chrysotile the silicon-oxygen layer of the unit cell is slightly smaller than the $Mg(OH)_2$ layer thus resulting in curvature and the formation of tubes. Bates and Mink point out that antigorite commonly contains more Al_2O_3 than chrysotile. The substitution of 4Al for 6Mg in a small percentage of the structure would be sufficient to make the layers equal in size, thus eliminating the curvature. Inasmuch as olivine is virtually devoid of Al_2O_3 and magnesian orthopyroxene normally contains 1.5% of Al_2O_3, the replacement of olivine by chrysotile and enstatite by bastite (antigorite) might thus be explained. If, however, the conclusion presented in the present paper that antigorite does not have the same Mg:Si

ratio as chrysotile, then the formation of the antigorite plates also may be explained on other grounds. The relative increase in Si^{+4} ions with respect to Mg^{+2} ions in the structure could also account for the lack of curvature of the antigorite plates. In this case the replacement of olivine by chrysotile and enstatite by bastite might be related to the higher silica content of pyroxene and antigorite relative to olivine and chrysotile.

Acknowledgments

The field work during which the antigorite was discovered was carried out under the sponsorship of the Direccion de Minería y Geología of the Estados Unidos de Venezuela, A. Schwarck, Director. The laboratory work was a detail in a broad investigation of the Caribbean region being carried on under a contract between the Office of Naval Research and Princeton University (N6onr-27008).

The work of Aruja, Brandenberger, Epprecht and Niggli, Caillere, Gruner, Hargraves and Taylor, Hey and Bannister, Selfridge, Warren and Bragg and others on serpentines have formed much of the background for this paper but have not been particularly cited in the text.

References

Bates, T. F., and Mink, J. F. (1950), Morphology and structure of serpentine minerals: *Tech. Rept.* No. **III,** Contract number N6onr 26914, Pennsylvania State College, Sept. 1950. 30 pp.

Bowen, N. L., and Tuttle, O. F. (1949), The System MgO-SiO_2-H_2O: *Bull. Geol. Soc. Am.*, **60,** 439–460.

Dengo, G. (1949), Geology of the Caracas Region, Venezuela. Ph.D. Thesis, Princeton University. (*Bull. Geol. Soc. Am.*, in press).

Leech, G. B. (1949), Petrology of the ultramafic and gabbroid intrusive rocks of the Shulaps Range, British Columbia: Ph.D. Thesis, Princeton University.

Switzer, G., Axelrod, J. M., Lindberg, M. L., and Larsen, E. S. 3rd (1948). Tables of *d* Spacings for Angle 2 θ: *U. S. Geological Survey, Circular* **39.**

Manuscript received June 29, 1951.

DETERMINATION OF SMALL QUANTITIES OF DOLOMITE BY DIFFERENTIAL THERMAL ANALYSIS*

Richards A. Rowland and Carl W. Beck,†
Shell Oil Company, Houston, Texas.

Abstract

A method which will be most useful in evaluating the product of laboratory synthesis of dolomite is described. The dolomite content of carbonate rocks can be quantitatively determined by differential thermal analysis when as little as 0.3 percent dolomite is present. Thermograms of prepared and natural mixtures containing small amounts of dolomite and calibration curves relating the area of the thermogram loops to the dolomite content are presented and compared with recast chemical analyses.

The general study of the problem of dolomites and the process of dolomitization frequently requires the determination of small quantities of the mineral dolomite in mixtures with other carbonates and other minerals. Likewise, in experimenting with different methods for the laboratory synthesis of dolomite, it is important that even a small percentage of the mineral be detected. Until now, there has been no reliable technique for this purpose. In small quantities, dolomite is most likely to be fine grained and intimately mixed with other carbonates; hence, the microscopic and staining techniques are not suitable. The recasting of chemical analyses becomes especially difficult when the magnesium content is less than 2 per cent, and, of necessity, the magnesia in the chemical analysis is assigned arbitrarily to the mineral dolomite. Frequently it is suggested in the literature that some of the magnesium may be present in the form of periclase or brucite. Dolomite in quantity less than 2 percent may not be detected by x-ray techniques.

In recent years the differential thermal analysis technique has been applied to the study of carbonate minerals (Cuthbert and Rowland, 1947), (Beck, 1950), (Faust, 1950), (Gruver, 1950). This technique can be used to distinguish dolomite in calcite-dolomite mixtures, both qualitatively and quantitatively. With an extremely sensitive recording apparatus and a controlled furnace atmosphere of CO_2, dolomite may be determined in prepared mixtures of dolomite and calcite when only 0.3 percent dolomite is present.

Differential thermograms of dolomite and calcite in an air atmosphere and in a CO_2 atmosphere are shown in Fig. 1. The thermogram of dolomite heated in air consists of two interfering loops. The first accompanies

* Publication No. 13, Exploration and Production Research Division, Shell Oil Company, Houston, Texas.

† Geology Department, University of New Mexico, Albuquerque, New Mexico.

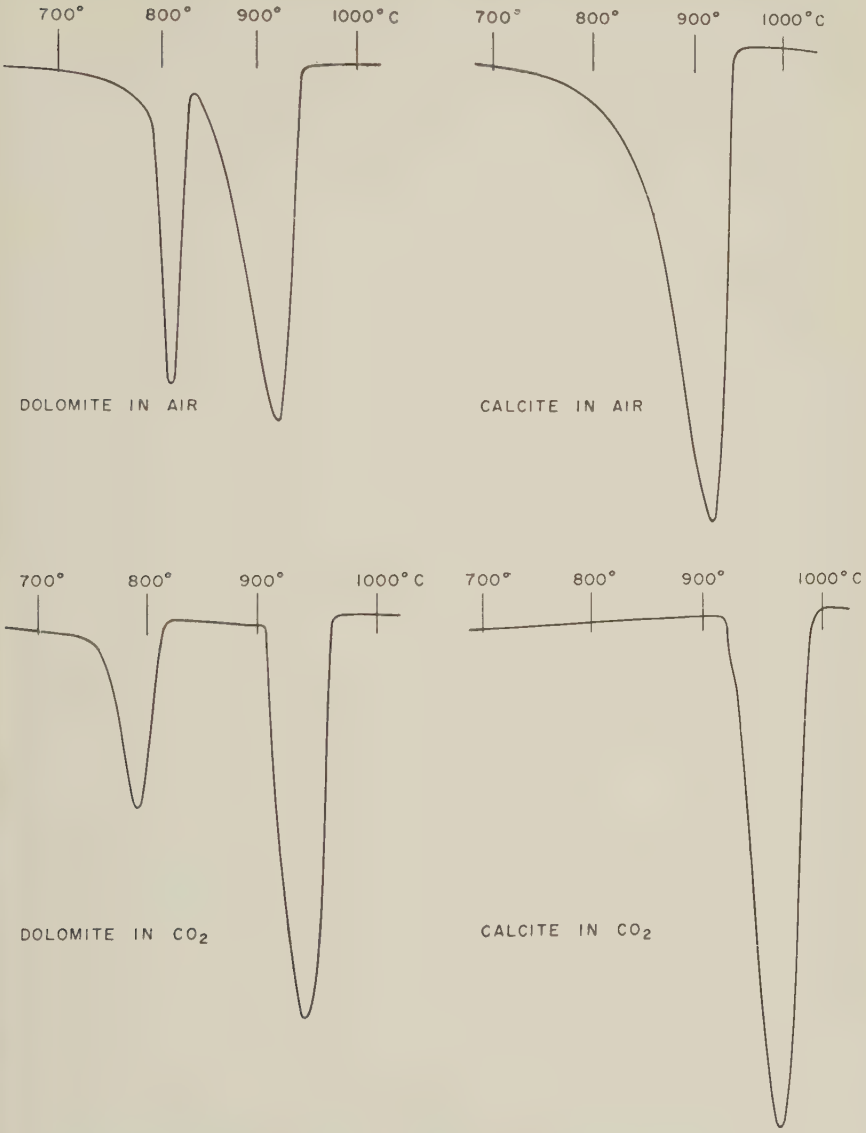

FIG. 1. Dolomite and calcite in air and carbon dioxide.

the decarbonation of the $MgCO_3$ part of the dolomite; the second, the dissociation of CO_2 from the $CaCO_3$ part of the dolomite. In a CO_2 atmosphere these two loops are separated largely because the dissociation temperature of the $CaCO_3$ portion is raised and the inflections are

sharpened (Fig. 1). Therefore, thermograms of dolomite in a CO_2 atmosphere are more useful for accurate measurement of the loop areas. In mixtures of dolomite and calcite, the $CaCO_3$ loop of dolomite and the calcite loop are superimposed. With decreasing amounts of dolomite the $CaCO_3$ loop becomes larger and the $MgCO_3$ loop diminishes. When the $MgCO_3$ loop becomes so small that it cannot be measured with any degree of accuracy, the technique described in the next paragraph is employed to overcome this difficulty.

The apparatus used is a standard DTA arrangment with platinum (platinum 10 per cent, rhodium difference) thermocouples, the e.m.f. from which is measured with a Leeds and Northrup Type R galvanometer having 50 ohms shunting resistance (sensitivity, 0.5 microvolt per mm.) (Rowland, 1948). The galvanometer deflections are recorded with a Beckman Photopen. With this apparatus dolomite normally is recorded with a 110-ohm series resistor in the galvanometer circuit. During the recording of the loop between 700° C and 800° C, when small amounts of dolomite are present, a 10-ohm series resistor replaces the 110-ohm resistor in the circuit. After the completion of this loop and before the inception of the loop between 900° C and 1000° C, the series resistance is changed to 310 ohms in order to contain the second loop within the dimensions of the chart. The sample is heated in a furnace atmosphere of CO_2, according to the method described by Rowland and Lewis (1951).

The area of each loop, described by the loop and a line joining the points at which a line 45° to the base line (Fig. 2, 1st two curves) is tangent to the maximum inflexion of the beginning and ending of each loop, was measured by planimetering. The method used can be extended to cover the range of dolomite-calcite mixtures, from 100 percent dolomite to 100 percent calcite. Berg's (1945) complicated construction of a line to close the loop was found to be unnecessary.

The experimental results of six prepared mixtures of dolomite and calcite are shown in Fig. 2; and the area of the $MgCO_3$ loop, as well as the percent factor of

$$\frac{\text{Area } MgCO_3 \text{ loop} \times 100}{\text{Area } MgCO_3 \text{ loop} + \text{Area } CaCO_3 \text{ loop}}$$

is shown in Table 1. Figure 3 plots the information of Table 1. Figure 4 presents the experimental results, using the above method, for three samples of the Trenton limestone, Clinton County, Illinois. Table 2 tabulates the area of the $MgCO_3$ loop, the percent factor, and the percent dolomite as determined by each method. Table 3 gives the chemical analyses of the three limestones. All the magnesia has been assigned arbitrarily to dolomite though there is no optical, x-ray, or staining evidence to indicate the presence of dolomite.

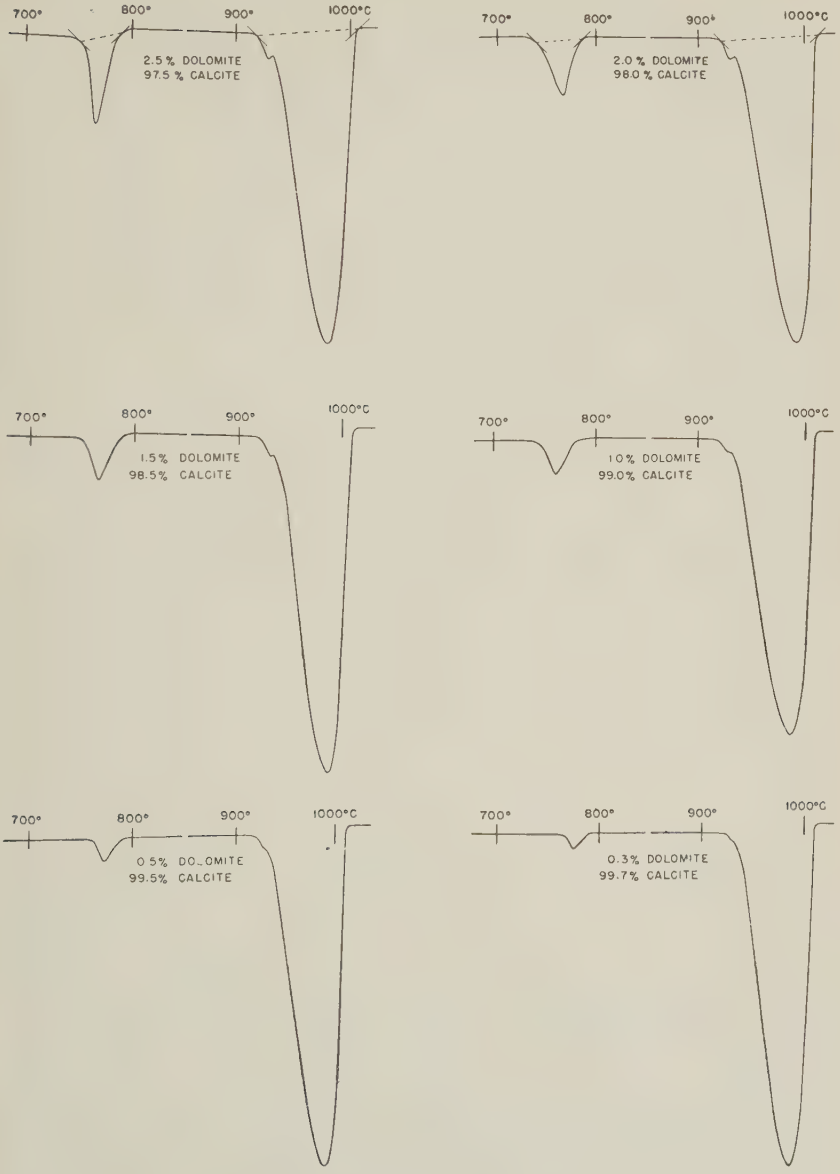

FIG. 2. DTA Calibration Curves of Small Percentages of Bureau of Standards Dolomite and Iceland Spar Calcite—10 Ohms and 310 Ohms. Undiluted.

TABLE 1. DATA FROM DTA CURVES OF SYNTHETIC MIXTURES OF BUREAU OF STANDARDS DOLOMITE AND ICELAND SPAR CALCITE

Percent Dolomite	Percent Factor	Area $MgCO_3$ Loop
2.5	8.58	68
2.0	6.90	54
1.5	5.04	39
1.0	3.27	25
0.5	1.85	14
0.3	0.93	7

TABLE 2. DATA FROM TRENTON LIMESTONE, CLINTON COUNTY, ILLINOIS

Depth	Percent Factor	Percent Dolomite from Percent Factor	Area $MgCO_3$ Loop	Percent Dolomite from Area $MgCO_3$ Loop
3496	2.38	0.64	15	0.70
3951	0.39	0.11	3	0.14
3960	1.98	0.55	14	0.67

TABLE 3. CHEMICAL ANALYSIS OF TRENTON LIMESTONE SAMPLES, CLINTON COUNTY, ILLINOIS

	Sample Number		
	3946	3951	3960
CaO	50.60%	54.00%	54.70%
MgO	0.64	0.65	0.04
CO_2	40.40	43.10	43.00
R_2O_3	1.20	0.44	0.27
−105° C	0.05	0.07	0.07
−1050° C	40.60	42.80	43.30
Recast percent dolomite	1.76	1.67	0.10

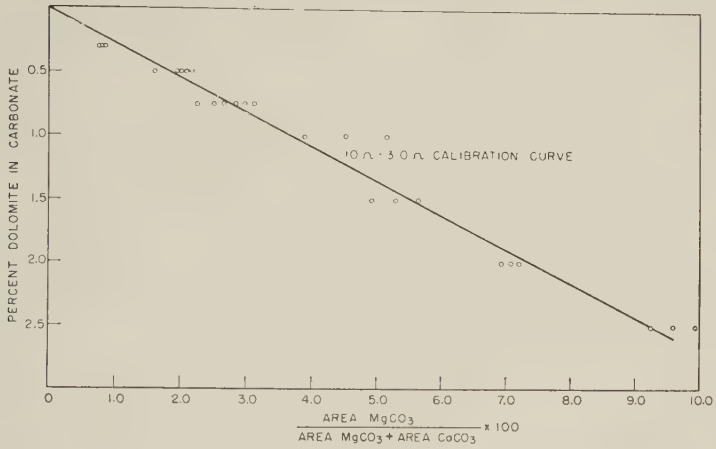

a

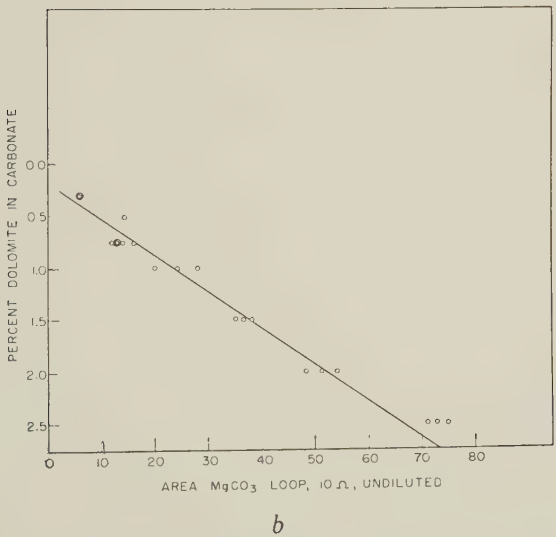

b

FIG. 3. Calibration Curves of Small Quantities of Dolomite Plotted (*a*) Percent Factor vs. Percent Dolomite in Carbonate, and (*b*) Area $MgCO_3$ vs. Percent Dolomite in Carbonate.

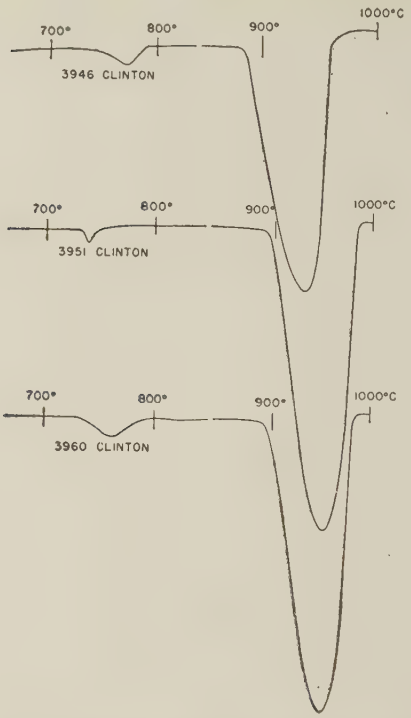

FIG. 4. DTA Curves of Three Samples from Trenton Limestone, Clinton County, Illinois.

The writers wish to express their appreciation for the helpful suggestions and assistance of Drs. Harold T. Byck and John F. Burst of the Exploration and Production Research Division staff.

REFERENCES

BECK, CARL W. (1950), Differential thermal analysis curves of carbonate minerals: *Am. Mineral.*, **35,** 985–1013.

BERG, L. G. (1945), Area measurements in thermograms for quantitative estimates and the determination of heats of reaction: *Compt. Rend. Acad. Sci. U.S.S.R.*, **49,** 648–651.

CUTHBERT, F. L., AND ROWLAND, RICHARDS A. (1947), Differential thermal analysis of some carbonate minerals: *Am. Mineral.*, **32,** 111–116.

FAUST, G. T. (1950), Thermal analysis studies on carbonates. I. Aragonite and calcite: *Am. Mineral.*, **35,** 207–224.

GRUVER, R. M. (1950), Characteristic heat effects of some carbonates: *Jour. Amer. Ceramic Soc.*, **33,** 90–101.

ROWLAND, RICHARDS A. (1948), Differential thermal analysis apparatus: *Exploration and Production Research Division, Report* **101,** 41 pp.

ROWLAND, RICHARDS A., AND LEWIS, DONALD R. (1951), Furnace atmosphere control in differential thermal analysis: *Am. Mineral.*, **36,** 80–91.

Manuscript received June 28, 1951.

TRICLINIC GNOMONOSTEREOGRAMS

D. Jerome Fisher, *University of Chicago, Chicago, Illinois.*

Abstract

The preparation of a combined gnomonic and stereographic projection of a triclinic crystal is a relatively simple procedure if carried out by the technique herein outlined. The method is suitable not only for the standard orientation, but for the first and second permutations; these latter are likely to be met when using the Buerger *x*-ray precession camera. Such a projection is useful because: (1) it enables one to make graphical calculations of crystal constants avoiding any gross errors; (2) it clearly shows which angles are obtuse, which acute; (3) it serves as a base from which to derive useful formulae. The principles herein elucidated may be applied readily to non-triclinic crystals, which are always simpler to handle.

Introduction

The preparation of a combined gnomonic and stereographic projection (a gnomonostereogram) of a triclinic crystal offers definite advantages in the interpretation of its geometry. Such a diagram can be made with both projections drawn to the same scale if the stereographic plane is taken as a central one of the unit sphere and if after drawing the gnomonic plane, it is projected orthographically to the stereographic plane; of course the two projection planes are originally parallel to one another, but offset by unit distance. This matter has been discussed previously by Fisher (1941, pp. 315–319.)

When the goniometry of crystals was limited to the optical technique, there was perhaps no advantage in preparing gnomonostereograms in any but the standard orientation, that with the *c*-axis at the center of the primitive circle. But when the goniometry is carried out with the *x*-ray precession camera (Buerger, 1944), it becomes desirable to handle both permutations of this orientation; first, with the *a*-axis at the center, second with the *b*-axis at the center; compare the orthorhombic cases (Palache *et al.* 1944, Fig. 11, p. 20); see Table 1. This matter is further discussed in the following paper.

Table 1. Triclinic Orientations

Orientation	At center	$\phi=0°$	$\phi=90°$	Unit value† (polar axial ratio)	Fig.
Standard	[*c*]	[*b**]	$[a]^t$	r_0	1
First Permutation	[*a*]	[*c**]	$[b]^t$	p_1	2
Second Permutation	[*b*]	[*a**]	$[c]^t$	q_2	3

† The radius of the fundamental sphere; see Palache *et al.* (1944, Fig. 1, p. 9).

The graphical technique herein described has the big advantage that it leaves no doubt as to which angles are obtuse and which acute. Thus in handling the formulae given, one need not be greatly concerned with negative trigonometric functions, or with the question of whether a given ϕ-angle is greater or less than 90°. These details all show up clearly in the projections, unless one of the interaxial angles is very close to 90°.

In preparing the gnomonostereograms it is time-saving to work on protractor paper with the aid of a scale for plotting (polar) ρ-angles in either projection; such scales are available as the top one of the projection protractor[1] (Fisher, 1941, Fig. 1) or of the crystallographic protractor (Barker, 1922, Fig. 1). Failing these, one may use an ordinary metric scale with the r. tangent tables (Goldschmidt, 1934, p. 162; or Wherry, 1920, p. 119), remembering that when one plots x° gnomonic, this is equivalent to plotting 2x° stereographic under the conditions stated.

The three figures used to illustrate this paper are based on chalcanthite with elements $a:b:c$ of 0.5693:1:0.5548 and $\alpha = 97°34'$, $\beta = 107°17'$, $\gamma = 77°26'$ (see Fisher, 1952). Had an example been chosen with obtuse γ, some of the conditions would be changed, but these should cause no difficulty to one employing the graphical techniques here outlined.

Definitions and Symbols

It is intended that this section may be consulted as one carries out the graphical procedure outlined in the remainder of the paper. Further definitions appear in an earlier paper (Fisher, 1941, pp. 296–300). First it may be desirable to make clear what is meant by the cyclographic projection (Fisher, 1941, pp. 315–316); the contrast between this and the stereographic is brought out in Table 2. The cyclographic is a *direct*

Table 2. Cyclographic and Stereographic Projections

Element to project	Type of Projection	
	Cyclographic (direct)	Stereographic (reciprocal)
Zone Axis (or other *direction*)	ZONE POLE (a point) Symbol [uvw]^c	ZONE LINE (a great circle) Symbol [uvw]^s
Crystal face (or other *plane*)	FACE LINE (a great circle) Symbol (hkl)^c	FACE POLE (a point) Symbol (hkl)^s

projection; that is, the element itself is projected (after moving it parallel to itself so that it goes through the center of the fundamental sphere).

[1] Obtainable from Ward's Natural Science Establishment, Rochester, N. Y.

On the other hand, the stereographic is a *reciprocal* projection; a normal to the element is projected. Thus in the stereographic a *plane* is represented by a point (a face pole) obtained by erecting a line through the center of the fundamental sphere normal to the plane. Where this line cuts the fundamental sphere establishes the face pole in the spherical projection. If this point is joined to the center of projection (typically the south pole) the resulting line cuts the plane of the stereogram at the point of the desired face pole. A *direction* appears in the stereographic as a line (a zone line) which is derived in a similar manner from the trace of the plane normal to the direction through the center of the fundamental sphere. Otherwise the stereographic and cyclographic projections are identical. In the past many writers have shown an axis or direction as a point in a so-called stereographic projection. This has, of course, confused the student and militated against clear thinking. This is particularly true when indicatrix directions and planes are added to those of morphology or structure. On the projection itself, the point (needle-prick) representing the pole of a face or other *plane* (stereographic) is surrounded by a small circle, one standing for the pole of a zone axis or some other *direction* (cyclographic) is in a small square. Thus $\boxdot^a$ on the projection corresponds to $[a]^c$ in the text; either one refers to the cyclographic projection of the *a*-axis.[2] The symbol $[a]^t$ is used to represent the *trace* of the *a*-axis; that is, the line in which a plane including [*a*] and the axis whose direct projection lies at the center of the primitive (divided) circle, cuts the plane of the projection.

Elements of the reciprocal lattice are indicated by the use of an asterisk*. Since the gnomonic projection of a crystal is nothing but a scaled enlargment of the 1-level of the reciprocal lattice (with the addition of "fractional" face poles, etc.), the polar axes of Goldschmidt (P, Q, & R) are closely related to *a**, *b**, and *c**. Goldschmidt (1934, Fig. 102, p. 67) shows his polar axes as going through the "center" of the crystal and also lying in the plane of the gnomonogram. In this paper the reciprocal axes are taken to go through the center of the crystal while two of the unprimed polar axes lie in the polar elements plane and two of the primed polar axes lie in the gnomonic plane. Elements in the polar elements plane are unprimed; those in the gnomonic plane are primed. The gnomonic plane in the standard orientation, is tangent to the unit sphere where it is cut by the *c*-axis; the polar elements plane is parallel the gnomonic plane, but goes through the point where the R = the *c**-axis cuts

[2] If one is also plotting in the gnomonic (reciprocal) and euthygraphic (corresponding direct) projections, the superscripts *g* and *e* may be employed; see Fisher, 1941, p. 318. As here used, the superscript *o* refers to a direct (i.e., non-reciprocal) version of the orthographic projection.

the unit sphere; thus r_0 is equal to unit distance; see Palache *et al.*, 1944, Fig. 1, p. 9. Goldschmidt's polar interaxial angles λ, μ, and ν, are the optical goniometric equivalents of the reciprocal lattice angles α^*, β^*, and γ^*, respectively, measured by *x*-ray goniometry.

A given face-pole or other *point* in the stereographic projection may be spoken of as a *ster*-point; a similar point in the gnomonic projection is a *gnom*-point. A *ster*-triangle is one whose sides are great circles which join any three non-colinear ster-points; it is the stereographic projection of a spherical triangle. The *primitive gnomonogram* (PG) gives the mesh of the reciprocal lattice at the scale of the projection; for standard orientation, it is the parallelogram made by joining the following gnomonic face-poles: (001), (101), (111), and (011). This excepts the hexagonal; see Barker, 1922, Figs. 27–34. The corresponding figure in the stereographic projection is the *primitive stereogram* (PS)

Case 0. Standard Orientation. Fig. 1

Given α, β, and γ (*or* γ^*); also for #7 the axial ratio $a:b:c$, *or* p_0' and q_0'.

1. Draw $[a]^t$, the *x*-axis, as a radius of the primitive circle of $r=1$ at $\phi=90°$ (Fig. 1*a*). Plot $[b]^t$ anticlockwise $(180-\gamma^*)°$ from $[a]^t$. [γ^* can be obtained from (3) below].

2. Plot the *gnom*-point E′ along $[b]^t$ at $(\alpha-90)°$ to the right of [*c*]. The line cE′ may be designated s_0'. If desired (see #5) also plot $[b]^c$ along $[b]^t$ at $\alpha°$ *ster.* to the right of [*c*].

3. Plot the *gnom*-point F′ along $[a]^t$ at $(\beta-90)°$ down from [*c*]. Then $cF'=x_0'$. If desired (see #5) also plot $[a]^c$ along $[a]^t$ at $\beta°$ *ster.* down from [*c*].

4. Erect normals through *common points*[3] E′ and F′ to $[b]^t$ and $[a]^t$ respectively, intersecting at R′, the gnomonic face pole (001). These normals are the P′ and Q′ axes of Goldschmidt, and E′ and F′ are their zone centers. The point R′ has cartesian coordinates x_0' and y_0' and polar coordinates ϕ_0 and d_0', where $d_0'=\tan \rho_0$.

5. If desired, one may draw the great circle $(001)^c$ using R′ as center and as radius the distance R′ to $[a]^c$ or R′ to $[b]^c$. This circle contains the cyclographic projection of γ, and also serves to locate $[\bar{a}]^c$ and $[\bar{b}]^c$. The ster-triangle *a b c* may be designated the *primitive octant.*

6. The *ster*-point (Fig. 1*b*) corresponding to R′ is $[c^*]^c$. A great circle (which may be traced from a stereonet) from here to [b^*] (which lies on the

[3] So-called because each one lies on both a polar axis and the trace of a (direct, primitive) crystal axis. Each of these points (geometrically) bisects the line joining the cyclographic projections of the (+) and (−) ends of the crystal axis on whose trace it lies.

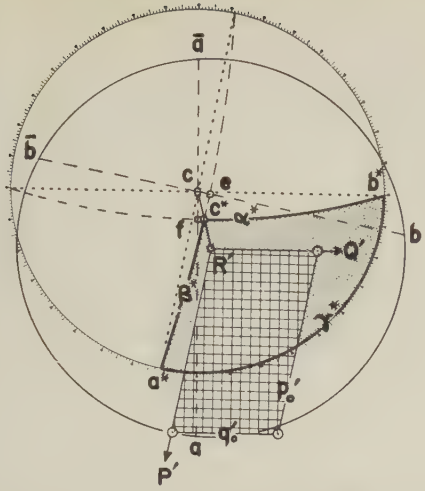

(b) Polar octant with primitive gnomonogram

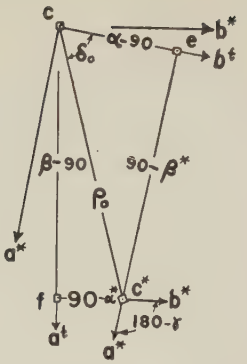

(c) Stereographic

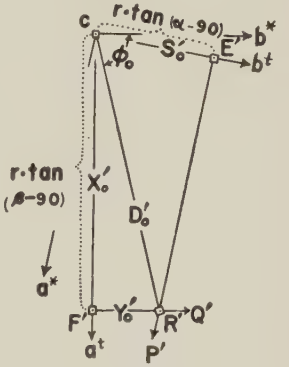

(d) Gnomonic

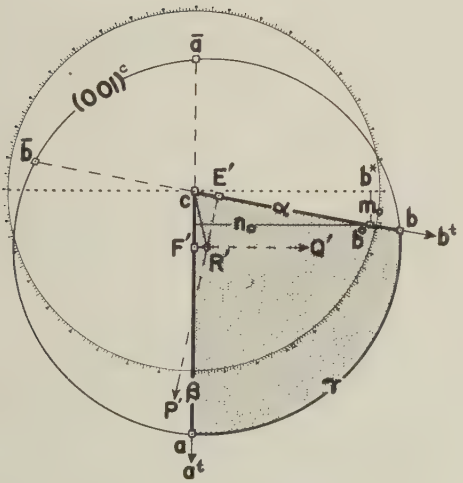

(a) Primitive octant

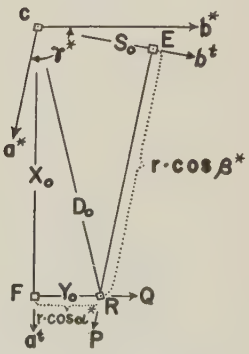

(e) Polar elements

FIG. 1. Gnomonostereogram of chalcanthite, standard orientation. a. The entire projection with primitive circle (graduated) of r=1. The primitive octant is stippled. b. The entire projection with primitive of r=1. The polar octant is stippled and the primitive gnomogram is reticulated. c. Central portion of stereoprojection (see *b*) with r=10. d. Central portion of gnomonogram with r=5. Note that distances D_0', S_0', X_0', and Y_0' are capitalized to emphasize $r \neq 1$. e. Central portion of polar elements plane with r=5. Here also D_0, S_0, X_0, and Y_0 are capitalized, since $r \neq 1$.

primitive at $\phi = 0°$) is the cyclographic projection of α^*. $[a^*]$ is γ^* degrees clockwise around the primitive from $[b^*]$. A great circle from $[a^*]$ to $[c^*]$ is the cyclographic projection of β^*. The ster-triangle $a^*b^*c^*$ may be called the *polar or reciprocal octant*. Its vertices are the face-poles of the three pinacoids in the stereographic projection.

7. The primitive gnomonogram (PG) may be plotted from the values of p_0' and q_0'; these may be obtained from the elements of crystallization by using (9) and (10) below. It should be noted that Figs 1*a* and 1*b* can be combined to advantage in a single diagram if colored inks (or sharp, colored crayons) are used to outline the primitive gnomonogram (blue), polar octant (green), and primitive octant (red).

Useful formulae—Standard Orientation

$$\cot \alpha^*/2 = \sqrt{\frac{\sin(\sigma - \beta)\sin(\sigma - \gamma)}{\sin\sigma \sin(\sigma - \alpha)}} \tag{1}$$

$$\cot \beta^*/2 = \sqrt{\frac{\sin(\sigma - \alpha)\sin(\sigma - \gamma)}{\sin\sigma \sin(\sigma - \beta)}} \tag{2}$$

$$\cot \gamma^*/2 = \sqrt{\frac{\sin(\sigma - \alpha)\sin(\sigma - \beta)}{\sin\sigma \sin(\sigma - \gamma)}} \tag{3}$$

Where $\sigma = (\alpha + \beta + \gamma)/2$

Note: Exactly analogous formulae permit one to compute α, β, or γ from α^*, β^*, and γ^*. Graphical solutions are given by Bond (1950, p. 239).

$$\cos \rho_0 = \sin \alpha^* \sin \beta = \sin \alpha \sin \beta^* \tag{4}$$

$$\tan \phi_0 = \cos \beta / \cot \alpha^* \tag{5}$$

$$s_0' = \cot \alpha = cE' \tag{6}$$

$$x_0' = \cot \beta = cF' \tag{7}$$

$$y_0' = \cot \alpha^* / \sin \beta = F'R' \tag{8}$$

$$q_0' = c/(\sin \alpha^* \sin \gamma) = c/(\sin \alpha \sin \gamma^*) \tag{9}$$

$$p_0' = c/(a \cdot \sin \beta \cdot \sin \gamma^*) = c/(a \cdot \sin \beta^* \sin \gamma) \tag{10}$$

Note: Any vector in the gnomonic plane (Fig. 1*d*) may be converted to one in the polar elements plane (Fig. 1*e*) by multiplying it by $\cos \rho_0$; thus $p_0' \cos \rho_0 = p_0$, etc. Thus the polar elements plane is like a gnomonogram at a slightly reduced scale; it does not represent an orthographic projection, in spite of the fact that $d_0 = \sin \rho_0$. Distances in these two diagrams (where $r = 5$) are represented by capital letters (D, S, X, and Y) to emphasize that $r \neq 1$.

The denominator of (9) is called v_2 by Bond (1946, p. 33) and by Evans (1948, p. 61). It is here designated n_0; it is the y-coordinate

(Fig. 1*a*) of the orthographic projection of one unit on [*b*]; that is, of where [*b*] cuts the unit sphere. The corresponding x-coordinate, called v_1 by Bond and by Evans, is here designated m_0, where:

$$m_0 = \sin \alpha \cos \gamma^* = n_0/\tan \gamma^* \qquad (11)$$

These coordinate values are useful in triclinic calculations according to Evans. They may be shown in the projection if one plots [*b*]° (the orthographic projection of unit distance on [*b*]) along [*b*]^t to the right of [*c*] a distance of sin α. Then n_0 is parallel to [*b**] and extends from [*b*]° to [*a*]^t, while m_0 is parallel to [*a*]^t and extends from [*b*]° to [*b**].

Derivation of equations

The first three are given in Buerger (1942, p. 355).

To get (4) apply Napier's rules (Phillips, 1947, p. 184) to right-angle triangles *c e c** and *c f c** of Fig. 1*c* where r = 10. Here *e* and *f* are ster-points corresponding to gnom-points E′ and F′, respectively.

To obtain (5) note from Fig. 1*e* that $y_0 = \cos \alpha^*$; thus $y_0' = \cos \alpha^*/\cos \rho_0$. But from Fig. 1*d* $\cot \bar{\phi}_0 = \tan \phi_0 = \cot \beta/y_0'$. Thus $\tan \phi_0 = \cot \beta/(\cos \alpha^*/\cos \rho_0)$. Substitute in this the value of cos ρ_0 from (4), and get (5).

(6) and (7) are self evident.

To get (8) substitute the value of cos ρ_0 from (4) in the equation $y_0' = \cos \alpha^*/\cos \rho_0$ obtained in deriving (5).

(9) and (10) are modified from Palache *et al.* (1944, p. 13) equations [24] and [25], where the latter should be written $c = (q_0' \cos \rho_0 \sin \nu)/\sin \mu$.

Case 1. First Permutation. Fig. 2

Given: β, γ, and α (or α^*) also for #7 the axial ratio *a*:*b*:*c*, *or* q_1' and r_1'.

1. Draw [*b*]^t, the *y*-axis, as a radius of the primitive circle at $\phi = 90°$ (Fig. 2*a*). Plot [*c*]^t anticlockwise $(180 - \alpha^*)°$ from [*b*]^t. [α^* can be obtained from (1)].

2. Plot *gnom*-point F_1' along [*c*]^t at $(\beta - 90°)$ to the right of [*a*]. The line aF_1' may be designated s_1'. If desired also plot [*c*]^c out $\beta°$ *ster.* to the right of [*a*].

3. Plot *gnom*-point G_1' along [*b*]^t at $(90 - \gamma)°$ up from [*a*]. (This assumes γ is acute). Then $aG_1' = y_1'$. If desired also plot [*b*]^c down $\gamma°$ *ster.* from [*a*].

4. Erect normals through common points F_1' and G_1' to [*c*]^t and [*b*]^t respectively, intersecting at P′, the gnomonic face-pole (100). These normals are the Q′ and R′ axes of Goldschmidt, and F_1' and G_1' are their zone centers. The point P′ has cartesian coordinates y_1' and z_1', and polar coordinates ϕ_1 and d_1', where $d_1' = \tan \rho_1$.[4]

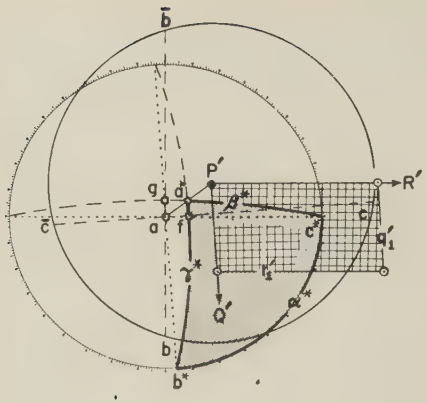

(b) Polar octant with primitive gnomonogram

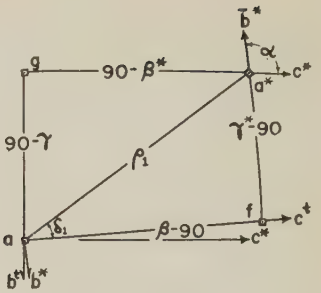

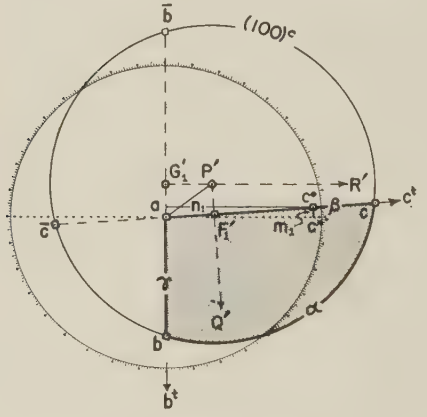

(a) Primitive octant

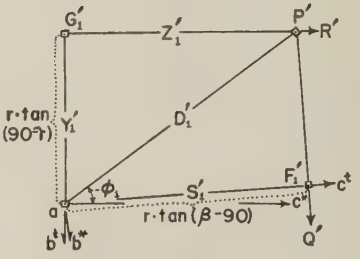

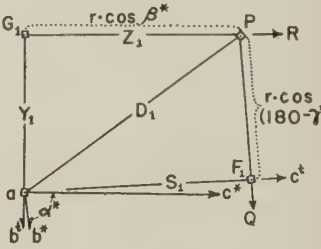

FIG. 2. Gnomonostereogram of chalcanthite, first permutation. a. The entire projection with primitive circle (graduated) of r=1. The primitive octant is stippled. b. The entire projection with primitive of r=1. The polar octant is stippled and the primitive gnomonogram is reticulated. c. Central portion of stereoprojection (see *b*) with r=10. d. Central portion of gnomonogram with r=5. Note that distances D_1', S_1', Y_1', and Z_1' are capitalized to emphasize that r≠1. e. Central portion of polar elements plane with r=5. Here also D_1, S_1, Y_1, and Z_1 are capitalized, since r≠1.

---

[4] ϕ_1 and ρ_1 are used here as the polar coordinates of (100). Palache *et al.* (1944, p. 20) use these in the orthorhombic system as the position angles of any given face in the first permutation.

5. If desired, draw great circle $(100)^e$ with center P′ and radius from here to $[c]^e$ or $[b]^e$; this circle contains $(\alpha)^e$ and also serves to locate $[\bar{b}]^e$ and $[\bar{c}]^e$.

6. The *ster*-point (Fig. 2*b*) corresponding to P′ is $[a^*]^e$. A great circle from here to $[c^*]$ (which lies on the primitive at $\phi = 0°$) is the cyclographic projection of β^*. Clockwise around the primitive α^* degrees from $[c^*]$ is $[b^*]$. The great circle from $[b^*]$ to $[a^*]$ is the cyclographic projection of γ^*.

7. The primitive gnomonogram may be plotted from the values of q_1' and r_1'; these may be obtained from the elements of crystallization by using (17) and (18) below.

Useful formulae—First permutation

$$\cos \rho_1 = \sin \beta^* \sin \gamma = \sin \beta \sin \gamma^* \quad (12)$$

$$\tan \phi_1 = \cos \gamma / \cot \beta \quad (13)$$

$$s_1' = \cot \beta = aF_1' \quad (14)$$

$$y_1' = \cot \gamma = aG_1' \quad (15)$$

$$z_1' = \cot \beta^* / \sin \gamma = G_1'P' \quad (16)$$

$$q_1' = a/(\sin \alpha \sin \gamma^*) = a/(\sin \alpha^* \sin \gamma) \quad (17)$$

$$r_1' = a/(c \cdot \sin \alpha^* \cdot \sin \beta) = a/(c \cdot \sin \alpha \cdot \sin \beta^*) \quad (18)$$

Note: Any vector in the gnomonic plane (Fig. 2*d*) may be converted to one in the polar elements plane (Fig. 2*e*) by multiplying it by cos ρ_1; thus $q_1' \cos \rho_1 = q_1$, etc.

Further note: In a manner similar to that described under "standard orientation," one (Fig. 2*a*) may plot $[c]^\circ$ out on $[c]^t$ to the right of $[a]$ a distance of sin β. The *z*-coordinate of $[c]^\circ$, called n_1, is given by (19). It is the distance to $[b]^t$ going parallel to $[c^*]$. The y-coordinate of $[c]^\circ$, called m_1, is given by (20). It is the distance to $[c^*]$ going parallel to $[b]^t$.

$$n_1 = \sin \alpha^* \sin \beta = \sin \alpha \sin \beta^* \quad (19)$$

$$m_1 = \cos \alpha^* \sin \beta = n_1 / \tan \alpha^* \quad (20)$$

It is clear that the denominator of (18) may be replaced by $c \cdot n_1$.

Case 2. Second Permutation. Fig. 3

Given α, γ, and β (or β^*); also for #7 the axial ratio $a:b:c$, *or* p_2' and r_2'.

1. Draw $[c]^t$, the *z*-axis, as a radius of the primitive circle at $\phi = 90°$ (Fig. 3*a*). Plot $[a]^t$ anticlockwise $(180 - \beta^*)°$ from $[c]^t$. [β^* can be obtained from (2)].

2. Plot *gnom*-point G_2' along $[a]^t$ at $(90 - \gamma)°$ to the left of $[b]$. (This assumes that γ is acute). The line bG_2' may be designated s_2'. If desired, also plot $[a]^e$ out $\gamma°$ *ster.* to the right of $[b]$.

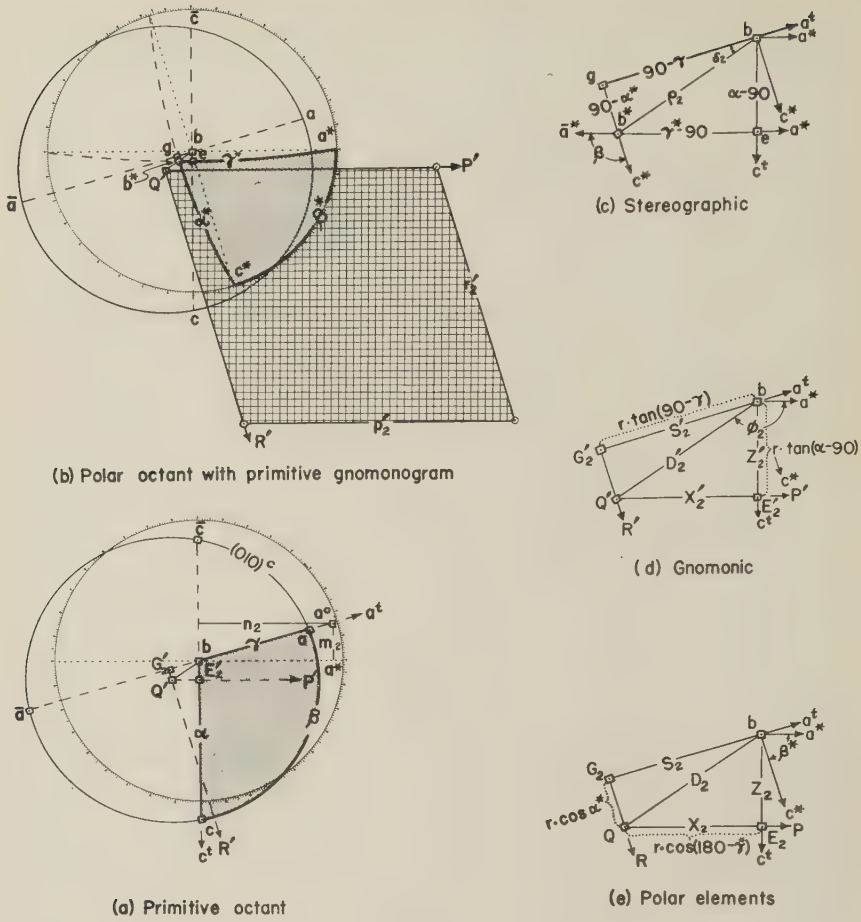

FIG. 3. Gnomonostereogram of chalcanthite, second permutation. a. The entire projection with primitive circle (graduated) of r=1. The primitive octant is stippled. b. The entire projection with primitive of r=1. The polar octant is stippled and the primitive gnomonogram is reticulated. c. Central portion of stereoprojection (see *b*) with r=10. d. Central portion of gnomonogram with r=5. Note that distances D_2', S_2', X_2', and Z_2' are capitalized to emphasize that r≠1. e. Central portion of polar elements plane with r=5. Here also D_2, S_2, X_2, and Z_2 are capitalized, since r≠1.

3. Plot *gnom*-point E_2' along $[c]^t$ at $(90-\alpha)°$ down from $[b]$. Then $bE_2' = z_2'$. If desired, also plot $[c]^c$ down $\alpha°$ *ster.* from $[b]$.

4. Erect normals through common points G_2' and E_2' to $[a]^t$ and $[c]^t$ respectively, intersecting at Q′, the gnomonic face-pole (010). These normals are the R′ and P′ axes of Goldschmidt, and G_2' and E'_2 are their zone centers. The point Q′ has cartesian coordinates x_2' and z_2' and polar coordinates ϕ_2 and d_2', where $d_2' = \tan \rho_2$.[5]

5. If desired, draw great circle $(010)^e$ with center Q′ and radius from here to $[a]^e$ or $[c]^e$; this circle contains $(\beta)^e$ and also serves to locate $[\bar{a}]^e$ and $[\bar{c}]^e$.

6. The *ster*-point (Fig. 3*b*) corresponding to Q′ is $[b^*]^e$. A great circle from here to $[a^*]$ (which lies on the primitive at $\phi = 0°$) is the cyclographic projection of γ^*. Clockwise around the primitive β^* degrees from $[a^*]$ is $[c^*]$. The great circle from $[c^*]$ to $[b^*]$ is the cyclographic projection of α^*.

7. The primitive gnomonogram may be plotted from the values of p_2' and r_2'; these may be obtained from the elements of crystallization by using (26) and 27) below.

Useful formulae—Second permutation

$$\cos \rho_2 = \sin \alpha \sin \gamma^* = \sin \alpha^* \sin \gamma \tag{21}$$

$$\tan \phi_2 = \cos \alpha / \cot \gamma^* \tag{22}$$

$$s_2' = \cot \gamma = bG_2' \tag{23}$$

$$x_2' = \cot \gamma^* / \sin \alpha = E_2'Q' \tag{24}$$

$$z_2' = \cot \alpha = bE_2' \tag{25}$$

$$p_2' = 1/(a \cdot \sin \beta \cdot \sin \gamma^*) = 1/(a \cdot \sin\beta^* \cdot \sin \gamma) \tag{26}$$

$$r_2' = 1/(c \cdot \sin \alpha \sin \beta^*) = 1/(c \cdot \sin \alpha^* \sin \beta) \tag{27}$$

Note: Any vector in the gnomonic plane (Fig. 3*d*) may be converted to one in the polar elements plane (Fig. 3*e*) by multiplying it by $\cos \rho_2$; thus $p_2' \cos \rho_2 = p_2$, etc.

Further note: In a manner similar to that described under "standard orientation," one (Fig. 3*a*) may plot $[a]°$ out on $[a]^t$ to the right of $[b]$ a distance of $\sin \gamma$. The x-coordinate of $[a]°$, called n_2, is given by (28). It is the distance to $[c]^t$ going parallel to $[a^*]$. The z-coordinate of $[a]°$, called m_2 is given by (29). It is the distance to $[a^*]$ going parallel to $[c]^t$.

$$n_2 = \sin \beta^* \sin \gamma = \sin \beta \sin \gamma^* \tag{28}$$

$$m_2 = \cos \beta^* \sin \gamma = n_2 / \tan \beta^* \tag{29}$$

It is clear that the denominator of (26) may be replaced by $a \cdot n_2$.

References

Barker, T. V. (1922), Graphical and Tabular Methods in Crystallography, London.

Bond, W. L. (1946), Computation of . . . angles, etc.: *Am. Mineral.*, **31**, 31–42.

——— (1950), Nomographs for triclinic cell computations: *Ibid.*, **35**, 239–244.

Buerger, M. J. (1942), *X*-ray Crystallography, New York.

——— (1944), The photography of the reciprocal lattice: *Am. Soc. X-ray & Electron Diffr. Monogr.* **1**, 37 pp.

[5] ϕ_2 and ρ_2 are used here as the polar coordinates of (010). Palache *et al.* (1944, pp. 18, 20) use these in the monoclinic and orthorhombic systems as the position angles of any given face in the second permutation.

Evans, H. T. (1948), Relations among crystallographic elements: *Am. Mineral.*, **33**, 60–63.
Fisher, D. J. (1941), A new projection protractor: *Jour. Geol.*, **49**, 292–323 and 419–442.
——— (1952), The lattice constants of synthetic chalcanthite by the x-ray precession technique using but a single mounting of the crystal. *Am. Mineral.*, **37**, 95–114.
Goldschmidt, V. (1934), Kursus der Kristallometrie. Berlin.
Palache, C., Berman, H., and Frondel, C. (1944), The System of Mineralogy of J. D. and E. S. Dana, vol. 1, New York.
Phillips, F. C. (1947), An Introduction to Crystallography, New York.
Wherry, E. T. (1920), Tangent Tables: *Am. Mineral.*, **5**, 119.

Manuscript received Aug. 14, 1951.

LATTICE CONSTANTS OF SYNTHETIC CHALCANTHITE BY THE *X*-RAY PRECESSION TECHNIQUE USING A SINGLE MOUNTING OF THE CRYSTAL

D. Jerome Fisher, *University of Chicago, Chicago, Illinois.*

Abstract

Chalcanthite is herewith returned to its pre-Barker setting with α and β obtuse, γ acute (rather than β and γ obtuse, α acute), but otherwise no change except for refinements in detail. The *x*-ray precession technique as applied to a triclinic crystal with but a single mounting is described for (1) precession along two axes, and (2) precession along but a single axis. A new angle table has been prepared.

Introduction

Following Romé de l'Isle's Essai de Cristallographie of 1772, chalcanthite ($CuSO_4 \cdot 5H_2O$) has frequently[1] been used as a textbook example of a triclinic crystal, since it is readily available, at least in the synthetic condition, shows good prismatic habit, and has pronounced obliquity of crystal axes. For this reason, and because the relatively new *x*-ray precession technique (Buerger, 1944) seems ideally suited to the mineralogists' use for getting crystal angles, this paper has been prepared. The present study was made on a single crystal 0.4 by 0.6 by 1.5 mm. which was grown on the overnight cooling of a slightly supersaturated solution made from the C. P. salt. This work was started to supply material for use in a beginning course in *x*-ray crystallography; it seemed of sufficient interest to warrant some further study which yielded the results herein reported.

Orientation

While many orientations have been used for chalcanthite (Goldschmidt, 1918, vol. 5, p. 105), since 1908 when Groth (1908, vol. 2, pp. 419–421) appeared, Barker's setting has become quite standard.[2] However, Barth and Tunell (1933) noted the unconventionality of Barker's orientation, though they retained it. Later Donnay (1943 *a*) suggested certain more or less arbitrary rules for orienting crystals; it is desirable to adopt these in order to achieve some degree of uniformity. The rules seem good for reasons stated by Donnay, but also because they preserve

[1] For example, see Barker (1922, pp. 36–38; 1930), Goldschmidt (1934, pp. 63–65), Terpstra (1946, pp. 91, 101, 147–151, 156–166, 236, 297), Tutton (1911, pp. 286–302; 1922, pp. 282–298).

[2] Apparently Barker's setting was first published in 1905 by Groth (1905, p. 349).

the standard orientation of the soda plagioclase feldspars.[3] In accordance with these rules, chalcanthite is here reoriented from the Barker setting by reversing the signs on the ends of the [a] and [c] axes.[4] The transformation formula from Barker is simply $\bar{1}00/010/001$.

A typical habit of chalcanthite is shown in Fig. 4[5] in the two settings. The prismatic zone carries the plus and minus unit hemi-prisms as well as front and side pinacoids; this is terminated by the large unit tetartodipyramidal form which is $\omega\{\bar{1}11\}$ in the Barker setting and $p\{\bar{1}\bar{1}1\}$

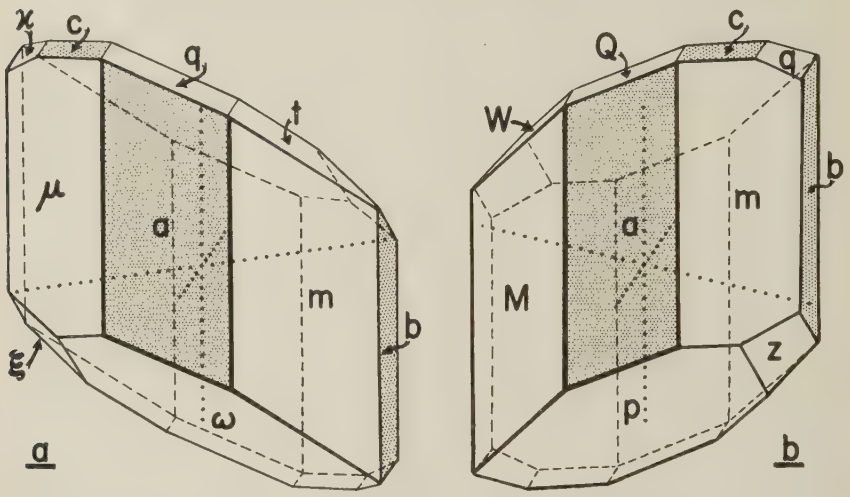

Fig. 4. Axonometric projections of chalcanthite in the (*a*) Barker setting, and (*b*) the old setting used in this paper. The pinacoids are stippled.

in the setting of this paper; the other terminal faces are generally quite small, but in the synthetic sample used in the present study $z\{\bar{1}2\bar{1}\}$ was several times as large as p. Figure 5 is a gnomonogram showing the main terminal forms in the two settings. One setting goes to the other by inversion followed by rotation of 180° on the [b^*] axis.[6] This is simpler

[3] The suggestion of Donnay (1943*b*) that the lime plagioclases be reoriented is unfortunate, and goes against first principles governing the treatment of a high-temperature solid solution series. Orientation of triclinic crystals has recently been discussed by Milne and Nuffield (1951, pp. 401–407).

The orientation of chalcanthite used in this paper is adopted by Palache *et al.* (1951, p. 488).

[4] This results in the first orientation of Donnay (1943*b*, p. 511); the second one is erroneous, due to a misprint in Wyckoff.

[5] The numbers here assigned to tables, figures, and formulas are in continuation of the numbers used for the same purposes in the preceding paper (Fisher, 1952).

[6] Elements of the reciprocal lattice are designated by an asterisk. The reciprocal axes are normal to the three pinacoidal planes of the direct lattice. The axes of the direct lattice (the "crystal axes") are normal to the three "pinacoidal" planes of the reciprocal lattice;

than considering that one setting goes to the other by reflection in (010), since the crystal is assumed to have a center of symmetry. Thus one can

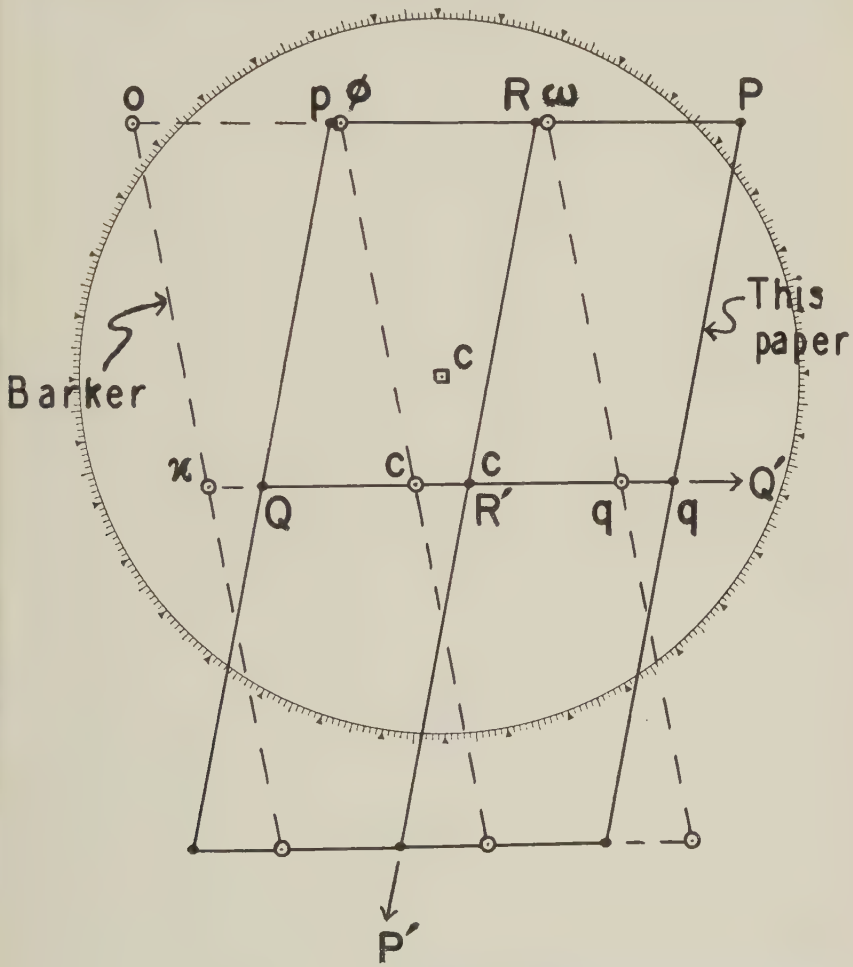

FIG. 5. Gnomonogram normal to the [c]-axis to fit the Barker setting (face-poles are open circlets, zone-lines are dashed) and the setting of this paper (face-poles are solid circlets, zone-lines are continuous).

take a model of the crystal held in the Barker position and rotate it 180° on [b^*] and it then has the position fitting the setting of this paper. In the Barker orientation the basal pinacoid c (001) slopes to the front

thus [a] is $\perp$ $|100|$, etc. Note that just as the symbol (100) designates a crystal face parallel to the b- and c-axes, so the symbol $|100|$ designates a plane of the reciprocal lattice parallel the b^*- and c^*-axes at a distance $d^*_{|100|}$ (measured along the a-axis) from the origin.

and to the left; in the setting of this paper it slopes to the front and to the right. Since synthetic crystals generally lack this form (Mäder, 1942, p. 198), and in any case it is small, the crystal was first oriented by Haüy (see Goldschmidt, 1918) with the large end face sloping to the front and right. Kupffer (1826), whose measurements were standard until Barker's work, used Haüy's orientation.

Sometime not long after the middle of the 19th century the setting of this paper was adopted, and it was the standard setting b.B. (before Barker). Groth (1874, p. 35) had it in 1874; probably Rammelsberg (see Tutton, 1922, p. 282) or Kobell (see Goldschmidt, 1918) used it as early as 1855 or 1856. It seems to have been used last in an article dealing mainly with twinning (Boeris, 1905). Why did Groth decide that a change should be made (see Groth, 1895, p. 340 and 1905, p. 349)?

Groth (1908) lists 10 isomorphous triclinic pentahydrates of bivalent metal sulfates, etc., the $A''ZO_4 \cdot 5H_2O$ compounds. These are mainly sulfates and selenates of Mn and Cu, but also of Mg, Co, Fe, and Zn (including the chromate and molybdate of Mg). He has them all in the same orientation, that of Barker for chalcanthite. It is likely that some of these were already described in the Barker orientation.

There is also another possibility, which is as follows. When one grows a synthetic chalcanthite crystal, better faces may develop on one end than on the other. The morphologist would of course mount the end with the poorer faces against the pin of his goniometer head. He would think of the $+[c]$-axis as extending out from his goniometer head. Then having measured and projected the crystal, he would find that his stereogram or gnomonogram fitted the setting adopted by Barker; to convert it to the setting of this paper he would need to reflect everything in (010), which is equivalent to rotating a centro-symmetric crystal 180° on $[b^*]$. If these crystals grow with a certain end having the better terminal faces, this may imply that the crystal is not centro-symmetric. In any case, the crystal used by the writer fitted this concept. Evidently this was also Tutton's (1922, pp. 282–283) experience, since he regarded Groth's pre-1905 values for α and γ as "the supplements of the true values," apparently not realizing that these earlier Groth values were the ones that fitted the orientation then used by Groth (1895, Fig. 184), and which is here adopted. Years later Winchell (1931, p. 233) seems to have made a similar error, which persists in his most recent book (Winchell, 1951, p. 160).

In summary, it thus seems that chalcanthite can be taken from the Barker orientation and returned to its earlier setting, which is in accordance with Donnay's rules, with a minimum of confusion. The transformation between the two settings is a very simple one. The axial ratios

are the same for the two, as is β. In the Barker setting α is acute, γ is obtuse; in the setting of this paper, α and γ are the supplements of their values in the Barker orientation. The optical goniometer measurements in the literature yield elements (orientation of this paper) as shown in Table 3.

Table 3. Chalcanthite Elements (optical goniometry)

	a		b		c	α	β	γ
Kupffer	.5656	:	1	:	.5507	97°39′	106°49′	77°37′
Barker	.5721	:	1	:	.5554	97°55′	107°08′	77°19′
Tutton	.5715	:	1	:	.5575	97°44′	107°26′	77°20′
Mäder	.5689	:	1	:	.5549	97°37′	107°16′	77°25′
Average	.5695	:	1	:	.5546	97°44′	107°10′	77°25′
±	.0039				.0039	0°11′	0°21′	0°12′

X-ray Data. Precession Along Two Axes

Many *x*-ray photographs of the synthetic chalcanthite crystal were taken using a number of different techniques and radiations. The crystal was oriented with [*c*] along the axis of a goniometer head in the ordinary manner on a two-circle optical goniometer, and a preliminary gnomonogram was prepared and its face-poles were indexed; compare Fig. 5.

For *x*-ray precession work, it is essential that a reciprocal axis be parallel to the axis of the goniometer head; this orientation for [*c**] was attained by the stereographic technique (Fisher, 1951). The goniometer head was then attached to the dial (vertical circle) axis of the precession camera (Fig. 6) and this axis was adjusted in azimuth (dial reading) so that, with the $\bar{\mu}$-arc set at 0°, the direct *x*-ray beam went along [*a*] or along [*b*]. Approximate dial readings to attain these ends were calculated from data taken from a preliminary stereogram rotated so that [*c**] lay at the center of the primitive; refined values were given by the precession orientation technique discussed ahead.

Zero-level films for these two precessing axes taken at $\bar{\mu}=20°$ and 30° with Mo K_α, Cu K_α, and Fe K_α radiations were measured, giving the results presented in Table 4.[7] The general appearance of such films is shown in Figs. 7*a* and 8*a*, if the 1-level spots are omitted from these. The films were given different values (as shown in Table 4) in terms of computing the weighted averages in accord with the sharpness of the spots or the size of the $\bar{\mu}$-angle. The Mo K_α films marked "double ex-

[7] The precession camera was set for F = 6.00 cms., but calibration showed this to be actually 5.985 cms. All film measurements in Tables 4 and 6 thus represent averaged read values multiplied by the factor 1.0025, so that F may be taken as just 6.00.

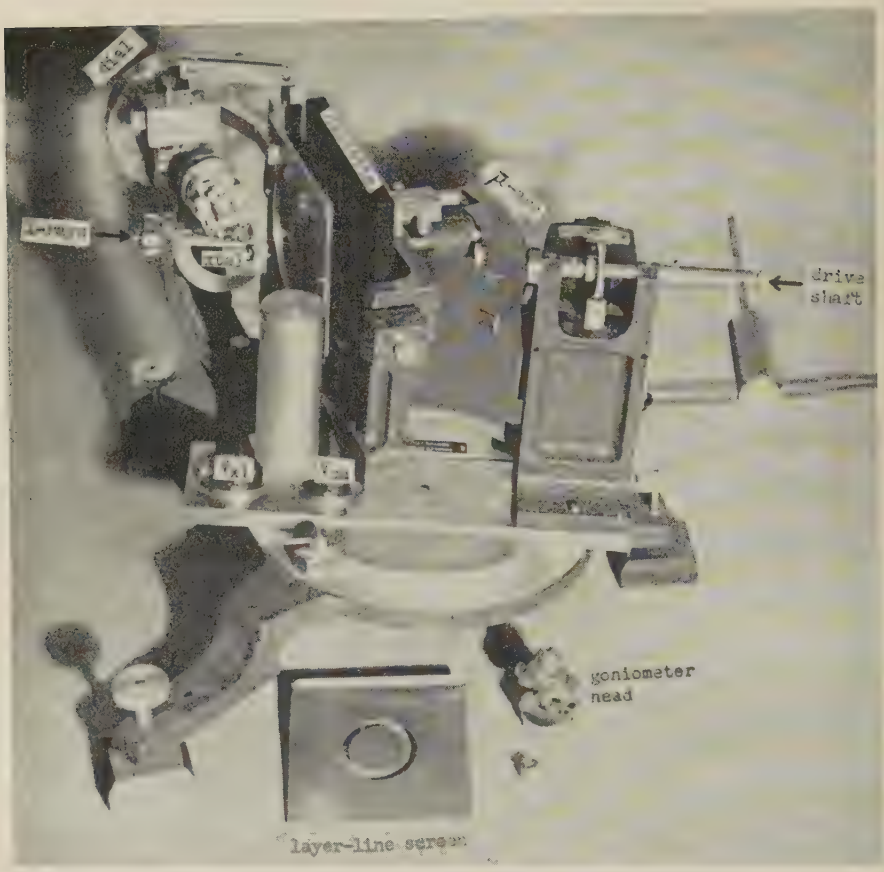

FIG. 6. The Buerger precession camera with the $\bar{\mu}$-arc set to 20°.

posure" were taken with a number of quartz spots which permitted calibration. All told, the results from 15 films are here presented.

These were studied on the measuring device shown by Buerger (1945, p. 553). This results in enlarged reciprocal lattice translation[8] values (in cms.) normal to reciprocal lattice axes in the plane of the film. For a triclinic crystal of course these are not enlarged reciprocal lattice spacings (d^*). Each film was measured in four azimuth positions, and the checked averaged results are given in Table 4. The pictures were taken over a period of about a year; differences shown are due in part to varying conditions of humidity and temperature, but buckling of the film (which is loose at the center) is serious at times, according to F. Laves, even with

[8] In the triclinic these are really "spacing" values between reciprocal lattice *lines* (the lines are parallel the reciprocal axes in the plane of the film).

TABLE 4. CHALCANTHITE MEASUREMENTS (F=6.000 CMS.)

Radiation	Average Weight	Precession on [a]			Precession on [b]		
		α^*	$t^*_{\perp b^*}$	$t^*_{\perp c^*}$	$t^*_{\perp c^*}$	$t^*_{\perp a^*}$	β^*
Mo	10	85°51′	.7506	.4059	.7109	.7214	73°49′
Mo	8				.7164	.7205	73°53′
Mo	6				.7194	.7275	73°53′
Mo	6				.7154	.7164	74°03′
Mo	4	85°53′	.7526	.4084			
Mo	Wt. Av.		.7512	.4066	.7150	.7214	
Mo	Double Ex.	85°53′	.7506	.4088	.7183	.7225	73°52′
Mo	Wt. Av.		.7509	.4077	.7161	.7218	
Mo	a*/λ				.17480		
Mo	b*/λ			.09586			
Mo	c*/λ		.17655			.17619	
Cu	10	85°53′	1.6253	0.8822	1.5504	1.5700	73°54′
Cu	10	85°55′	1.6297	0.8857	1.5499	1.5674	73°51′
Cu	2				1.5542	1.5723	73°50′
Cu	Wt. Av.		1.6275	0.8840	1.5505	1.5690	
Cu	a*/λ				.17446		
Cu	b*/λ			.09581			
Cu	c*/λ		.17639			.17655	
Fe	2	85°47′	2.0548	1.1128			
Fe	1				1.9453	1.9744	73°43′
Fe	a*/λ				.17420		
Fe	b*/λ			.09598			
Fe	c*/λ		.17723			.17680	
Weighted Averages	a*/λ				.17468		
	b*/λ			.09584			
	c*/λ		.17650			←	
	Angles	85°53′					73°53′

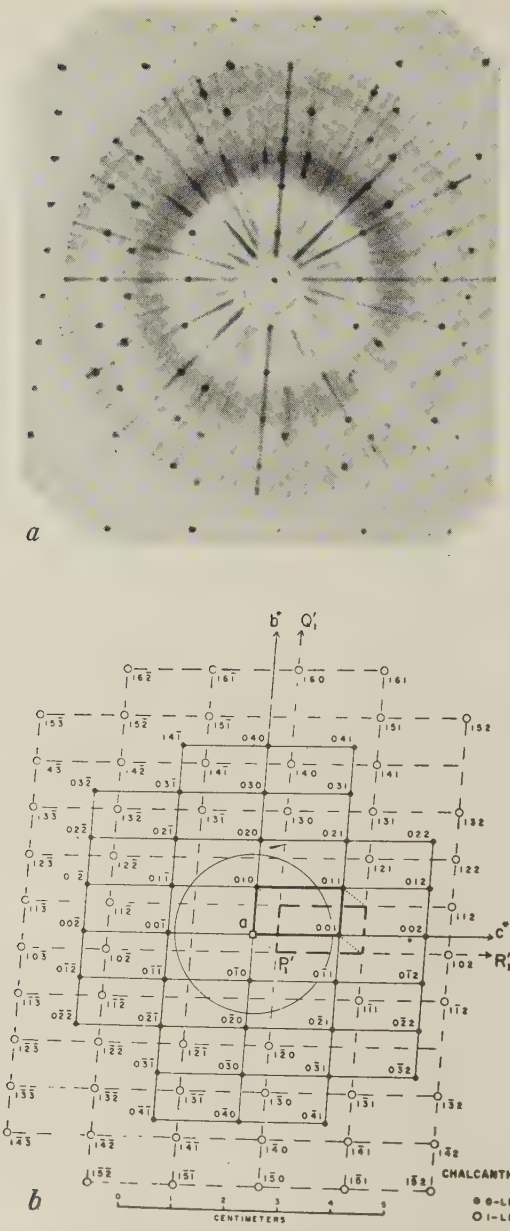

FIG. 7. (*a*) Chalcanthite diffraction pattern with precession on [*a*] for the 0- and 1-levels. F = 6.00 cms., $\bar{\mu} = 20°$, Cu K_α rad. at 45 KV. and 15 ma. (*b*) Reciprocal lattice 0- and 1-levels projected on the b^*c^* or the $|100|$ plane to the same scale as (*a*). The 1-level corresponds to the gnomonogram of the Goldschmidt method; its unit circle is also shown.

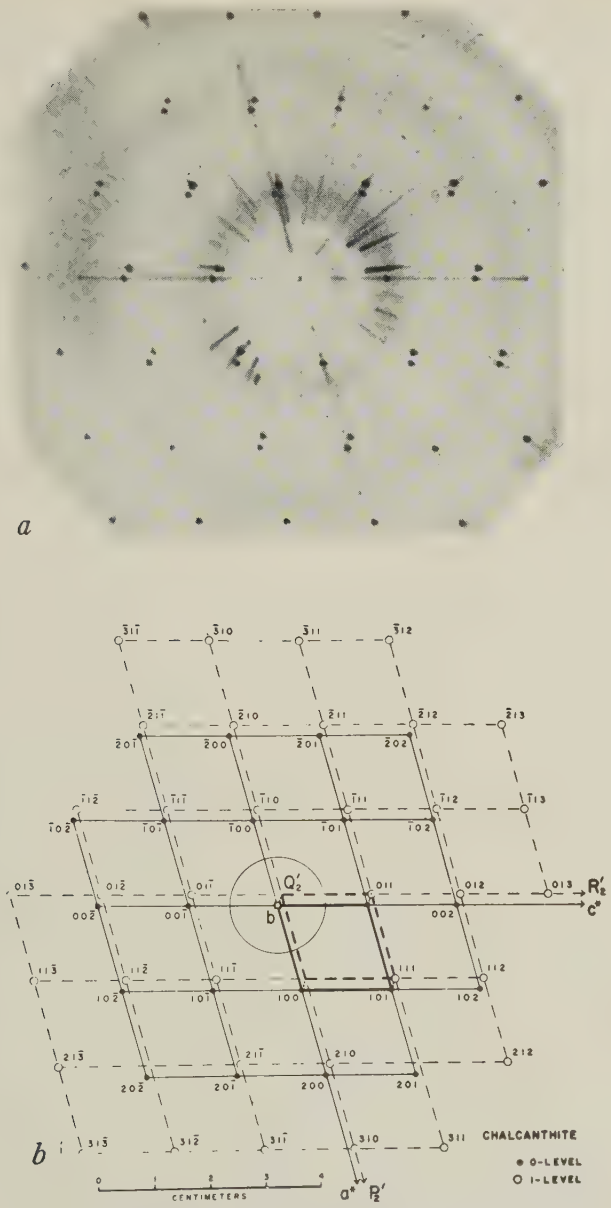

FIG. 8. (*a*) Chalcanthite diffraction pattern with precession on [*b*] for the 0- and 1-levels. F = 6.00 cms., $\bar{\mu} = 20°$, Cu K_α rad. at 45 KV. and 15 ma. (*b*) Reciprocal lattice 0- and 1-levels projected on the a^*c^* or the $|010|$ plane to the same scale as (*a*). The 1-level corresponds to the gnomonogram of the Goldschmidt technique; its unit circle is also outlined.

constant temperature and humidity conditions. The center of the film may be held to the metal plate backing the film cassette by a tiny spot of Duco cement, or a small alnico magnet may be inset at the center of the metal plate backing the cassette and another one placed at the center of the film outside the light-tight cover forming the front of the cassette. Or if no central spot is desired, a small screw could be put through the center of the film from the front of the cassette.

The values of a,* b,* and c* for assumed unit radiation ($\lambda = 1$Å.) are obtained by use of the following formulae,[8a] where F = the distance from the center of the film to the crystal:

Precession on [b]

$$a^* = t^*_{\perp c^*}/(\sin\beta^* \cdot F \cdot \lambda) \quad (30)$$

$$c^* = t^*_{\perp a^*}/(\sin\beta^* \cdot F \cdot \lambda) \quad (31)$$

Precession on [a]

$$b^* = t^*_{\perp c^*}/(\sin\alpha^* \cdot F \cdot \lambda) \quad (32)$$

$$c^* = t^*_{\perp b^*}/(\sin\alpha^* \cdot F \cdot \lambda) \quad (33)$$

Given the results for these three reciprocal lattice translations, as well as the values of α* and β,* all shown at the bottom of Table 4, it was still necessary to secure one more parameter before the desired triclinic calculations could be carried out. Moreover it was hoped that re-mounting of the crystal could be avoided.

Of course since $\gamma = [a] \wedge [b]$, it is possible to obtain this angle by taking the difference in dial readings for precession on [a] and on [b]. Since the dial circle is only 9 cms. in diameter, graduated to degrees with a 5-minute vernier, it seemed doubtful that this would lead to an accurate result. However two series of precession orientation pictures (Buerger, 1944, pp. 21–26) were made two weeks apart as shown in Fig. 9. The dial readings were taken (estimating to the nearest minute) before each picture was started and again, independently, after each picture was completed. For the eight pictures three identical results were obtained, three differed by 1′, one differed by 2,′ and inadvertently but one reading

[8a] Other formulae of interest in this connection are as follows:

Precession on [c]

$a^* = t^*_{\perp b^*}/(\sin\gamma^* \cdot F \cdot \lambda)$ (34); and $a = (F\lambda)/(t^*_{\perp b^*} \sin\beta)$ (34′)

$b^* = t^*_{\perp a^*}/(\sin\gamma^* \cdot F \cdot \lambda)$ (35); and $b = (F\lambda)/(t^*_{\perp a^*} \sin\alpha)$ (35′)

Precession on [b]	*Precession on* [a]
$a = (F\lambda)/(t^*_{\perp c^*} \sin\gamma)$ (30′)	$b = (F\lambda)/(t^*_{\perp c^*} \sin\gamma)$ (32′)
$c = (F\lambda)/(t^*_{\perp a^*} \sin\gamma)$ (31′)	$c = (F\lambda)/(t^*_{\perp b^*} \sin\beta)$ (33′)

was made on one (that at the upper right). Averaged values are given.[9]

In the precession orientation technique, in which no screen is placed in the layer-line screen holder, the ends of the zero-level general radiation streaks outline the circumference of a circle of precession, of which the streaks themselves should be the radii or spokes, providing precession is occurring exactly along a translation direction of the direct lattice. This is rarely the case, however, since it is very difficult to make a precession camera in which the dial axis is exactly normal to the direct x-ray beam (when $\bar{\mu}=0°$).[10] On the instrument used in this study, when the crystal is in perfect orientation the center of this diffraction circle is 0.8 mm. (corresponds to 23 minutes) to the right of the center of the hub (the point where the "spokes" meet) under the conditions stated in the caption of Fig. 9. Scratches made along the streaks on the film intersect at the hub-center, (the direct-beam spot), and a needle-prick appears at the center of the circle of precession. This latter point is determined easily by placing the film on a light box topped with a glass positive made from polar coordinate paper. It will be noted that streaks in the two left pictures of Fig. 9 correspond to those of the zero-level of Fig. 7*a* and those in the right-central pictures of Fig. 9 correspond to the 0-level streaks of Fig. 8*a*.

As the "east-west" streaks of Fig. 9 trace out $[c^*]$,[11] it is only necessary to note the relation of the needle-prick at the center of the diffraction circle to the trace of $[c^*]$ to find the error in the dial setting. Since with an error of 1° there is a streak difference of 4.2 mm. (difference in length of a "north spoke" and a "south spoke") where F = 6.00 cms. and the orientation error is small, this is easily calculated. Thus in the left-center picture (upper row of Fig. 9) since the needle-prick is 0.50 mm. below the trace of $[c^*]$, the dial reading must be increased from the value given by $(2 \cdot 0.5 \cdot 60)/4.2 = 2 \cdot 0.5 \cdot 14.3 = 14'$ to have precession exactly along $[\bar{a}]$. In this way averaged dial readings for precession along $[b]$ and $[a]$ were obtained. The corrected values for the two left-hand pairs of pictures (subtracting 180° from the $[\bar{a}]$ values) were 48°52′, 48°58′, 48°54′, and 48°56′. For the two right-hand pairs the results were 126°20′, 126°22′,

[9] In actual practice it is better to take double exposures made when dial readings are approximately 180° apart. One exposure has twice the time of the other, so that the two are easily differentiated. If there is any difficulty in interpreting this, a new picture is made with the (approximately) horizontal arc of the goniometer head about one degree off its position for true orientation. Such pictures are not very good for illustration purposes. thus the principle is here elucidated by single exposure as shown in Fig. 9.

[10] The latest model precession instrument (Fig. 6) has a collimator which is adjustable for both height and direction.

[11] All x-ray photos are shown just as they appear looking at the film in the cassette from the x-ray source with the dial on the left.

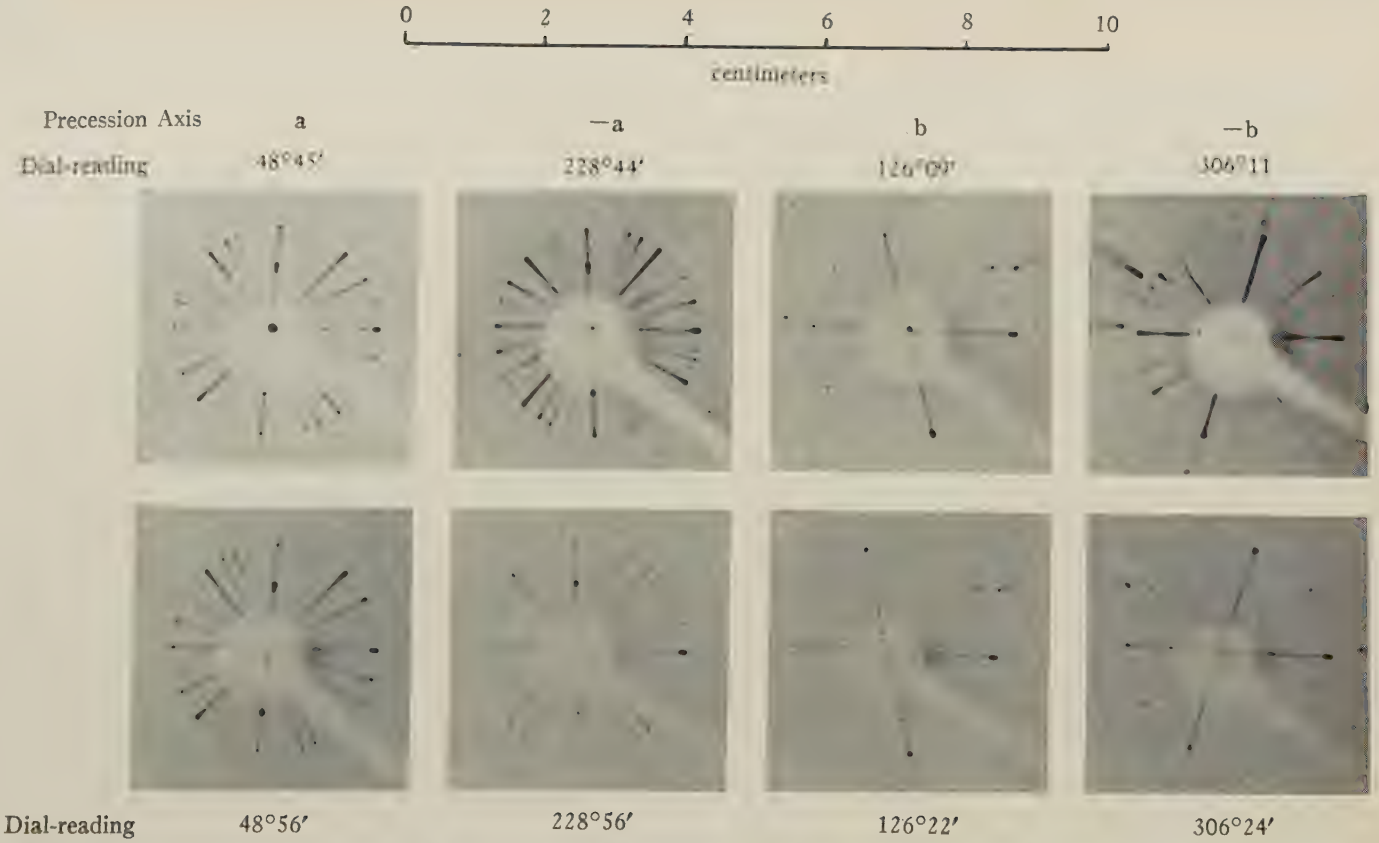

FIG. 9. Precession orientation pictures of chalcanthite with [c^*] the dial axis. The dial reading is indicated for each example. The differences for the averaged dial readings for precession along [a] and [b] indicate that $\gamma = 77°36'$. $R = 6.00$ cms., $\mu = 7°$, unfiltered Cu rad. at 45 KV. and 15 ma.

126°19′, and 126°21′. This yields an average value for γ of $126°20\frac{1}{2}'-48°55'=77°25\frac{1}{2}'$. It seems likely that the probable error in the γ value does not exceed 3′, which may give this reading about the same order of accuracy as those for α^* and β^* as shown at the base of Table 4.

Given $a^*=0.1747$, $b^*=0.0958$, $c^*=0.1765$, $\alpha^*=85°53'$, $\beta^*=73°53'$, and $\gamma=77°26'$, the elements for chalcanthite can be calculated using standard formulae (for example see Buerger, 1942, pp. 360–361). The results are given in Table 5, along with those of previous workers employing x-ray techniques. Angles used by earlier x-ray workers are those of Table 3. Barth and Tunell (1933) found $\alpha^*=85°48'$, $\beta^*=74°00'$, and $\gamma^*=100°45'$; however they considered Tutton's angles to be better than these. The writer's figures yield $\alpha=97°34'$, $\beta=107°17'$, $\gamma^*=100°52'$.

TABLE 5. CHALCANTHITE ELEMENTS (X-RAY GONIOMETRY)[12]

Name	Date	a_0	b_0	c_0	a	b	c	Technique	Angles used
G. & B.	1929	6.08	10.80	5.90	0.563	1	0.546	Rotation	Barker
B. & T.	1933	6.122	10.695	5.96	.5725	1	.5575	Weiss.	Tutton
B. & L.	1934	6.13	10.7	5.98	0.572	1	0.558	Rotation	Tutton
D. J. F.	1952	6.104$_5$	10.72	5.949	.5693	1	.5548	Precession	D. J. F.

A graph of the results obtained by various workers appears in Fig. 10; in this the data of Gossner and Brückl (1929) and of Beevers and Lipson (1934) are not shown, because neither of these pairs was interested in accuracy better than about one per cent. The very close agreement between the writer's values and those of Mäder (1942) is here emphasized.

X-RAY DATA. PRECESSION ALONG ONE AXIS

What is probably the most accurate general technique for determining the elements of a triclinic crystal from a single setting on the precession camera has just been described; this involved precession along two directions. It is perhaps worth emphasizing that precession along one crystal axis furnishes sufficient data to obtain these elements, providing one gets an n-level pattern. This is brought out from Figs. 7 and 8; these should be compared with Figs. 2*b* and 3*b* of the previous paper (Fisher, 1952). The method of obtaining the triclinic elements from a picture made by precession on a single axis may be illustrated by the example of Fig. 7. The close similarity between Fig. 7*b* and Fig. 2*b* becomes clearer if the

[12] Corrected to fit wave lengths where (kX units) · 1.00202 = Å units. Cf. *Am. Mineral.*, **32**, 591–592 (1947).

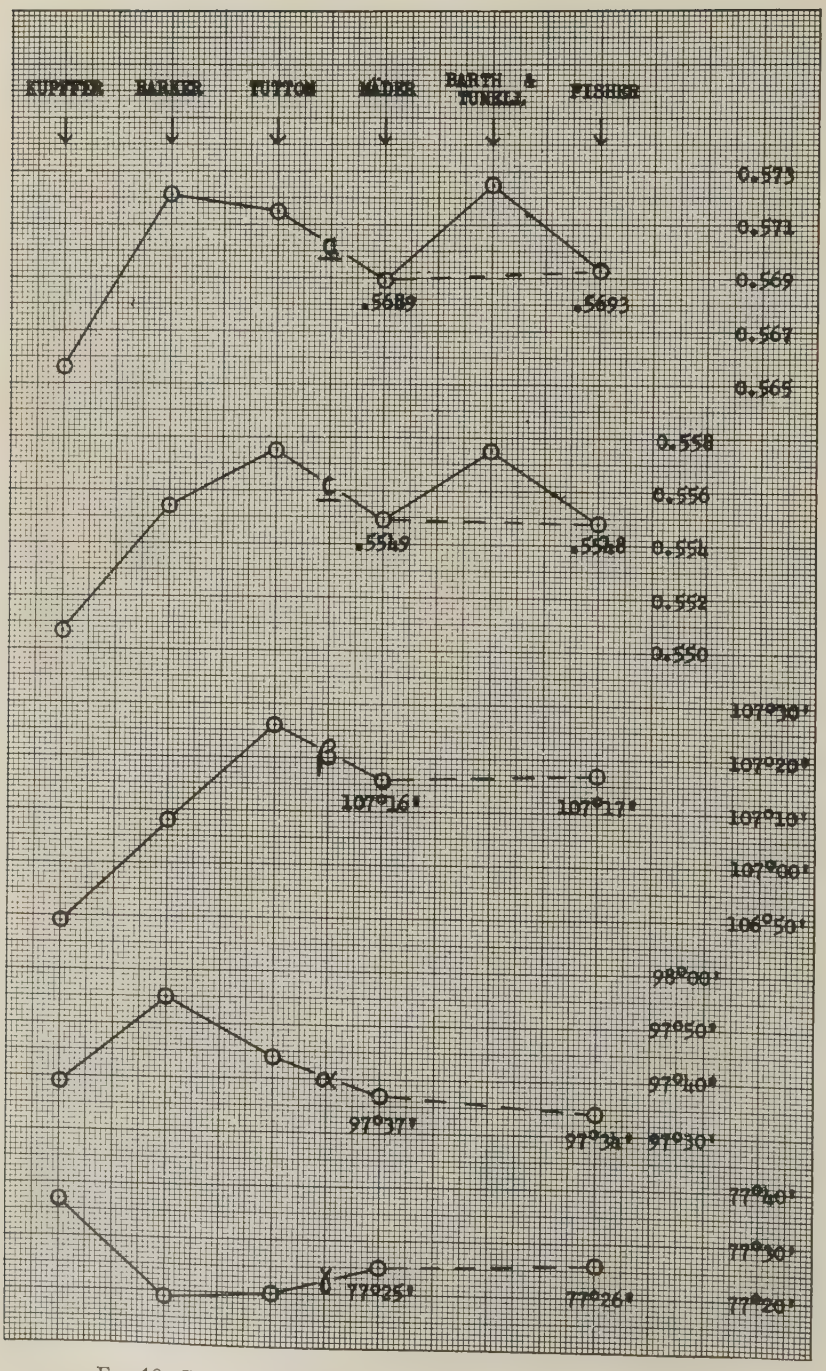

FIG. 10. Graph showing values obtained for chalcanthite elements.

former is rotated 180° about [c^*].[13] Before a 1-level picture such as is shown in Fig. 7*a* can be made, it is necessary to know the reciprocal spacing $d^*_{|100|}=\lambda/a_0$. This can be obtained from a cone-axis photograph (Buerger, 1944, p. 8).[14] Having such an n-level precession pattern, one can measure values that are analogous to the projection constants of the Goldschmidt two-circle technique. For the films of Figs. 7*a* and 8*a* these were as shown in Table 6.

TABLE 6. FILM MEASUREMENTS (in cms.)

Fig. 7*a*	Fig. 8*a*	Special film[a]
$d^*_{\|100\|}=\lambda/a=0.2526$	$d^*_{\|010\|}=\lambda/b=0.1438$	$2d^*_{\|010\|}=0.2876$
$\alpha^*=85°51'$	$\beta^*=73°53'$	$\beta^*=75°54'$
$t^*_{\perp c^*}=0.887$	$t^*_{\perp c^*}=1.546$	$t^*_{\perp c^*}=1.549$
$t^*_{\perp b^*}=1.627$	$t^*_{\perp a^*}=1.555$	$t^*_{\perp a^*}=1.562$
$aG_1'=0.332$ (cf. Y_1')	$bE_2'=0.109$ (cf. Z_2')	$bE_2'=0.112$ (cf. Z_2')
$aF_1'=0.464$ (cf. S_1')	$bG_2'=0.188$ (cf. S_2')	$bG_2=0.190$ (cf. S_2')

[a] The results in this column were measured from a film identical with that of Fig. 8*a* except that the 2-level was taken in place of the 1-level; thus the values shown for the bottom two figures in this column are half those actually measured.

The bottom two values in Table 6 for Fig. 7*a* represent the components of the shear between the 0- and 1-levels of the reciprocal lattice in directions normal to the [c^*]- and [b^*]-axes respectively. Thus these are the central distances of the common points; see Fig. 2*d* of the previous paper. Using formulas (32) and (33) with the values given in Table 6 for Fig. 7*a* yields b^* and $c.^*$ Similarly formulas (14) and (15) of the previous paper furnish β and γ, if one remembers that $r=F\cdot d^*_{|100|}=1.515$ cms. From the six parameters now available (shown in italics in the two lines marked Row 1 of Table 7), the other values given in Row 1 of Table 7 were calculated by standard procedures. The results shown in the second and third rows of Table 7 were derived in analogous fashion from the data given in the middle and right-hand columns of Table 6.

The last row in Table 7 contains the assumed best values for chalcanthite, obtained as described in an earlier section of this paper by using precession photos taken along both the [a] and [b] axes. The weakness of the single axis precession picture technique would seem to be that the shear-components between adjacent layers of the reciprocal lattice must be used for findings γ and α or β. While these components are given to

[13] To make Fig. 8*b* fit Fig. 3*b* rotate the former 74° anticlockwise on [b] and then 180° about [a^*].

[14] While the reciprocal spacing value obtained from a cone-axis photograph does not have great precision, the first result can be refined by the precession technique; see Buerger (1944, pp. 27–32).

Table 7. Results of Computations

Row	Film	α	β	γ	α^*	β^*	γ^*
1	Fig. 7*a*	97°29′	*107°02′*	*77°38′*	*85°51′*	74°07′	100°43′
2	Fig. 8*a*	*97°12′*	107°13′	*77°42′*	86°12′	*73°53′*	100°42′
3	Special	*97°24′*	107°14′	*77°35′*	86°00	*73°54′*	100°46′
4	Best Values	97°34′	107°17′	*77°26′*	*85°53′*	*73°53′*	100°52′
Row	Film	a	b	c	a^*	b^*	c^*
1	Fig. 7*a*	*6.105*	10.68	5.95	0.1744	*0.0961*	*0.1763*
2	Fig. 8*a*	6.12	*10.72*	6.00	*0.1740*	0.0956	*0.1750*
3	Special	6.12	*10.72*	5.97	*0.1743*	0.0958	*0.1758*
4	Best Values	6.104_5	10.72	5.949	*0.1747*	*0.0958*	*0.1765*

0.01 mm. in Table 6, the order of their accuracy is probably only about 0.03 mm., though this might well be improved if several films were measured, and if each of these was taken by a technique that inhibited any buckling. Any errors due to temperature or humidity changes could be cancelled out by taking a pattern of a standard sample (halite or quartz) on each film.

Comparison with Two-Circle Goniometry

Those familiar with the Goldschmidt technique will recognize the close similarity between the gnomonogram given by this and the 1-level precession film, as well as the calculations based on these. Of course the x-ray method yields the absolute size of the unit cell, and thus the results given by it far exceed in value those obtainable from the optical goniometer. The latter is a superseded instrument as far as determination of the fundamental geometrical crystal constants is concerned. But the Goldschmidt method is still a fine training tool for those who wish to study x-ray methods first by the precession camera, later by the Weissenberg. It will continue to be fundamental in morphologic and habit studies. The optical goniometer is often useful in preliminary orientation work. For these reasons the writer has computed an angle table (Table 8) based on the measurements herein reported. The stereogram of Fig. 11 gives the position of the optical indicatrix[15] in the present setting using

[15] The optic triangle is an equilateral right-angled spherical triangle representing an indicatrix octant. The arcs bounding it can be drawn readily by plotting its apices both cyclographically and euthygraphically in a single projection (from the position angles given in Table 8). The apices of the *gnom*-optic triangle are the centers of the required arcs.

the results of Mäder (1942). Figure 12 shows a model representing the unit cell (lucite sheets; scale 1 inch = 1 Å.) and 8 cells of the reciprocal lattice (nodes on wire rods; same scale) to fit Mg K_α radiation of $\lambda = 9.889$Å.;

TABLE 8. CHALCANTHITE: $CuSO_4 \cdot 5H_2O$

Triclinic, P$\bar{1}$

$a:b:c = 0.569:1:0.555$; $\alpha = 97°34'$, $\beta = 107°17'$, $\gamma = 77°26'$

$p_0:q_0:r_0 = 0.994:0.543:1$; $\alpha^* = 85°53'$, $\beta^* = 73°53'$, $\gamma^* = 100°52'$

$p_0' = 1.0441$, $q_0' = 0.5700$, $x_0' = 0.3111$, $y_0' = 0.0754$, $m_0 = 0.1869$, $n_0 = 0.9735$

No.[a]	Form	ϕ	ρ	A	B	C	Barker
1	$c(001)$	76°22′	17°45½′	73°53′	85°53′	00°00′	$c(001)$
2c	$b(010)$	00 00	90 00	100°52	00°00′	85 53	$b(0\bar{1}0)$
3b	$a(100)$	100 52	90 00	00 00	100 52	73 53	$a(100)$
4	$n(130)$	34 07	90 00	66 45	34 07	76 57	$\pi(1\bar{3}0)$
5d	$h(120)$	47 24	90 00	53 28	47 24	74 31	$\lambda(1\bar{2}0)$
6c	$m(110)$	70 00	90 00	30 52	70 00	72 21	$\mu(1\bar{1}0)$
7	$d(210)$	85 05	90 00	15 47	85 05	72 27	$\nu(2\bar{1}0)$
8	$F(3\bar{1}0)$	110 40	90 00	9 48	110 40	75 25	—(310)
9	$T(2\bar{1}0)$	115 10	90 00	14 18	115 10	76 15	—(210)
10a	$M(1\bar{1}0)$	126 48	90 00	25 56	126 48	78 48	$m(110)$
11	$L(1\bar{2}0)$	142 31	90 00	41 39	142 31	82 56	$l(120)$
12	$N(1\bar{4}0)$	157 31	90 00	56 39	157 31	87 20	$p(140)$
13d	$w(021)$	14 22	51 26	87 17	40 46	45 07	$\tau(0\bar{2}1)$
14	$q(011)$	25 44	35 37	81 24	58 22	27 31	$\kappa(0\bar{1}1)$
15c	$Q(0\bar{1}1)$	147 50	30 18	69 52	115 17	29 24	$q(011)$
16b	$W(0\bar{2}1)$	163 43	47 59	70 11	135 31	49 37	$t(021)$
17	$e(201)$	97 40	67 14	22 59	97 04	50 55	$d(201)$
18	$R(\bar{1}01)$	−69 08	37 24	126 52	77 30	52 51	$\phi(\bar{1}01)$
19	$u(141)$	31 46	68 30	70 37	37 44	56 33	—(1$\bar{4}$1)
20	$x(131)$	40 04	64 17	63 56	46 25	50 36	$\psi(1\bar{3}1)$
21d	$Z(\bar{1}21)$	−26 50	57 42	121 07	41 02	63 15	$\sigma(\bar{1}2\bar{1})$
22	$P(111)$	−40 18	47 50	125 16	55 35	57 28	$o(\bar{1}\bar{1}1)$
23a	$p(\bar{1}\bar{1}1)$	−112 38	37 44	120 41	103 37	55 20	$\omega(\bar{1}11)$
24d	$z(\bar{1}2\bar{1})$	−140 33	48 20	110 56	125 14	63 12	$\xi(\bar{1}21)$
25	$X(\bar{1}3\bar{1})$	−153 35	58 05	103 09	139 29	72 55	$\zeta(\bar{1}31)$
	Direction						
	α(Na)	168 47	75 53	68 37	162 02	77 18	
	β	75 25	76 51	28 27	75 48	59 06	
	γ	−55 03	19 29	107 44	78 59	33 51	
	A_1	−17 42	76 44	117 44	22 00	78 37	
	A_2	177 17	48 46	79 50	138 42	54 15	
	$[c]$	—	00 00	90 00	90 00	17 45½	
	$[\bar{b}]$	−169 08	82 26	90 00	166 47	90 00	
	$[\bar{a}]$	−90 00	72 43	159 40	90 00	90 00	

[a] The letters in this column give a crude idea of the relative importance of the various forms. Those marked (a) are most important, the (b) ones are of lesser importance, etc.

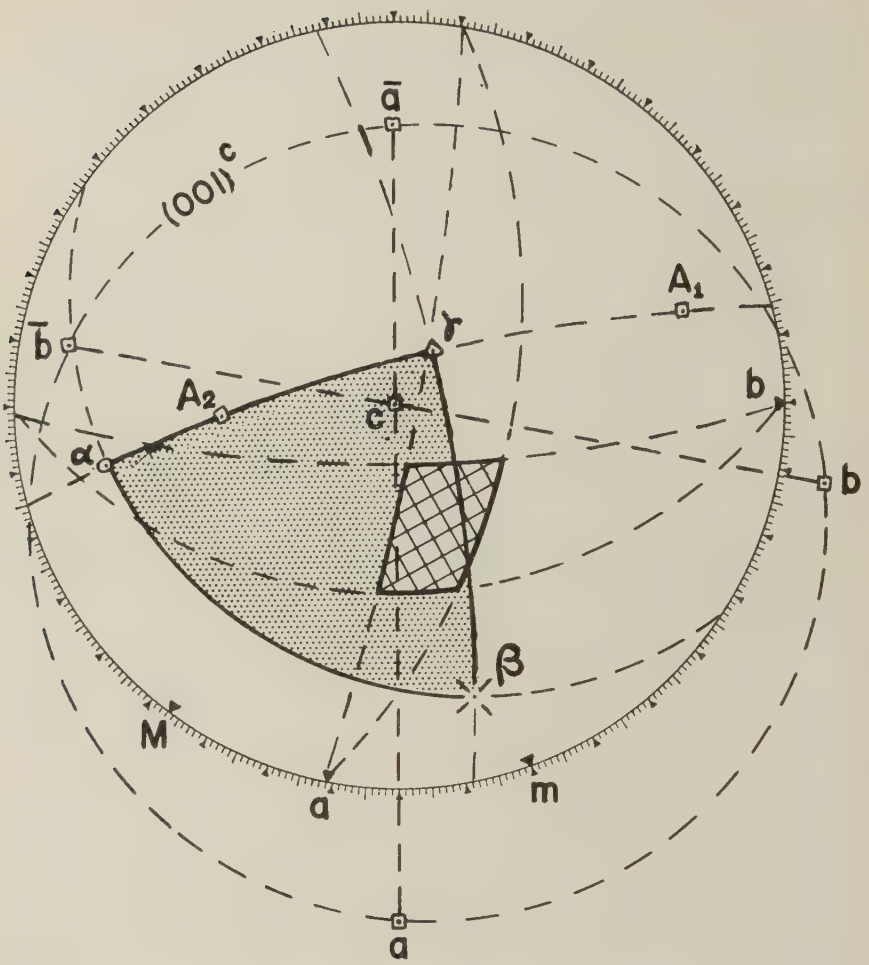

FIG. 11. Stereogram of chalcanthite showing indicatrix directions, standard orientation. The optic triangle is stippled and the primitive stereogram is reticulated.

thus $a^* = 1.7255$, $b^* = 0.9472$, and $c^* = 1.7446$ Å. In the picture the c-axis is vertical and the view is from the upper right octant. The model may be fitted into its support base with any axis vertical. In each case some plane of the reciprocal lattice is horizontal. Similarly it is clear that the wires of the reciprocal lattice network are normal to the pinacoid faces. Or the model may be held in the two hands by the opposite ends of any axis and slowly rotated or oscillated. If one imagines a sphere of reflection to be present, it is then easy to visualize the development of the straight layer lines.

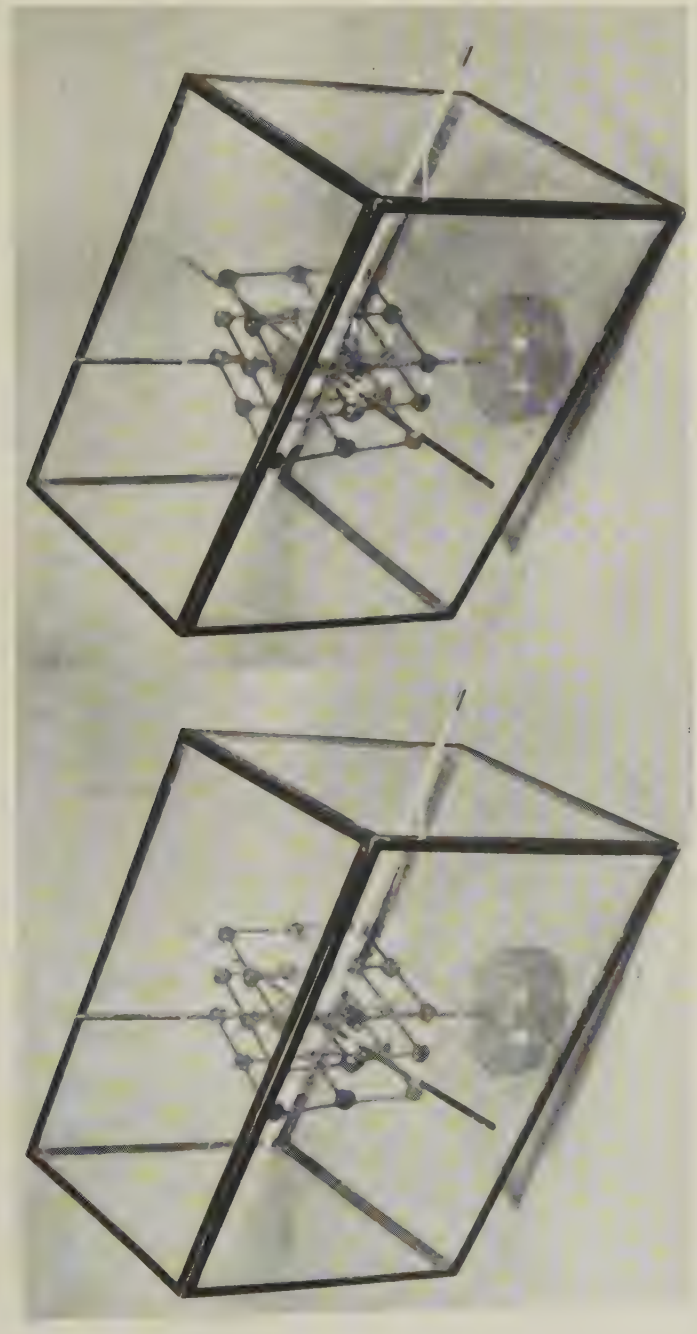

FIG. 12. Stereo-photograph of a model of the chalcanthite unit cell containing a portion of the chalcanthite reciprocal lattice.

Acknowledgments: F. L. Koucky and B. P. Asanachinta helped with the drawings, and W. F. Schmidt did the photography. The members of two classes (and particularly F. D. Bloss) served as stimulating subjects.

References

Barker, T. V. (1922), Graphical and Tabular Methods in Crystallography, London.
——— (1930), The Study of Crystals, London.
Barth, T. F. W., and Tunell, G. (1933), The space-lattice and optical orientation of chalcanthite: *Am. Mineral.*, **18,** 187–194.
Beevers, C. A., and Lipson, H. (1934), Crystal structure of copper sulphate pentahydrate: *Proc. Royal Soc.* (London), **146A,** 570–582.
Boeris, G. (1905), Osservazioni cristallografiche sopra il Solfato di Rami: *Atti d. Soc. ital. sc. nat. Milano,* **44,** 73–85. Reprinted in 1907: *Riv. min. crist. ital.* (Padova), **33,** 5–17. Cf. *Zeit. Krist.*, **43** (1906), 489–490.
Buerger, M. J. (1942), *X*-ray Crystallography, New York.
——— (1944), The photography of the reciprocal lattice: *Am. Soc. X-ray and Electron Diffr., Monogr.* **1,** 37 pp.
——— (1945), Soap crystals: *Am. Mineral.*, **30,** 551–571.
Dana, E. S. (1892), A System of Mineralogy, p. 944, New York.
Donnay, J. D. H. (1943*a*): Rules for the conventional orientation of crystals: *Am. Mineral.*, **28,** 313–328.
——— (1943*b*), Resetting a triclinic unit-cell in the conventional orientation: *Ibid.*, 507–511.
Fisher, D. J. (1951), Setting a given direction parallel to the axis of a goniometer head: *Am. Mineral.*, **36,** 123–128.
——— (1952), Triclinic gnomonostereograms: *Ibid.*, **37,** 83–94.
Goldschmidt, V. (1897), Winkeltabellen, 210, Berlin.
——— (1918), Atlas der Kristallformen, **5,** Heidelberg.
——— (1934), Kursus der Kristallometrie, Berlin.
Gossner, B. u. Brückl, K. (1929), Die Gitterkonstanten von Kupfervitriol: *Zeit. Krist.*, **69,** 422–426.
Groth, P. (1874), Tabellarische Uebersicht der Mineralien, Braunschweig.
——— (1895), Physikalische Krystallographie, Leipzig.
——— (1905), *Ibid.*, Leipzig.
——— (1908), Chemische Krystallographie, **2,** Leipzig.
Kupffer, A. F. (1826), Ueber die Krystallisation des Kupfervitriols, etc.: *Pogg. Ann.*, **8,** 215–229.
Mäder, J. (1942), Kristallographie und Optik des Kupfervitriols: *Schweiz. Min. u. Petr. Mitt.*, **22,** 197–232.
Milne, I. H., and Nuffield, E. W. (1951), Vandenbrandeite: *Am. Mineral.*, **36,** 394–410.
Palache, C., Berman, H., and Frondel, C. (1951), The System of Mineralogy of J. D. and E. S. Dana, Vol. **2**, New York.
Terpstra, P. (1946), Kristallometrie, Groningen.
Tutton, A. E. H. (1911), Crystallography and Practical Crystal Measurement, London.
——— (1922), *Ibid.*, London.
Winchell, A. N. (1931), The Microscopic Characters of Artificial Inorganic Solid Substances or Artificial Minerals, New York.
Winchell, A. N. (1951), Elements of Optical Mineralogy, Part II, New York.

Manuscript received Aug. 14, 1951.

NOTES AND NEWS

NOMOGRAMS FOR CORRECTING ANGLE OF TILT OF THE UNIVERSAL STAGE

A. W. Kleeman, *Adelaide University, South Australia.*

The writer and senior students at Adelaide University have for some time been using nomograms for correcting the angle of tilt on the universal stage when the refractive index of the mineral differs from the refractive index of the hemisphere. Unlike the Federow diagram (cf. Emmons, 1943, plate 8) a separate nomogram must be used for each hemisphere.

The nomograms consist of three parallel scales, one for the observed angle of tilt, one for the refractive index of the mineral and the third for true or corrected angle of tilt. The two scales for angle of tilt are identical and are graduated with the logarithm of the sine of the angle. In the original drawing from which Fig. 1 was prepared two angles of which the logarithms of the sines differed by 0.10 were placed 2 inches apart.

The scale for refractive index has been plotted so that two numbers, the logarithms of which differed by 0.10 are 1 inch apart.

In constructing the nomogram the two scales for angle of tilt were drawn parallel and 5 inches apart. As one is inverted with respect to the other, lines joining the pairs of graduations on the two scales all intersect in a common point. This point represents the condition when the true angle of tilt is the same as the observed angle of tilt, i.e. when the refractive index of the mineral is the same as the refractive index of the hemisphere. For the high index prism (Leitz 1.648 or Bausch and Lomb 1.649) the 1.65 point of the refractive index scale is placed at this point with the scale paralled to the other two scales.

If the scales for angle of tilt were graduated for all angles 1°–55°, they would be 33 inches long. In order to keep the nomogram to a reasonable size and still keep the graduations of the refractive index scale open the main scale was restricted to a range of 17°–55° (larger upright figures), and a supplementary scale with smaller sloping figure drawn to cover the range 7°–19°. A third scale covering the range 3°–8° can be added (preferably in another colour of ink) to complete the range of angles when dealing with minerals in which the refractive index differs widely from that of the hemisphere.

The momograms for other hemispheres differ only in that the refractive index of the hemisphere (1.516 or 1.559) lies on the intersection point.

The nomograms are used by placing a straight edge on the point representing the observed angle and the refractive index of the mineral

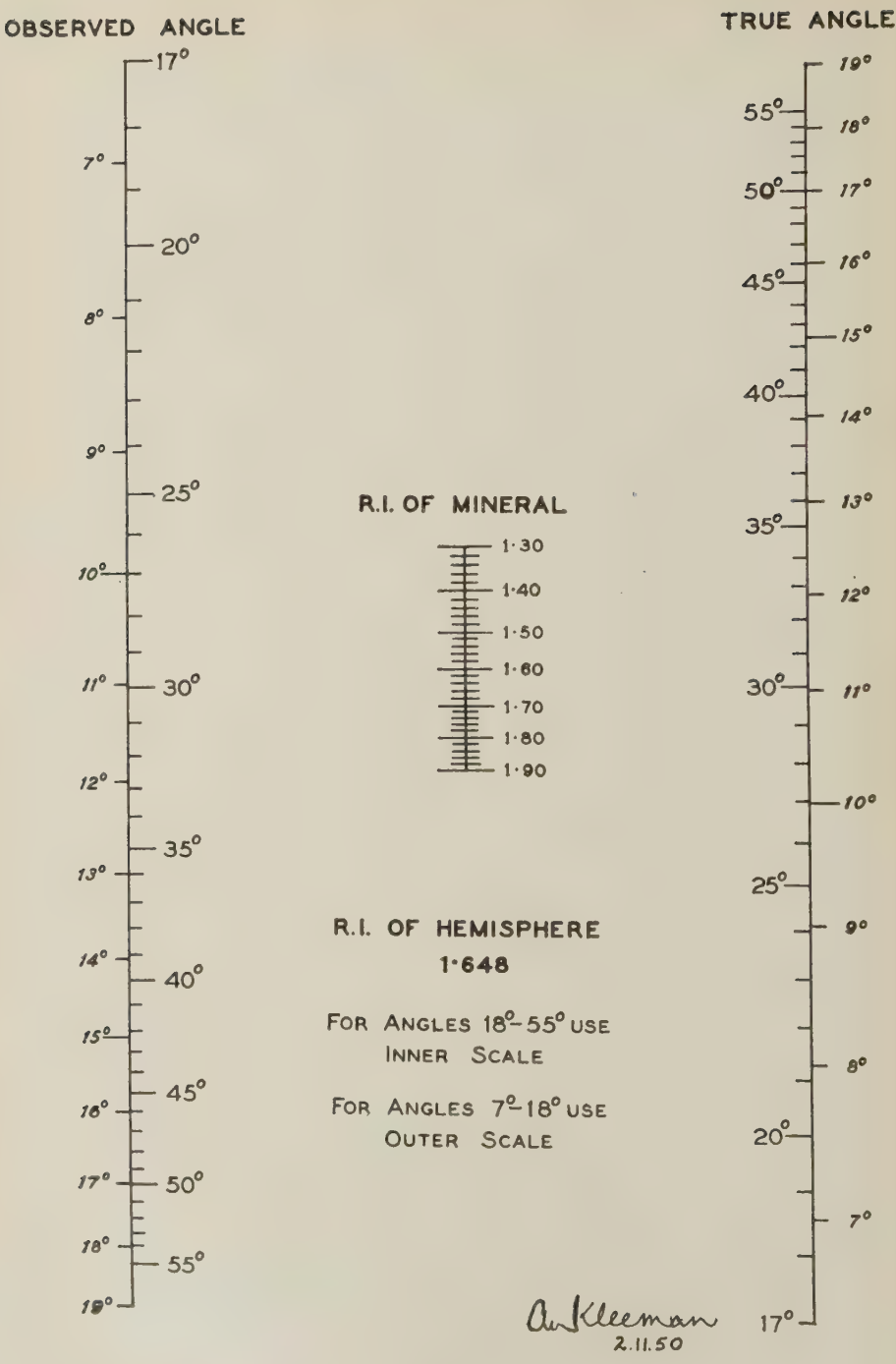
OBSERVED ANGLE
17°
7°
20°
8°
9°
25°
10°
11°
30°
12°
35°
13°
14°
40°
15°
16°
45°
17°
50°
18°
55°
19°
R.I. OF MINERAL
1·30
1·40
1·50
1·60
1·70
1·80
1·90
R.I. OF HEMISPHERE
1·648
FOR ANGLES 18°–55° USE
INNER SCALE
FOR ANGLES 7°–18° USE
OUTER SCALE
TRUE ANGLE
19°
55°
18°
50°
17°
45°
16°
15°
40°
14°
13°
35°
12°
30°
11°
10°
25°
9°
8°
20°
7°
17°
A. J. Kleeman
2.11.50

FIG. 1.

on the left hand and middle scale, respectively, and reading the true angle from the right hand scale.

REFERENCE

EMMONS, R. C. (1943), The Universal Stage: *Geol. Soc. Am., Memoir* **8**.

ANOMALOUS BEHAVIOR OF MONTMORILLONITE CLAYS IN CLERICI SOLUTION

J. L. RODDA*

Clerici solution (thallium formate-malonate mixture) is a very useful medium for separating minerals because of the high specific gravities attainable and the ease with which specific gravities may be changed by dilution or concentration. Occasionally reactions occur between mineral and solution which may prove troublesome or even be useful.

Holzner, working with stilpnomelane[1] and stilpnochloran,[2] later shown by Gruner[3] to be nontronite, demonstrated a base exchange reaction in which thallium replaced the alkalies, and in the case of stilpnochloran, the calcium and part of the water as well. The treated mineral contained up to about 13% thallium oxide. The specific gravity of stilpnomelane was raised from 2.823 to 3.068, and of stilpnochloran from 2.523 to 3.111. Behavior was normal in acetylene tetrabromide-benzol solution.

During some recent work in this laboratory, differences were noted in the behavior toward Clerici solution of kaolinite on the one hand, and of montmorillonite and its zinc-bearing variety, sauconite, on the other. Ninety-two per cent of the kaolite sample floated at a specific gravity of 2.70 while 97% and 87%, respectively, of the montmorillonite and sauconite samples sank at 3.55 specific gravity. Semiquantitative spectrographic analyses of the washed samples showed that the montmorillonites had taken up appreciable amounts of thallium (Table 1). Both montmorillonite and sauconite floated in methylene iodide at specific gravity

* Research Department, The New Jersey Zinc Company (of Pa.), Palmerton, Pennsylvania.

[1] Holzner, J., Beiträge zur Kenntnis der varistischen Gesteins und Mineralprovinz in Lahn-Dillgebiet.-2. Über den Stilpnomelane von Grube Theodor (Lahngebiet) und einem beim Trennen mit Clerici-lösung auftretenden Basenaustausch: *Neues Jahrbuch für Min. Geol. u. Pal., Beilage Band*, **66**, Abt. A, pp. 213–225 (1933).

[2] Holzner, J., Neue Daten über den Stilpnochloran von Gobitschau (Mähren), zugleich Bericht über eine ungewöhnliche Umtauschreaktion: *Centralblatt für Min., Geol. u. Pal.*, Abt. **A**, pp. 250–256 (1934).

[3] Gruner, John W., The structural relationship of nontronites and montmorillonite: *Am. Mineral.*, **20**, 475–483 (1935).

3.25. *X*-ray diffraction patterns of the kaolinite fractions were normal, but the montmorillonite and sauconite fractions showed the 14.72 Å dimension either increased beyond the scope of the camera or too diffuse to be observed, while montmorillonite showed the 4.5 Å line greatly weakened and the 3.04 Å line missing entirely.

Table 1. Thallium Content of Washed Specific Gravity Fractions—Percent

	>3.55	*<3.55*	*<2.70*
Montmorillonite	15.0	3.4	
Sauconite[a]	6.2	2.9	
Kaolinite	0.9	0.7	1.0

[a] Quantitative analysis showed the zinc content of the >3.55 and <3.55 fractions to be 17.1% and 8.8%, respectively.

Up to this point, the behavior of montmorillonite parallels that described by Holzner. In a further experiment montmorillonite first separated in Clerici solution at specific gravity 3.33 showed over 99% greater than 3.33 specific gravity.* This same sample after washing and drying was centrifuged in methylene iodide, when over 99% of it separated in the less than 3.25 specific gravity fraction. It appears that the thallium taken up by base exchange, as shown by Holzner, and which will survive ordinary washing with water, produces a moderate permanent increase in specific gravity, but a much larger, temporary, increase in specific gravity occurs *while the montmorillonite is in contact with the Clerici solution*. This property may prove useful as a separation technique.

Application to Mixtures

A 50-50 mixture of montmorillonite and kaolinite was taken, ground together in a mortar, screened through 200 mesh, put through a homogenizer with Clerici solution at 3.55 specific gravity and centrifuged. The mixture split, 51.42% greater than 3.55, and 48.58% less than 3.55 specific gravity. *X*-ray patterns showed only montmorillonite in the >3.55 fraction and only kaolinite in the <3.55 fraction. The method might well be applied to natural mixtures of active and inactive clays as a separation and diagnostic technique. Care should be taken not to use too high a specific gravity. In a Clerici solution of specific gravity 3.75

* The sample loading was so light, 2 gms. in about 60 ml. of Cleric solution, that the adsorption by the clay of thallium salts must have a negligible effect on the specific gravity of the solution. 60 ml. of solution contains about 185 grams of thallium salts.

only 39% of a pure montmorillonite sample separated in the heavy fraction.

Discussion

The known behavior of montmorillonite in adsorbing water and organic materials into the interlayer position offers a probable explanation of the above phenomena. It seems possible that the thallium salts are more strongly attracted to the interlayer position than the solvent water, thereby raising the specific gravity of the swollen clay above that of the solution. That methylene iodide is also taken into the interlayer position seems quite probable but, since it is a pure compound the specific gravity of the clay could not be increased to a greater value than that of the liquid.

Method of Carrying Out the Separations

A brief description of the method of centrifuging fine materials in heavy liquids may be useful. The sample, crushed through 200 mesh or finer, is mixed with the heavy liquid, sometimes with the aid of a "homogenizer" to insure dispersion. Separations are carried out in Lusteroid plastic tubes. Twenty to thirty minutes may be required at 3500 r.p.m. or approximately 1500 times gravity.

After centrifuging, each tube is pinched together at the center with a laboratory clamp. Provided the tube is not too cold, this may be done without leakage. The "float" fraction may then be poured off and the top of the tube washed out. The pinch clamp is released, the tube squeezed back into shape with a vise, and the "sink" fraction removed. Tubes which have been pinched cannot be used again, but the facility with which heavy and light fractions may be separated is well worth the few cents which the tubes cost.

Acknowledgments

The montmorillonite and kaolinite samples used in this study were two of the clay mineral standards (Polkville, Miss., No. 19 and Bath, S. C., McNamee No. 1 Mine, respectively), of The American Petroleum Institute and were furnished this laboratory through the courtesy of Professor Paul F. Kerr. The sauconite sample, designated "Stadiger vein," was collected at Friedensville, Pa., by Dr. Thomas L. Hurst.

The centrifuge separations were carried out by Mr. C. W. Bartholomew. The x-ray interpretations were supplied by Messrs. George Vaux and W. R. Smith. Suggestions and counsel from Mr. M. L. Fuller are gratefully acknowledged.

TINGUAITE AND BOSTONITE IN NORTHWESTERN NEW JERSEY

A. S. WILKERSON, *Rutgers University, New Brunswick, New Jersey.*

ABSTRACT

The possible utilization of tinguaite and bostonite intrusions in northwestern New Jersey is given. The petrography of these rocks is discussed.

INTRODUCTION

In Sussex County, northwestern New Jersey, there is a zone of alkali-rich intrusions which parallels the northeastward strike of the enclosing Martinsburg shale, of Ordovician age, from half-way between Libertyville and Sussex southwestward to $1\frac{1}{2}$ miles southwest of Wykertown. These intrusives as a group have been briefly described by Wolff.[1] Individual intrusives have been mentioned by Parker,[2] and Milton and Davidson.[3] About 2.5 miles northwest of this zone is the better known intrusion of nepheline syenite described by Emerson,[4] Kemp,[5] Iddings,[6] Wolff,[7] Aurousseau and Washington,[8] Wilkerson,[9] and Parker.[10]

The possible utilization of these rocks for ceramic use (glass making) has led several investigators to re-examine the area. In 1937 the United States Bureau of Mines,[11] and in 1945 the Rutgers University Bureau of Mineral Research,[12] came to the conclusion that from the main nepheline syenite area northwest of Beemerville a product acceptable for glass making could not be obtained.

[1] Wolff, J. E., Post-ordovician igneous rocks: *U. S. Geol. Survey, Folio* **161,** 13 (1908).

[2] Parker, J. M., New Jersey's potential feldspar resources: *Rutgers University Bureau of Mineral Research,* **5,** 57 (1948).

[3] Milton, C., and Davidson, N., An occurrence of natrolite, andradite, and allanite in the Franklin Furnace quadrangle, N. J.: *Am. Mineral.* **35,** 500–507 (1950)

[4] Emerson, B. K., On a great dyke of foyaite or elaeolite syenite, cutting the Hudson river shales in N. W. New Jersey: *Am. Jour. Sci.,* (3) **23,** 302–308 (1882).

[5] Kemp, J. F., The elaeolite syenite near Beemerville, Sussex County, New Jersey: *N. Y. Ac. Sci., Tr.* **11,** 71, (1892).

[6] Iddings J. P., Nepheline syenite from Beemerville, Sussex County, New Jersey: *U. S. Geol. Survey, Bull.* **150,** 209–211 (1898).

[7] Wolff, J. E., Leucite tinguaite from Beemerville, N. J.: *Harvard Coll. Mus. C.Z. Bull.* **38** (Geol. Ser. 5), 273–277 (1902). Wolff, J. E., *op. cit.,* pp. 12–13.

[8] Aurousseau, M., and Washington, H. S., The nepheline syenite and nepheline porphyry of Beemerville, N. J.: *Jour. Geol.,* **30,** No. 7, 571–586 (1922).

[9] Wilkerson, A. S., Nepheline syenite from Beemerville, Sussex County, New Jersey: *Am. Mineral.,* **31,** 284–287 (1946).

[10] Parker, J. M., *op. cit.,* p. 53.

[11] Metcalf, R. W., Feldspar chapter in Mineral Yearbook, 1938 (Review of 1937): *U. S. Bur. Mines,* 1218 (**1938**).

[12] Wilkerson, A. S., and Comeforo, J. E., New Jersey nepheline syenite: *Ceramic Age,* **48,** no. 3, 103–104 (1946).

The northeastward-trending zone of somewhat closely spaced intrusions consists of tinguaites and bostonites. Although fair to good quarry sites and good roads are usually available, and ample tonnages are often possible above ground water level, and the overburden consists only of residual soil and some boulders; however, the fineness of grain, the locally relatively large amounts of mafic constituents present, the alteration of the feldspar and/or nepheline, and the local presence of numerous mafic inclusions in the feldspar and/or nepheline make all the rocks of the zone unsuitable for glass manufacture. Some of the rocks are probably suitable for roofing granules and most could be used for local road ballast. These facts have also been stressed by Parker.[13]

Following is presented a detailed petrographic description of the rocks of this northeastward-trending zone. The area was re-mapped and several intrusions are located differently from their positions as originally shown in the Franklin Furnace folio. The mislocation of one of the dikes was first called to our attention by Parker.[14]

Petrography

Tinguaite

Intrusions of tinguaite occur at nine localities: nos. 1, 3, 4, 5, 6, 7, 13, 14 and 15 (see Fig. 1). In length they range from 150 ft. (no. 6) to 2400 ft. (no. 3); in width they range from 50 ft. (no. 6) to 150 ft. (nos. 1 and 13). The usual strike is N 35° E to N 50° E and apparently follow the strike and dip of the enclosing Martinsburg shale, although contacts are not exposed. At locality no. 15 the tinguaite occurs as a dike with an eastwardly trend and is seemingly vertical. These intrusions, as well as those of bostonite to be described, usually form low-ridges in an otherwise flat or gently rolling country.

The rock is medium gray to dark gray in color but locally has a slightly greenish tint. Usually it is altered, and fresh specimens would be difficult to obtain. In texture it is aphanitic or porphyritic. Phenocrysts of feldspar 2.5 cm.×1 cm. in size, cross-sections of greasy appearing nepheline, about 5 mm. in diameter, and biotite crystals 1.5 mm. across locally are prominent against the gray or greenish-gray groundmass. There is a wide range in the phenocryst-to-groundmass ratio, which varies from 5 per cent (no. 3) to 50 per cent (no. 7), but the phenocrysts normally comprise about 20 per cent of the rock. The phenocrysts are orthoclase, microperthite, nepheline, biotite, and aegirine-augite. Feldspar and nepheline are present usually in approximately equal amounts and great-

[13] Parker, J. M., *op. cit.*, pp. 55, 57.
[14] Parker, J. M., *op. cit.*, p. 54.

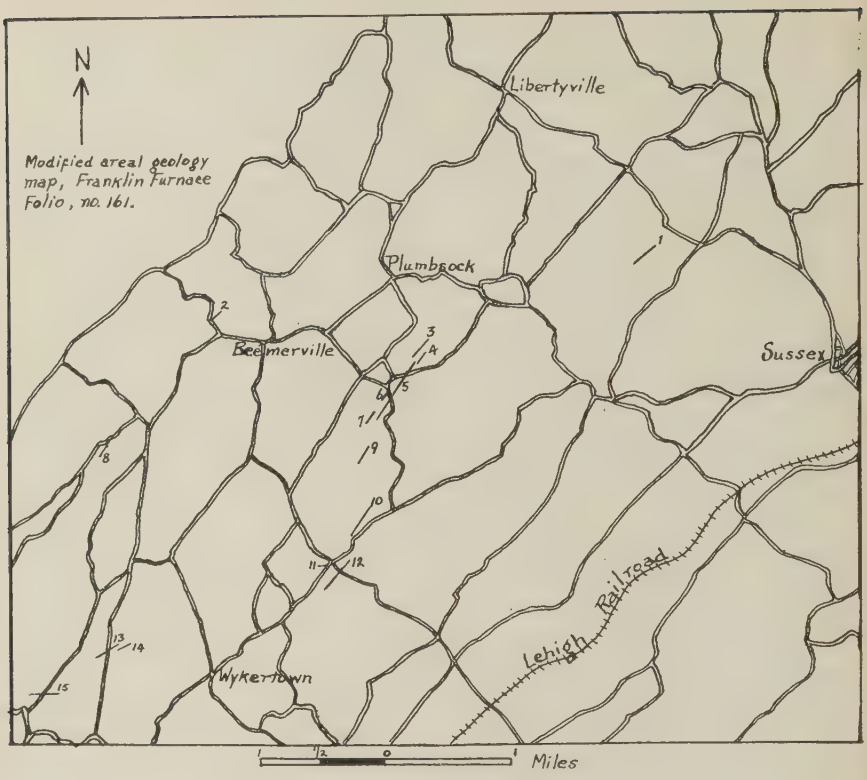

FIG. 1. Index map showing locations of intrusions.

ly exceed the quantity of either biotite or pyroxene.

Feldspar phenocrysts seldom attain a size greater than 10 mm.×3.5 mm., are subhedral, and are frequently twinned on the Karlsbad law. They frequently have numerous inclusions of all the primary minerals, but especially nepheline. Much of the feldspar is altered to clay materials and a colorless mica; locally it is altered to calcite or epidote; locally sodalite replaces portions of the orthoclase.

Phenocrysts of nepheline seldom are greater than 6.0 mm.×3.0 mm. in prismatic sections. Sphene and soda pyroxene are the most common inclusions. Much of the feldspathoid has altered to a colorless mica and calcite; locally to sodalite. Some phenocrysts have been completely altered and are recognizable only by their hexagonal outline.

Biotite seldom comprises as much as 10 per cent of the phenocrysts and usually does not exceed 1.5 mm.×0.75 mm. in size. Inclusions of sphene and apatite are common. Where unaltered the pleochroism is: X = light yellow, Y = Z = reddish brown. Biotite usually is much altered,

however, to a mixture of chlorite, magnetite, locally epidote, and some calcite.

Aegirine-augite seldom comprises as much as 10 per cent of the phenocrysts and usually is not greater than 3.0 mm.×0.05 mm. in size. Pleochroism is: X = pale greenish brown, Y = medium yellow-brown, Z = medium greenish brown. It is usually rimmed with aegirine. Sphene is the only inclusion.

The groundmass is a fine aggregate of nepheline, orthoclase, microperthite, biotite or soda pyroxene, sphene, apatite, magnetite, and zircon, stated in the usual sequence of decreasing abundance. Nepheline and feldspar occur in relatively the same amounts and generally together comprise about 90 per cent of the minerals. Biotite or soda pyroxene seldom is present in an amount greater than 15 per cent. At the middle portion of the sill at location 5 and at location no. 15, garnet comprises 10 per cent of the minerals. The size of the minerals of the ground mass varies slightly in the different intrusions, but the average size is 0.50 mm.×0.10 mm. to 0.10 mm.×0.05 mm. Locally there is an ill-defined flow structure.

Nepheline usually occurs as small squares and as prismatic sections 0.50 mm.×0.20 mm. in size. Locally it contains inclusions of soda pyroxene and magnetite. Much is altered to a colorless mica, calcite and cancrinite but usually it is less altered than where it occurs as phenocrysts.

Orthoclase is more abundant than microperthite. Both occur in subhedral to anhedral forms, and infrequently orthoclase is twinned on the Karlsbad law. The usual size is 0.40 mm.×0.10 mm. Somewhat common are inclusions of nepheline, sphene, apatite, and zircon. Orthoclase is less altered than where it occurs as phenocrysts, but much of it has altered to a colorless mica and calcite. Parker[15] states that nepheline and orthoclase at no. 15 are considerably altered to cancrinite and melilite, which locally compose about 12 per cent of the rock.

Anhedra of biotite, some containing inclusions of aegirine, are partially to almost completely altered to chlorite, magnetite, and calcite.

Aegirine exceeds aegirine-augite in quantity in the groundmass and occurs as small prisms 0.15 mm.×0.03 mm. in size. The pleochroism of aegirine is: X = blue-green, Y = yellow-green, Z = pale yellow to colorless.

Sphene, magnetite, apatite, and zircon also occur. Highly birefringent sphene occurs as wedges, some of which are twinned and which measure up to 1.3 mm.×1.0 mm. in size. Locally sphene comprises one percent of the mineral assemblage. Locally it is altered to leucoxene, other places to calcite and anatase in shades of blue.

[15] Parker, J. M., *op. cit.*, p. 57.

Magnetite locally comprises 5 per cent of the groundmass. It usually is only 0.02 mm. to 0.30 mm. in diameter. Much is altered to red iron-oxide.

Apatite occurs in prisms up to 1.5 mm.×1.1 mm. in size but usually it is 0.30 mm.×0.10 mm.

At location no. 6 garnet(?) of undetermined variety occurs in perfect dodecahedrons. It has completely altered to an aggregate of a fine, black, opaque substance part of which is magnetite, or to this opaque material plus biotite and/or calcite and/or chlorite. The average size of the crystals is 0.08 mm. in diameter and comprises 10 per cent of the mineral assemblage. At location no. 17 garnet, variety melanite, is dark brown in color. These crystals, which average 0.10 mm. in diameter and seldom attain a diameter greater than 0.3 mm., are frequently so filled with small inclusions of nepheline and orthoclase that melanite occurs here as skeleton crystals.

Bostonite

Intrusions of bostonite occur at six locations: nos. 2, 8, 9, 10, 11, and 12. In length they range from 200 ft. (no. 2) to 1400 ft. (no. 12); in width they range from perhaps 1 or 2 feet (no. 8) to 125 ft. (no. 12). All but one strike N 35°–45° E and, since contacts are not exposed, are apparently conformable with the bedding of the Martinsburg shale. The strike of the intrusion at location 11 is N 80° E and thus cuts across the strike of the shale.

The rock is medium gray to dark gray but locally has a greenish hue. In texture it is aphanitic and usually porphyritic. Phenocrysts of weathered feldspar up to 8 mm.×1.5 mm. in size usually are identifiable. At locality no. 11 the rock has a scoriaceous appearance due to numerous solution cavities.

Under the microscope the bostonite is holocrystalline, fine grained, and porphyritic except at locations nos. 8 and 12 where it is fine grained, hypautomorphic-granular. At location no. 8 the rock is composed almost entirely of tabular orthoclase crystals, 0.3 mm.×0.03 mm. in size, with outlines that are moderately sutured. It has a trachytic texture. At location no. 12 it is composed essentially of orthoclase laths and microperthite which average 0.80 mm.×0.13 mm. in size and which contain numerous inclusions of aegirine and magnetite. Here the feldspars have a rough trachytic texture; locally they have a tendency to sperulitic groupings. At all other localities phenocrysts of orthoclase and microperthite comprise about 10 per cent of the rock. They seldom exceed 2.5 mm.×1.5 mm. in size and are moderately altered to clay materials, a colorless mica, and calcite.

The groundmass has a rough trachytic texture. The principal constituent is orthoclase, but at location no. 11 there is also microperthite. The feldspar, normally 0.25 mm.×0.10 mm. in size, makes up 95 per cent of the mineral assemblage. Much of the feldspar is altered to a colorless mica and calcite. Locally a small amount of plagioclase (Ab_{68} at no. 2 and Ab_{90} at no. 11) is present. Aegirine, with pleochroism in yellow and shades of green, occurs in irregular bunches and as needles up to 1.0 mm.×0.02 mm. in size. At locality no. 9 aegirine comprises 30 per cent of the minerals but usually the amount does not exceed 5 per cent. Remnants or 'ghosts' of biotite are numerous, the biotite having altered to chlorite and magnetite. Sphene locally altered to leucoxene, magnetite altered to red iron oxide, and unaltered apatite and zircon are invariably present in minor amounts. Many irregularly shaped patches of calcite are present. Locally, as in portions of the intrusions at nos. 2, 8 and 11, a small amount of nepheline may have been present but has altered to cancrinite and a colorless mica.

TORBERNITE IN MISSOURI FIRE CLAY

W. D. Keller, *University of Missouri, Columbia, Mo.*

Torbernite, $Cu(UO_2)_2P_2O_8 \cdot 12\,H_2O$, hitherto unreported from Missouri, has been found filling thin cracks in a fire clay deposit of Pennsylvanian age in the north central fire clay district of Missouri. The occurrence is about 14 miles east of Auxvasse and $4\frac{1}{2}$ miles south of Martinsburg, on a farm owned by Mr. Robert Bailey.

Metatorbernite was reported by Grawe (1943) from a fire clay deposit near Gerald, Missouri, in the diaspore region south of the Missouri River, about 50 air miles from the torbernite occurrence. An isolated find of carnotite near Ste. Genevieve, located about 80 air miles southeast across the flank of the Ozark dome was reported by Muilenberg and Keller (1950).

The torbernite occurs in a soft, gray, semi-flint fire clay which has been open-pit mined intermittently. A pocket or seam of torbernite-bearing clay was encountered in a shallow prospecting shaft at a depth of about 10 feet below the upper surface of unweathered fire clay. Rain water filled the shaft which was abandoned and the water has remained high in the shaft ever since, due to the impervious nature of the clay. The writer did not see the walls of the shaft before water filled it, but collected the torbernite from the subsequently slaked fire clay which had been thrown out of the shaft. The clay is typical of Missouri Cheltenham (Keller, 1946) semi-flint fire clay.

The torbernite occurs invariably in a thin coating or scales on the clay

along relatively tight joints. Rarely is a torbernite film continuous with an area as much as one-half square inch. Usually tiny flakes are isolated, or the mineral forms tiny, flat, circular, scaly rosettes one-half millimeter or less in diameter. A few of the joints are lightly and discontinuously stained with brown iron oxide upon which (later) the torbernite rosettes were deposited.

Mineralogical Properties

The torbernite is pale, slightly bluish, apple-green in color against the light gray fire clay. Although the flakes adhere closely to the clay, they spring away slightly when pried with a needle. The tiny flakes vary in color in transmitted light from pale green to slightly yellowish green, and show first order yellow interference color between crossed Nicols. Bluish abnormal interference color also is characteristic. Radial structure (probably plates) in the rosettes is shown by the presence of undulatory extinction crosses.

Individual crystals are too small to furnish indices of refraction, but a mean index of 1.584 was determined on the cleanest material. Diffuse interference figures are obtained, similar to those on dried clay film aggregates, ranging from a hazy uniaxial cross to shadowy biaxial brushes of an optic angle of about 65°. Optical character is always negative. Winchell (1951) gives for torbernite: "Nearly uniaxial and negative with $N_o = 1.592$, $N_e = 1.582$." Metatorbernite on the other hand, has indices of refraction in the range 1.620 to 1.640.

A Geiger counter is slightly but definitely activated by the small amount of torbernite available.

By prolonged picking under a binocular microscope, enough of the mineral was segrated to irradiate for an x-ray powder diffraction pattern. Using CuK_α-Ni radiation the following d spacings were obtained, which are compared with those of torbernite from Old Gunnis Lake, Calstock 7112, furnished by Dr. Michael Fleischer[1] from the files at Harvard. Correlation of the patterns is good. Variability in the widest d spacing may be attributed to variation in the degree of hydration between layers.

Origin of the Torbernite

Evidence for the origin of the torbernite indicates that it was dissolved from endogenetic and superjacent Pennsylvanian sedimentary rocks. Missouri fire clay deposits usually give a slightly higher impulse count on a Geiger counter than do adjacent limestones, but not enough difference to be useful in prospecting for fire clay. The fire clay is therefore a potential source of radioactive elements which might be concen-

[1] Personal letter from Dr. Fleischer, Dec. 27, 1950.

Torbernite (This paper)		Torbernite—Phase 13 Old Gunniss Lake, Calstock 7112 Harvard Univ. data	
d	*I*	*d*	*I*
10.2	w	9.41	1
8.84	s	8.85	5
5.49	m	5.47	2
4.93	m	4.96	2
4.32	w	4.37	3
3.70	s	3.69	10
3.59	w	3.52	4
3.24	m	3.26	5
2.99	vw	2.95	3
2.67	m	2.68	5
2.54	w	2.56	3
		2.49	2
		2.39	2
2.25	w	2.26	1
		2.22	2
2.17	m	2.18	5
2.12	w	2.14	3
2.05	m	2.07	4
1.98	m	1.989	6
		1.892	1
1.84	w	1.852	2
		1.821	1
1.77	w	1.781	2
		1.746	1
		1.713	1
1.64	s	1.642	7
		1.613	2
1.58	vw	1.583	2
1.55	s	1.556	8
		1.461	1
1.45	w	1.449	1
1.42	m	1.419	5
1.39	w	1.389	2
1.369	m	1.366	5
1.336	w	1.336	3
1.313	w	1.313	4
		1.264	1
		1.247	1
		1.243	2
		1.222	2
		1.211	2
		1.197	1
		1.159	5

s —strong line
m—medium
w—weak
vw—very weak

trated into minerals. A lateral secretion mode of origin is not likely because of the imperviousness of the clay.

The Cheltenham fire clay was covered in all Missouri fire clay districts by a sequence of Pennsylvanian shales which were subsequently eroded. Some of the shales are black and are slightly radioactive. Pleistocene (Kansan) glacial drift overlay the torbernite-bearing clay most recently. The Burlington (Mississippian) limestone is the thick country rock beneath the conglomeratic and sandy floor of the clay deposit which contains the torbernite.

The clay deposit which contained the metatorbernite reported by Grawe is underlain by the Jefferson City (Ordovician) dolomite. Glacial deposits did not extend to this region but Pennsylvanian shales did cover this region as well as the torbernite one to the north (Keller, 1951).

Hence the two occurrences of the radioactive minerals have in common the possibility that the torbernite and metatorbernite elements were leached out of the overlying Pennsylvanian shales and the upper zones of fire clay while they were being eroded. Descending ground water probably carried them into the jointed clay below but there is no recognizable evidence of any chemical or mineralogical cause for precipitation where the torbernite was deposited. Deposition occurred after iron-oxide bearing solutions had penetrated the joints in the clay. Although a hypogene origin remains a possibility, it seems less logical than a supergene one.

Acknowledgments

It is a pleasure to acknowledge the help of Mr. Ben K. Miller who called the attention of the writer to the torbernite occurrence, and who helped collect the samples. Dr. Michael Fleischer furnished verified metatorbernite for comparison purposes and a copy of the Harvard data on torbernite. Funds from the University Research Council (Grant No. 415) defrayed the cost of the x-ray patterns.

References

Grawe, Oliver R. (1943), Metatorbernite in Missouri flint fire clay; in Fire clay districts of east central Missouri, by McQueen, H. S.: *Missouri Geological Survey and Water Resources*, **XXVIII**, 2nd series, p. 153.

Keller, W. D. (1946), Evidence of texture on the origin of the Cheltenham fire clay of Missouri and associated shales: *Jour. Sed. Petrol.*, **16**, 63–71.

Keller, W. D. (1951), Observations on the origin of Missouri high alumina clays: *AIME*, in press.

Muilenburg, G. A., and Keller, Walter D. (1950), Carnotite and radioactive shale in Missouri: *Am. Mineral.*, **35**, 323.

Winchell, Alexander N., and Winchell, Horace (1951), Elements of Optical Mineralogy, Part II, Fourth Edition, John Wiley & Sons, New York, p. 206.

USE OF AEROSOL IN GRAIN SORTING

FRED A. HILDEBRAND, *U. S. Geological Survey, Washington 25, D. C.*

It is common practice for mineralogists to sort grains by using a dissecting needle moistened with saliva or some oily substance to which grains will adhere. In the U. S. Geological Survey laboratories, where samples for *x*-ray identification are frequently purified by grain-sorting, a wetting agent such as "Laboratory Aerosol" manufactured by Eimer & Amend Company of New York, was found to be an excellent needle moistener. Aerosol, because of its low surface tension, forms a thin, uniform layer over the tip of the needle, and even the tiniest grains can be picked up and easily removed from the needle. Saliva tends to "ball up" some distance back from the point and hence is ineffective. It was found convenient to use a small shallow container (about 2 cm. in diameter) such as a biological-specimen jar with an inside ground-glass stopper or an outside ground-glass cover, in the bottom of which is placed a wad of cotton saturated with aerosol. The tip of the dissecting needle is coated with aerosol simply by touching it lightly to the aerosol-saturated cotton. In *x*-ray examination by the powder method, the aerosol used does not contribute to the pattern, even when the grains are completely saturated or coated with aerosol.

X-RAY DEFRACTION CARDS ON CLAY MATERIALS

Extracted from Preliminary Report No. 7 of the API Research Project 49, these cards present *x*-ray diffraction data on 19 clay materials from different localities. On 3 by 5 inch cards in the format of the *x*-ray diffraction data card file published by the American Society for Testing Materials for the Joint Committee on Chemical Analysis by *x*-ray Diffraction Methods. Cards cover complete patterns given in "d" values for lines, including relative intensities, as well as single crystal data where available. Materials covered include the following:

Clay	*Locality*
Attapulgite	Attapulgus, Georgia
Dickite (96.29%)	St. George, Utah
Dickite (94.43%)	San Juanito, Mexico
Halloysite (93.9%)	Eureka, Utah
Halloysite (91.06%)	Bedford, Indiana
Kaolinite (Unknown Purity)	Macon, Georgia
Kaolinite (97.44%)	Lewistown, Montana
Kaolinite (97.19%)	Murfreesboro, Arkansas
Kaolinite (95.30%)	Mesa Alta, N. Mexico
Kaolinite (95.18%)	Bath, S. Carolina
Montmorillonite	Polksville, Mississippi
Montmorillonite	Chambers, Arizona
Montmorillonite	Santa Rita, N. Mexico
Montmorillonite	Lorena, Mississippi
Nacrite (Unknown Purity)	Augustusburg, Saxony
Nontronite	Garfield, Washington
Nontronite	Manito, Washington
Pyrophyllite	Robbins, N. Carolina
Saponite	Hector, California

Total of 24 cards because of necessity in some cases for two cards to cover complete diffraction pattern. Available from American Society for Testing Materials, 1916 Race Street, Philadelphia 3, Pennsylvania, at $2.00 per set of 24 cards.

The Cordilleran Section of the Geological Society of America will hold its forty-eighth annual meeting, the 11th and 12th of April, 1952, at Tucson, Arizona. A mineralogical session will be sponsored by the Mineralogical Society of America.

Members and fellows are requested to submit at their earliest convenience the titles and abstracts of papers they hope to present at this session. Abstracts should be submitted in duplicate and must not exceed 250 words. Titles and abstracts must be in the hands of Dr. V. L. Vanderhoof not later than February 1, 1952. Abstract blanks may be secured from the various geology departments or from the Secretary of the Section, Professor V. L. Vanderhoof, School of Mineral Sciences, Stanford University, Stanford, California.

At the recent meeting of the International Union of Chemistry in New York and Washington, the Commission on Geochemical Localization of the Elements, organized by the Section of Inorganic Chemistry, held its first meetings. It was agreed that one of the needs of the field that could be met by the Commission was to act as a central source of information as to what research in geochemistry was being undertaken and where. It is therefore requested that persons and organizations that now have under way or that expect in the near future to undertake research projects or bibliographic projects in the field of geochemistry to inform the Commission of these projects and their scope. Those in the Western Hemisphere should write to Dr. Michael Fleischer, U. S. Geological Survey, Washington 25, D. C.; those elsewhere should write to Professor T. F. W. Barth, Geological Museum, Oslo 45, Norway.

The 1952 Spring Meeting of the Society for Experimental Stress Analysis will be held at the Hotel Lincoln, Indianapolis, Indiana, on May 14, 15, and 16.

BOOK REVIEWS

CONFERENCE ON THE ORIGIN AND CONSTITUTION OF COAL, sponsored by Nova Scotia Department of Mines and Nova Scotia Research Foundation, Crystal Cliffs, Nova Scotia, June 21–23, 1950. 159 pp., 1951.

The proceedings of the conference on the origin and constitution of coal at Crystal Cliffs centered around two major papers relating to coal geology in Nova Scotia, one by Dr. P. A. Hacquebard, Coal Petrographer, Fuel Division, Geological Survey of Canada, entitled "The Nomenclature and Classification of Coal Petrography," and the other by Dr. T. B. Haites, Geologist, Fuel Division, Geological Survey of Canada, on "Some Geological Aspects of the Sydney Coal Fields with Reference to their Influence on Mining Operations." Only the first paper is printed in these proceedings, the other being published in the *Proceedings of the Canadian Institute of Mining and Metallurgy*. In addition to the paper by Dr. Hacquebard the volume contains articles by Dr. A. T. Cross entitled "Plant microfossils and the application of their study to coal stratigraphy," and "Pennsylvanian stratigraphy and sedimentation of the Northern Appalachian region," one on "Metamorphism of coal" by Dr. A. Lahiri, which, however, was not given at the conference, and a version of which appears in *Economic Geology*, **46,** no. 3, 252–266 (1951); a paper on "The vacuum differential thermal analysis of coals," by Prof. W. L. Whitehead; one on "The chemical and structural relationships of lignin to humic substances," by Dr. Irving A. Berger, Illinois (also *Fuel*, **30,** no. 9, 1951), and one by I. A. Berger and W. L. Whitehead on "A thermographic study of the role of lignen in coal." Dr. B. R. MacKay, Chief Coal Division, Geological Survey of Canada, presented a short discussion on the coal resources of Nova Scotia at the opening of the conference.

In addition to these papers there is a fairly complete record of the discussion obtained with the aid of a tape or wire recorder.

The paper by Dr. Hacquebard is noteworthy because it represents the first presentation in North America of the European method of coal petrography based almost exclusively on polished surface technique rather than upon thin sections. The article is an exceedingly good presentation of the general principles and nomenclature of coal petrography from the point of view adopted. A useful system of coal petrography classification defines the limits between the different varieties of coal on the basis of the proportion of the vitrain on the one hand and opaque matter (micrinite) on the other. Likewise 5 varieties of banded coal grading from bright through semi-bright, intermediate coal, semi-dull coal to dull coal are proposed on the basis of the amount of the megascopically bright ingredients present (vitrain, clarian, and fussain). One of the chief items of discussion following the paper concerned the method and validity of identification of opaque matter (micrinite) that forms the ground mass of splint coal (durain) using incident light. Some of the pictures on display showing what was identified as micronite (Pl. IV, no. 3, Pl. VI no. 2 and no. 6) seemed to some of those present to be resin bodies which are translucent in thin sections, although somewhat less so than vitrain. Comparison of photographs of polished surfaces and of thin sections in half tone reproductions fail to show the full value of thin sections because the colors of the thin sections are very important aids in the identification of the constituents.

Dr. Cross's paper on plant microfossils explained the nature of spores and pollen grains and the use of these fossils in coal bed correlation. The procedure of stratigraphic studies followed by the West Virginia Geological Survey was outlined. The stratigraphic studies of the Pennsylvanian system in the Northern Appalachians have been carried on by making considerable use of the cyclic repetition of beds which characterizes the Pennsylvanian in this region as well as in other coal fields in eastern United States. At the same time the

importance of "key" beds in mapping is recognized. Both of the papers by Dr. Cross were profusely illustrated at the conference.

The article by Dr. Lahiri, Director of Fuel Research Institute, Bahar, India, which was not presented at the conference, presents a number of controversial ideas, adequate consideration of which is impossible here. In his summary the author states that "coal is a polydispersed colloidal system, the degree of polymerization being enhanced by metamorphic processes." Ignoring the fact, as coal paleobotanists have long since demonstrated, that vitrain represents coalified woody tissue, Lahiri suggests that the banded structure is of secondary origin arising from a process of gel coagulation and expulsion. One wonders whether or not the Lahiri theory could be adjusted to fit more consistently with the facts in regard to coal banding as determined by botanical studies.

The articles in the field of thermal analysis and the study of lignin by Breger and Whitehead present the results of some studies that have recently been carried on at the Massachusetts Institute of Technology. Various thermograms are shown, but Dr. Whitehead definitely recommends caution in the interpretation of results. There is so little published information concerning the thermal analysis of coal that the significance of the curves shown in this publication cannot be fully understood, if indeed it is certain that they have significance. However, Dr. Breger seems somewhat more inclined to regard the early part of the thermograms of lower rank coal as more indicative of the origin of coal from lignin rather than from cellulose. It may be pointed out that the thermograms of the bituminous coals, except low volatile coal (Fig. 7, no. 88, p. 133) tend to a fairly strong exothermic reaction around 400 to 450 degrees C followed by an exothermic reaction between 450 and 600 degrees C which is again followed by an endothermic reaction. This intermediate endothermic action appears to correspond to the loss of bituminous smoke-producing substances that characterizes the early stages of the carbonization of these coals as has been pointed out many times. Breger presents three infra-red absorption analysis curves for humic acid and spruce lignin. This method of analysis would appear to be applicable in determining the nature of the chemical substances found in coal. It is possibly applicable in the determination of the presence of bituminous substances—waxes and resins in coal. It may be noted that for the various bituminous coals examined by thermal analysis (Fig. 7, p. 137) low volatile coal alone does not show the exothermic rise between 400 to 450 degrees. This might provide a basis for classification of this and higher ranks of coal.

It is believed that this publication deserves the careful attention of people interested in the geology of coal.

Gilbert H. Cady,
State Geological Survey Division, Urbana, Illinois

STRUKTUR UND EIGENSCHAFTEN DER KRYSTALLE. Eine Einführung in die physikalische und chemische Krystallkunde by Helmut G. F. Winkler. Springer Verlag, Berlin/Göttingen/Heidelberg (1950). viii+258 pp., 1 pl., 62 text figs., 78 tables. Price DM 16.80.

Professor Winkler's book is a synthesis of the current concepts of the relations between crystal structure and a few of the selected physico-chemical properties of crystals. Although intended for a wide audience, the subject matter emphasizes the mineralogic approach. After a brief introduction, the book is divided into two sections: "Crystal Structure and Properties" and "Property and Crystal Structures," representing two approaches to the same subject. The first section contains descriptions of chemical bonding, general kinds of crystal structures and their chemical compositions, and ideal and real crystals. A discussion of the significance of the varying structural features of crystals to the physical and chemical

properties is included in these descriptions. The second part deals with the variations of the following properties with respect to the lattice geometry and to the nature of the chemical bond: heat conduction, compressibility, thermal expansion, optical properties, hardness, and cleavage. An appendix treats mostly of the Hermann-Mauguin symbols for symmetry classes and space groups. As a means of emphasizing the theme of the book, crystal structures are classified as isometric or anisometric; the anisometric group is further separated into sheetlike, sheet, chainlike, and chain structures.

The book is an outgrowth of Professor Winkler's lectures at the University of Göttingen in 1949. The reader is constantly reminded of this origin by the organization, the repetition of fact and kind of example, and by the uneven treatment of the different subjects. In a few places, the subject matter is discussed too briefly for adequate comprehension. The text is exceptionally clear and lucid. The illustrations are in unfavorable contrast to the text; they are poorly tied into the text, and very few are self-explanatory. Several complicated points would be clearer had more illlstrations been used. The numerous tables add little, being a sort of repetition of what has been clearly stated in the text.

The book is essentially an excellent introduction to the subject matter and is not a reference book. The treatment is qualitative and the more important references are included for those who wish to delve deeper into the subject. The German is unusually simple and clear. For these reasons the book should be well received by the many geologists interested in this aspect of crystallography, but who are unwilling to wade through the usual complex mathematical presentations. The section on cleavage is especially interesting and is the latest attempt to explain cleavage on the basis of inherent structural properties rather than on lattice defects. This section is a condensation of Winkler's article in the Heidelberger *Beiträge zur Mineralogie und Petrographie* (Bd. **2**, p. 255, 1950).

The book is clearly printed on good quality paper; the covers are paper.

George J. Neuerburg,
U. S. Geological Survey, Washington, D. C.

SCHWEFEL IN SCHLACKE UND SCHLACKENWOLLE, by Dr. Ing. Walther Fischer and Dr. rer. techn. Siegfried Wolf. E. Schweizerbort'sche Verlagsbuchhandlung, Stuttgart, Germany (**1951**), 231 pp., 1 fig., 53 tables, paper DM 25, bound DM 27.

The title of this book suggests a work of limited interest. To this reviewer, however, the many facets of the problem of sulfur in silicate melts was indeed revealing. The many forms in which sulfur may occur in slags: elemental, sulfide, sulfite, sulfate, silico-sulfate and others, and their intricate equilibrium relationships, create problems of considerable complexity. This book brings together the known data.

Even small quantities of sulfur in silicate melts may have important effects, some beneficial, some deleterious. The utilization of slags, of which tremendous quantities are available, is hindered by the nature of their sulfur content. Through an adequate knowledge of the role of sulfur in these slags appropriate manipulations can often be devised to convert the useless into valuable materials.

The book is divided into six sections: (1) the general nature of slags, devoted to the mineralogy of silicate slags, (2) source of sulfur in slags, from fuels as well as the raw materials, (3) effects of sulfur in slags and slag products, (4) the various forms of sulfur in slags, including the numerous sulfur-bearing compounds occurring in them, (5) thermochemical considerations, and (6) a résumé. A pertinent bibliography of 162 titles is included, as well as an author and thorough subject indices.

The book should be of particular interest to the technologist in smelting and steel manufacture, cement, glass and rock-wool insulation products, and concrete construction.

There is also much of interest to the geochemist, mineralogist, petrologist and economic geologist with a particular interest in sulfide ores.

W. F. FOSHAG

STRUCTURE REPORTS FOR 1947–1948. Vol. 11. General Editor, A. J. C. WILSON; Section editors: C. S. BARRETT (Metals), J. M. BIJVOET (Inorganic compounds), J. M. ROBERTSON (Organic). Published for the International Union of Crystallography. N.V.A. Oosthoek's Uitgevers Mij, Utrecht. x+779 pp. (1951). Price 55 Dutch guilders, postpaid.

It is gratifying that this very important compilation of crystal structure data is now available, and that plans are underway to fill the gap between this volume and the last *Strukturbericht*, Vol. 7 (1939), as well as to continue the series for the years since 1948. The structures of about 800 substances, published in 1947–8, are included. It has been the aim of the editors to make these reports such a complete record of the data that reference to the original work will be unnecessary in most cases. On the other hand, data of non-structural interest is not included, even though it be of great importance in the original article.

Separate sections in the volume are devoted to Metals, Inorganic Compounds, and Organic Compounds. The order of listing differs from that used in the *Strukturbericht*, and is described in the introduction. In most cases readers will find it desirable to use the indices. Both subject and formula indices are included, as well as an author index.

This volume represents an international undertaking, and in spite of the difficulty of having editors in different countries, a very creditable volume has resulted, and has appeared in a remarkably short time. The editors and abstractors who have labored to produce this volume are very deserving of thanks from the many workers in the field of crystal structure who will be using these reports for years to come.

LEWIS S. RAMSDELL,
University of Michigan
Ann Arbor, Michigan

DIE LAGERSTÄTTE DER TREPČA UND IHRE UMGEBUNG, by Professor Dr. Ing. F. SCHUMACHER. Published by Izdavačko Preduzeće Saveta Za Ernegetiku I Ekstraktivnu Industriju Vlade Fnrj. Belgrade, 1950, 65 pages, 6 illustrations and 12 tables with geological horizontal sections through the deposit. Two colored geological maps, scale 1:5000 and 1:20,000. Can be obtained for DM 10. at the following address: Professor F. Schumacher, (14b) Spaichingen, P.O. Box 41, Württenberg, Germany.

The author of this bound book, written in German, was formerly Director of the Geological Institute at the Bergakademie in Freiberg, Saxony. During recent years he has served as geologist at Trepča and had an opportunity to make a thorough study of this unique deposit. The Trepča deposit was developed by The Selection Trust, London, and is in the mountainous district of southern Serbia.

According to Professor Schumacher, Trepča is considered one of the most remarkable lead-zinc ore deposits of the world, formed by metasomatic action and related to young volcanic intrusions.

It is not only for the unusual character of this ore deposit that the book by Schumacher is mentioned here, but more especially to call attention to the exceptional mineral specimens that may be collected at Trepča. To mention only a few the reviewer should like to stress the extraordinary large and beautiful crystals of dolomite, rhombohedrons measuring 16 cm. on edge; the large hexagonal plates of pyrrhotite; the unexcelled pseudomorphs of

pyrite after pyrrhotite; choice specimens of plumosite; vivianite crystals (7 cm.×2 cm.), transparent, with a green color and of superb quality, etc.

A detailed crystallographic description of these minerals will be published later.

ALFRED SCHOEP,
Ghent, Belgium

NEW MINERAL NAMES

Allevardite = Caillèrite = Tabulite = Déribérite

This spate of names refers to a peculiar mineral previously described as kaolinite (S. Caillère, *Compt. Rend.*, **198,** 179 (1934)), as mica (E. Lemoine, *Bull. hist. nat. Savoie*, **23,** 199 (1935)), as palygorskite (S. Caillère and S. Hénin, *Compt. rend.*, **222,** 238 (1946)), and finally as a new mineral named allevardite (S. Caillère and S. Hénin, *Compt. Rend.*, **230,** 668–669 (1950); S. Caillère, A Mathieu-Sicaud, and S. Hénin, *Bull. soc. franc. mineral. crist.*, **73,** 193–201 (1950). In discussion (*Bull. soc. franc. mineral. crist.*, **73,** 142, 146 (1950)), the name allevardite was objected to on the ground that the occurrence was 15 km. distant from the Allevard region, the alternative names caillèrite, tabulite, and déribérite were proposed, and it was agreed that the name caillèrite was preferred.

Analyses of 1. A yellow variety. #2. A greenish-white variety gave:

	SiO_2	Al_2O_3	Fe_2O_3	FeO	CaO	MgO
1.	45.20	30.05	1.07	0.20	4.62	0.34
2.	46.17	29.43	0.59	0.15	3.20	0.45

	K_2O	Na_2O	H_2O^-	H_2O^+	Sum
1.	0.33	2.83	9.72	6.04	100.40
2.	0.92	3.81	9.23	5.59	99.54

From analysis (1), after deducting CaO, "which is very probably present as impurities," the formula "$[Al_2(OH)_2(Al_{0.5}Si_{3.5})] \cdot 0.5\ (Na_2O)O_{10}$" is deduced. The mineral swells in water to form a gelatinous mass. Base exchange occurs on treatment with ammonium carbonate. Dehydration curves are given.

The mineral is fibrous, matted like papyrus. Electron microscope photographs show it to be made up of ribbons, some of which are folded or bent. The ribbons are 0.5 to 1μ wide by 10μ long and are about 100 Angstroms thick. Cleavage basal, perfect. Yellow to greenish-white. Biaxial, mean $n = 1.550$. G. = 2.36.

X-ray study gives $d_{001} = 22.5$ Å.; when the mineral is saturated with glycerol, $d_{001} = 25.6$ Å. The powder pattern of material heated at 500° is apparently that of a mica, with $d_{001} = 9.5$ Å. The mineral is believed to consist of mica layers, generally grouped in pairs and separated by a layer of water molecules.

NAMES: Allevardite for the Allevard region, Isère, France; tabulite for La Table, Savoy, France (the actual locality); déribérite for Mr. Déribére; caillèrite for Miss S. Caillère.

DISCUSSION: The evidence is insufficient to justify a new name. In the present confused state of the nomenclature of the clays and micas, restraint is desirable and new names should not be proposed for poorly defined material. In particular, the deduced formula can not be accepted, since it was derived by deducting 4.62% CaO and nothing else. Obviously the analysis is faulty, or something else has to be deducted, or both.

G. T. FAUST
MICHAEL FLEISCHER

NEW DATA

Schafarzikite

J. ZEEMANN, Formel und Kristallstruktur des Schafarzikite: *Anzeiger Osterreich. Akad. Wissenschaften, Math.-naturwiss. Klasse*, **87**, 200–201 (1950).

Schafarzikite was originally described in 1921, but was not analyzed until 1932, when a microanalysis by Hueber led to the formula $Fe_5Sb_4O_{11}$. *X*-ray study shows the mineral to be tetragonal, space group $D^{13}{}_{4h}-P4/mbc$, with $a=8.59\pm.02$, $c=5.92\pm0.20$ Å. It is isomorphous with synthetic $ZnSb_2O_4$, so that the formula is probably $FeSb_2O_4$.

M. F.

DISCREDITED MINERALS

Taosite = (Hoegbomite)

JACQUES DE LAPPARENT, Composition mineralogique, structure et origine des emeris de Turquies: *Compt. rend.*, **223**, 227–228 (1946).

The mineral named taosite (see *Am. Mineral.*, **21**, 678 (1936)) is stated to be apparently identical with hoegbomite.

GERALD M. FRIEDMAN